LOAD-SETTLEMENT BEHAVIOUR OF GRANULAR PILES

by

Nigel P. Balaam B.E.

A Thesis submitted for the Degree of Doctor of Philosophy in the University of Sydney.

June, 1978.

CONTENTS

Synopsis		v
Preface		vii
Acknowledgements		x
Notation		xi
CHAPTER 1	INTRODUCTION	1
CHAPTER 2	HISTORICAL REVIEW	6
2.1	INTRODUCTION	6
2.2	HISTORICAL NOTE	9
2.3	LITERATURE REVIEW	10
2.3.1	Methods for Predicting the Ultimate Load of Single Stone Columns	11
2.3.2	Methods for Predicting the Settlements of Clays Reinforced with Stone Columns	20
2.3.3	Some Applications of the Process	31
2.3.4	Field Load Tests	37
CHAPTER 3	FINITE ELEMENT ANALYSES	48
3.1	INTRODUCTION	48
3.2	FINITE ELEMENT ANALYSIS OF A SINGLE CONVENTIONAL PILE	50
3.2.1	Elastic Analysis	50
3.2.2	Analysis Taking Slip Between the Pile and Soil into Account	56
3.2.3	Modified Analysis to Take Soil Failure into Account	57
3.3	FINITE ELEMENT ANALYSIS OF A SINGLE GRANULAR PILE	62
3.3.1	Elasto-Plastic Behaviour	63

3.3.2 Finite Element Analysis 66

3.3.3 Analysis Taking Account of Slip 68

3.3.4 Analysis of an Adhesive-Frictional Dilatant Interface 76

3.4 AN ECONOMICAL METHOD FOR PERFORMING ELASTO-PLASTIC FINITE ELEMENT ANALYSES 82

3.4.1 Method of Analysis 82

3.4.2 Application of the Method to Elastic and Elasto-Plastic Analyses 88

3.5 THE CHOICE OF ELEMENT 100

3.5.1 Rectangular Isoparametric and Constant Strain Triangular Elements 101

3.5.2 Elastic Analyses - The Two Elements Compared 104

3.5.3 Elasto-Plastic Analyses - The Two Elements Compared 112

3.5.4 Conclusions 118

APPENDICES: 3A ELASTICITY MATRIX 121

3B EXPRESSIONS FOR NODAL FORCES 122

CHAPTER 4 ANALYSIS OF SINGLE GRANULAR PILES AND SMALL GROUPS 127

4.1 INTRODUCTION 127

4.2 SINGLE PILES 127

4.2.1 Typical Results From Finite Element Analysis 128

4.2.2 Comparison Between Theoretical Results and a Full Scale Load Test 137

4.3 SMALL GROUPS 146

4.3.1 Load-Settlement Analysis of Small Groups 148

4.4 ESTIMATION OF THE MATERIAL PROPERTIES FOR USE IN THE ANALYSES 162

4.5 SUMMARY AND CONCLUSIONS 167

CHAPTER 5 STABILISATION OF EXTENSIVE AREAS 169

5.1 INTRODUCTION 169

5.2 SETTLEMENT ANALYSIS OF REINFORCED CLAY 170

5.2.1 Finite Element Analysis 170

5.2.2 Comparisons Between Observed Settlements, Existing Methods for Predicting Settlements and Elastic Analyses 186

5.3 STABILITY OF EMBANKMENTS SUPPORTED BY STONE COLUMNS 193

5.4 SUMMARY AND CONCLUSIONS 195

CHAPTER 6 ANALYSIS OF 'SAND DRAIN' ACTION OF GRANULAR PILES 197

6.1 INTRODUCTION 197

6.2 CONSOLIDATION THEORY 198

6.2.1 Biot Consolidation Theory 198

6.2.2 Diffusion Theory 201

6.2.3 Comparison Between Diffusion and Biot Theory Solutions 203

6.3 EFFECT OF PILE DIAMETER, SPACING AND DEGREE OF PENETRATION ON RATE OF PORE PRESSURE DISSIPATION 212

6.4 EFFECT OF ANISOTROPY AND DRAINAGE CONDITIONS ON RATE OF PORE PRESSURE DISSIPATION 225

6.5 EXAMPLE ILLUSTRATING THE USE OF SOLUTIONS PRESENTED IN CHAPTERS 5 AND 6 238

6.6 SUMMARY AND CONCLUSIONS 243

APPENDIX 6A: FINITE DIFFERENCE EXPRESSIONS FOR DIFFUSION THEORY EQUATION 245

CHAPTER 7 ANALYSIS OF RIGID RAFTS SUPPORTED BY GRANULAR PILES 250

7.1 INTRODUCTION 250

7.2 ANALYSIS OF SETTLEMENT 250

7.2.1 Description of Problem 251

7.2.2 Analytic Solution 256

7.2.3 Effect of Domain of Influence on Solutions 269

7.3 ANALYSIS OF THE RAFT 274

7.3.1 Method of Analysis 274

7.3.2 Effect of the Domain of Influence on the Moment and Shear Distributions Across the Raft 284

7.4 ANALYSIS OF THE TIME-DEPENDENT BEHAVIOUR 293

7.5 SUMMARY AND CONCLUSIONS 311

CHAPTER 8 EXPERIMENTAL RESULTS 313

8.1 INTRODUCTION 313

8.2 PRESSURE VESSEL TESTS 314

8.2.1 Apparatus 314

8.2.2 Test Procedure 316

8.2.3 Experimental Results and Theoretical Predictions 317

8.3 CYLINDER TESTS 332

8.3.1 Apparatus and Test Procedure 332

8.3.2 Comparison Between Theoretical and Experimental Results 335

8.4 CONCLUSIONS 337

CHAPTER 9 CONCLUDING REMARKS 339

REFERENCES 346

SYNOPSIS

In this thesis an examination is made of the vibro-replacement technique for the stabilisation of cohesive soils. Improvement is achieved by the formation of stiffer columns of granular material within the soil deposit using a large cylindrical vibrator referred to as a vibroflot. Granular piles (also termed stone columns) are used either singly or in small groups to support isolated footings or large numbers are installed in a regular array to support widespread loads. Each of these modes of application are investigated. For convenience, the work may be divided broadly into four sections.

(a) Presentation of a finite element method for analysing a single granular pile in which slip at the pile-soil interface is taken into account. Both the pile and soil are treated as ideal elasto-plastic materials. The soil is taken to be purely cohesive while the pile is treated as a purely frictional dilatant material which does not necessarily obey an associated flow law. A finite element method suitable for the analysis of single conventional piles is also described.

(b) The finite element analysis is used to investigate the load-settlement behaviour of a single granular pile. The theoretical results indicate the general effects of the pile and soil properties on the load-settlement behaviour of the piles. The analysis is then used to reproduce the results of a field load test. Settlement influence factors for single piles, produced from an elastic analysis, are presented. These influence factors are used in conjunction with interaction factors, derived from the same ana-

lysis, to estimate the settlement of small groups of granular piles.

(c) Attention is then focussed on the use of large numbers of granular piles installed in a regular array to stabilise an extensive area. Except near the edges of the loaded area, the behaviour of all pile-soil units is virtually the same, and consequently only one pile-soil unit need be analysed. Improvement of the soil behaviour is due to (i) the presence of the stiffer pile, (ii) the sand-drain action of the pile which promotes more rapid consolidation of the clay. The results of elastic finite element analyses are presented which quantify the reduction in settlement under drained conditions of soft clays reinforced with granular piles and subjected to a uniform pressure applied over a large area. A series of diffusion theory solutions have been obtained for a parametric study of the increased rate of consolidation of the clay due to the installation of the piles. An analytic solution is then presented for the settlement of a rigid raft supported by the reinforced clay. Finite element solutions to Biot's equations are presented for the rate of settlement of the rigid raft. Expressions are also given for the bending moment and shear force distributions in the raft.

(d) Finally, the results of a limited laboratory programme, designed to verify the applicability of the finite element analysis and elastic settlement theory, are presented.

PREFACE

The candidate carried out the work described in this thesis during the period 1973-1978. All the work was conducted in the School of Civil Engineering, The University of Sydney. The candidate was supervised by Dr. H.G. Poulos, Reader in Civil Engineering, except for a period during 1976 when he was supervised by Dr. P.T. Brown.

The By-Laws of the University of Sydney require a candidate for the degree of Doctor of Philosophy to indicate which sections of the thesis are original. Any information or ideas derived from the many references used during this research programme have been acknowledged in the text. In accordance with the abovementioned By-Laws the Author claims originality for the following work:

(i) In Chapter 3 the method of separating the pile and soil bodies to overcome the necessity of using special joint elements is claimed as original, although analyses following a similar basic procedure have been presented previously.

(ii) In Chapter 3 the method of incorporating dual nodes at the pile-soil interface for the analysis of slip are claimed as original. The treatment of frictional-dilatant slip and in particular the transformations of the governing equations so that the same solution procedure used for the analysis of an adhesive interface can be retained, is claimed as original. In addition, the technique of reducing the size of the equation set for elasto-plastic finite element analyses is claimed as original.

(iii) In Chapter 4 the application of the finite element analysis. in which a pile-soil interface strength can be specified, for predicting the results from field load tests is claimed as original.

(iv) In Chapter 5 all numerical results for the reduction in settlement under drained conditions of soft clays reinforced with granular piles and subjected to a uniform pressure are claimed as original.

(v) In Chapter 6 all numerical results showing the increased rate of consolidation of the clay due to the installation of the piles are claimed as original.

(vi) In Chapter 7 the analytic solution for the settlement of a rigid raft, seated on clay stabilised by granular piles, is claimed as original.

A number of papers were prepared and published by the author and others during the period of the author's candidature. These are submitted in support of his candidature. They are:

1. BALAAM, N.P., POULOS, H.G. and BOOKER, J.R. (1975), "Finite Element Analysis of the Effects of Installation on Pile Load-Settlement Behaviour", Geotechnical Engineering, Vol. VI, No. 1, pp. 33-48.

2. BALAAM, N.P., BOOKER, J.R. and POULOS, H.G. (1976), "Analysis of Granular Pile Behaviour using Finite Elements", Proc. Int. Conf. on Finite Element Methods in Eng., Adelaide, pp. 29.1-13, 1976.

3. ROWE, R.K., BOOKER, J.R. and BALAAM, N.P. (1976), "Application of the Initial Stress Method to Soil Structure Interaction", accepted for publication, Int. J. Num. Meth. in Engng., see also Res. Report No. 294, School of Civil Engineering, University of Sydney.

4. BALAAM, N.P., POULOS, H.G. and BROWN, P.T. (1977), "Settlement Analysis of Soft Clays Reinforced with Granular Piles", Proc. 5th S.E. Asian Conf. on Soil Engineering, Bangkok, pp. 81-92.

ACKNOWLEDGEMENTS

The work described in this thesis was made possible by the award of a Commonwealth Research Scholarship and a Blackwood Hodge Foundation Scholarship.

I am indebted to my fellow research workers for their help during the course of this work. I gratefully acknowledge the value of discussions with, and the helpful supervision of, Dr. P.T. Brown. I wish to express my gratitude and most sincere thanks to Dr. H.G. Poulos for his supervision, guidance and enthusiasm in all aspects of this work. I should also like to record my sincere thanks to Dr. J.R. Booker for his invaluable contributions and generous help during the time of my candidature.

Finally, I should like to thank my parents, Les and Wyn, for their continual moral and financial support.

N.P.B.

NOTATION

All notation and symbols are defined where they first appear in the text. For convenience, the more frequently used symbols and their meanings are listed below.

A_p	Cross-sectional area of pile
a	Radius of footing, radius of pile
b	Footing width, radius of equivalent circular domain of influence of pile
c_a	Adhesion at pile-soil interface
c_u	Undrained cohesion
c'	Cohesion of soil skeleton
c_{rl}	Coefficient of consolidation in the radial direction for one dimensional strain conditions
c_{vl}	Coefficient of consolidation in the vertical direction for one dimensional strain conditions
c_{v3}	Coefficient of consolidation in the vertical direction for three dimensional strain conditions
$[D_E]$	Elasticity matrix
d	Pile diameter
d_e	Effective diameter of a pile's domain of influence
E_p', E_p, E_1	Young's modulus of pile
E_s	Undrained Young's modulus of soil
E_s', E_2	Young's modulus of soil skeleton
$E_s(0)$	Young's modulus of soil at surface
$E_s(h)$	Young's modulus of soil at depth h
$\{F\}$	Force vector

G	Shear modulus
G_o	Shear modulus at surface
h	Depth of soil layer
I_ρ	Displacement influence factor
K	Relative stiffness of pile and soil
$[K_E]$	Elastic stiffness matrix
$[K_{EP}]$	Plastic stiffness matrix
k_h	Permeability in the horizontal direction
k_v	Permeability in the vertical direction
L	Length of pile
M_1	Major principal moment
M_2	Minor principal moment
M_r	Moment in the radial direction
M_t	Moment in the tangential direction
m_{v1}	Coefficient of volume change for piles
m_{v2}	Coefficient of volume change for soil
P	Applied load
p	Magnitude of applied traction
p_1	Reaction stress in pile minus the applied traction
Q	Shear force
q, q_A	Magnitude of applied traction
R_s	Sum of interaction factors for group settlement
r	Radial co-ordinate
r_e	Effective radius of a pile's domain of influence
r_w	Radius of pile
s	Pile spacing
T_h	Time factor defined in terms of c_{r1}
T_{v1}	Time factor defined in terms of c_{v1}
t	Time

t_{50}	Time for 50% consolidation
U_o	Pore water pressure
U_p	Degree of pore pressure dissipation
U_R	Degree of pore pressure dissipation for radial flow
U_s	Degree of settlement
u	Excess pore pressure
u_o	Initial excess pore pressure
u_r	Radial displacement
u_t	Excess pore pressure at time t
x, y, z	Cartesian co-ordinates
z	Cartesian co-ordinate
α_f	Interaction factors computed from an elastic analysis of two identical piles
γ_t, γ	Bulk density
γ_w	Density of water
Δ	Footing displacement, finite increment
$\delta_{elastic}$	Footing displacement for elastic continuum
δ	Footing displacement
∂	Differential operator
ε_z	Vertical strain
ε_v	Volume strain
θ	Bulk stress, angular measure
ν	Poisson's ratio
ν_p', ν_p, ν_1	Poisson's ratio of pile
ν_s', ν_2	Poisson's ratio of soil skeleton
ν_{RAFT}	Poisson's ratio of raft
σ_1, σ_2, σ_3	Principal stresses
σ_h	Horizontal stress
σ_R	Radial stress

σ_θ	Circumferential stress
σ_z	Vertical stress
ϕ, ϕ'	Angle of internal friction
ϕ_a	Angle of friction for interface slip
ψ	Angle of dilatancy of pile material
ψ_a	Angle of dilatancy of interface

CHAPTER ONE

INTRODUCTION

1.1 INTRODUCTION

The vibroflotation method of stabilising unsuitable deposits of soil has been widely used in the last two decades although the technique was first conceived in the early 1930s. In this process a large poker vibrator, referred to as a vibroflot, is sunk into the ground usually by the combined action of vibration and a jetting fluid emerging from the tip of the vibroflot. Initially the process was restricted to the improvement of granular soils by compaction. However, it was found that where compaction was made difficult by the presence of soils with cohesion, the formation of columns of coarse backfill at each compaction centre resulted in reduced settlements. This development led to the establishment of the stone column method in which cohesive soils are improved by the partial replacement (wet process - jetting fluid used) or displacement (dry process - no jetting fluid) of the native soil with columns of compacted granular material.

Granular piles or stone columns are used singly or in small groups to support isolated footings when conventional foundations are considered uneconomical. Frequently large numbers of stone columns are installed in a regular array to stabilise soft clays over an extensive area. Despite the widespread use of such piles, present design methods are largely based on empirical data or very simplified concepts of the action of the piles. In this thesis an attempt is made to present rational design methods for each of the modes of application referred to above.

The most fundamental problem to consider is the bearing capacity of an isolated single stone column. The bearing capacity is a function of the rate of application of the load with a minimum value generally occurring when the soil deforms under undrained conditions. When the ultimate load is reached plastic failure will have occurred in both the pile and soil materials. The compacted gravel is a dilatant work softening material whereas normally consolidated soft clay deformed under undrained conditions behaves as an incompressible elastoplastic material. Thus, to obtain an analytic solution for the bearing capacity of a single granular pile radical simplifications need to be made.

In this thesis a finite element loading path method is presented which enables the load-settlement relationship of a single isolated granular pile to be computed. In order to model the soil and pile behaviour realistically and to avoid excessive computational effort both the pile and soil are treated as elastic, perfectly plastic materials obeying a Mohr-Coulomb yield criterion. The soil is taken to be purely cohesive while the pile is treated as a purely frictional dilatant material. The plastic deformation within the pile and soil is described by a flow rule characterised by a dilatancy angle which governs the volumetric behaviour of the plastic component of strain. The analysis allows for three modes of failure within the granular pile-soil system,

a) interface slip between the pile and soil

b) failure within the soil under undrained conditions

c) failure within the gravel pile under drained conditions.

The analysis is capable of allowing for an interface strength which is either purely adhesive, purely frictional or adhesive-friction

After this method of analysis is described, it is used to reproduce the results from a previously published field load test. The use of small groups of granular piles is then investigated. A small group may be installed to support an isolated footing when a single pile is considered inadequate. The ultimate load of the group can be estimated from an analysis of a single pile. Thus, no attempt is made to formulate a method exclusively for predicting the ultimate load of a small group of granular piles. However, results from an elastic analysis are presented which enable the load-settlement response of small groups to be estimated.

An examination is then made of the use of large numbers of granular piles installed in a regular array to stabilise a clay over an extensive area. In this case, except near the edges of the loaded area, the behaviour of all pile-soil units is virtually the same, and consequently only one pile-soil unit need be analysed. Improvement of the soil behaviour is due to:

a) the presence of the stiffer pile

b) the sand-drain action of the pile which promotes more rapid consolidation of the clay.

A mechanism for a bearing capacity type failure of the stabilised clay only exists at the edges of the loaded area. The results from conventional slip circle analyses can be used to estimate a factor of safety against this type of failure occurring. Away from the edges

of the loaded area the required size and spacing of the columns is dictated by the maximum allowable settlement. Elastic finite element results are presented which show the effect of changes in material properties and geometric factors such as pile penetration, spacing and soil layer depth on the settlement of the clay when subjected to a uniform applied pressure. An analytic solution is presented for the settlement of the clay reinforced by fully penetrating piles and loaded by a rigid raft. These results should provide a sound basis for estimation of the reduction in settlement of the clay due to the presence of the stiffer pile. However, if the soil is highly inhomogeneous a separate elastic analysis may be necessary to model the site conditions realistically. In addition, if the magnitude of the loading pressure causes significant yield in the pile or soil, the elastic analysis will underestimate the settlement and an elasto-plastic analysis of a pile-soil unit may be required.

The sand drain action of the piles causes more rapid consolidation of the clay. To utilise this advantage piles could be installed followed by a short period of preloading before commencement of construction. A series of diffusion theory solutions, in the form of a parametric study, is presented from which the required time for preloading or the rate of settlement of a flexible foundation can be determined. Finite element solutions to Biot's equations of consolidation are presented for the rate of settlement of a rigid raft.

Finally, the results of a laboratory programme are presented. These results show that the analytic solution for the settlement of a rigid raft placed on stabilised clay predicts settlements which are in good agreement with measured values. In addition, the

results from model footing tests are in reasonable agreement with predictions from the elasto-plastic finite element analysis in which slip along potential shear planes can be taken into account.

CHAPTER TWO

HISTORICAL REVIEW

2.1 INTRODUCTION

The vibroflotation process is now well established as an effective method for mechanical improvement of soil deposits. Improvement is achieved by the formation of stiffer columns of material within the soil deposit using a large cylindrical vibrator referred to as a vibroflot. Cohesionless soils are improved by compaction due to the vibrations of the vibroflot. This method is referred to as vibro-compaction. Cohesive soils are not responsive to vibrations; the method used to improve soft cohesive soils is vibro-replacement. A sieve analysis chart shown in Fig. 2.1 is a guide to the range of granular and cohesive soils which can be stabilised by these two methods.

Step-by-step diagrams of the vibro-compaction and vibro-replacement methods are shown in Fig. 2.2. In the first stage of the vibro-compaction method the vibroflot is sunk into the soil to the desired depth by the action of the vibrations and jetting fluid emerging from the tip of the vibrator when the wet process of construction is employed. The vibrator is then slowly withdrawn resulting in densification of the loose granular deposits as the intergranular forces are nullified and the grains rearranged into a denser state.

For cohesive soils, the vibrator is sunk to the desired depth and then partially withdrawn while the jetting fluid (wet process) prevents collapse of the hole. The hole is backfilled with coarse granular material. The vibrator is lowered and the backfill compacted. This is repeated until the hole takes no further backfill.

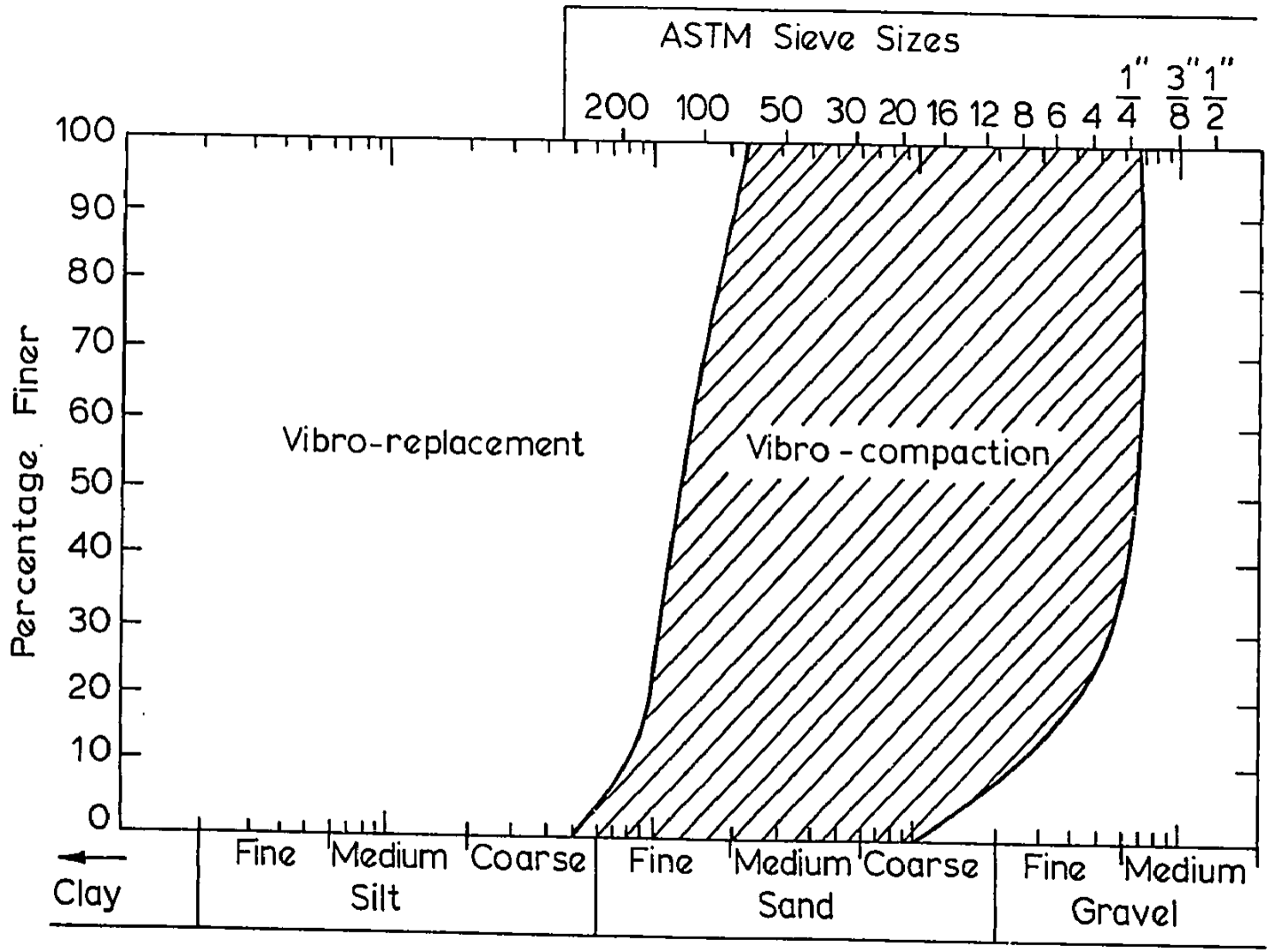

FIG. 2.1 SUITABLE RANGE IN SIZES FOR STABILISATION BY VIBRO - FLOTATION

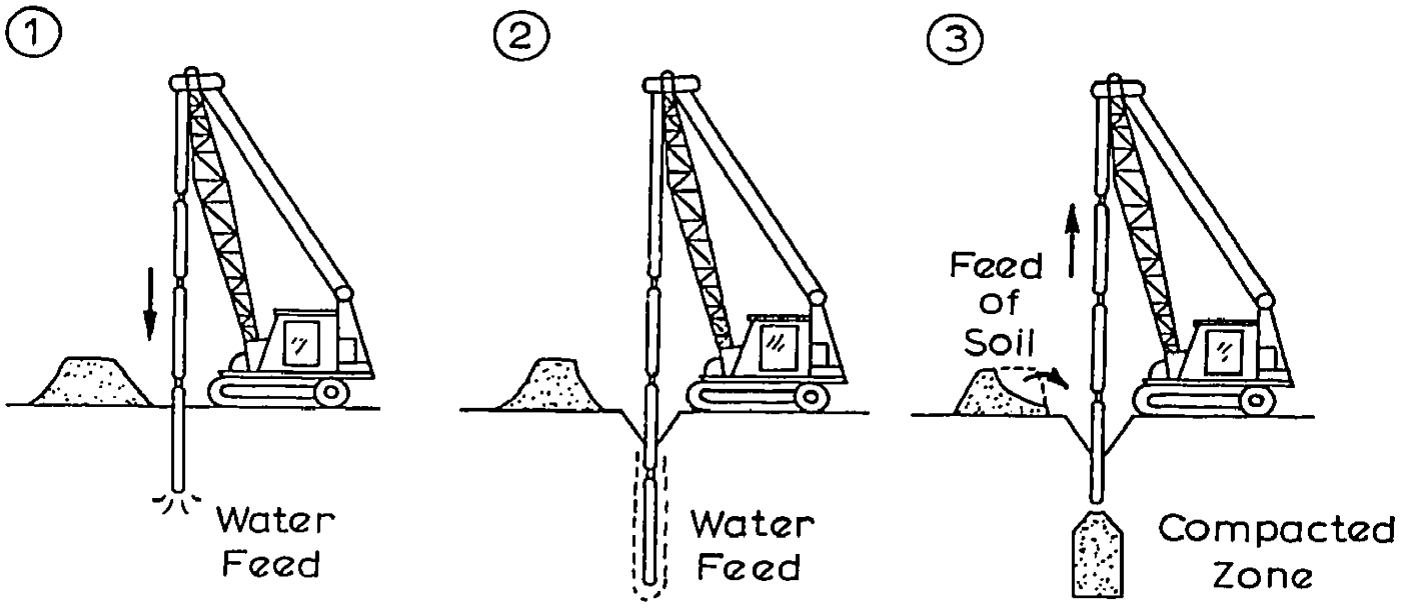

(a) Vibro - Compaction Method

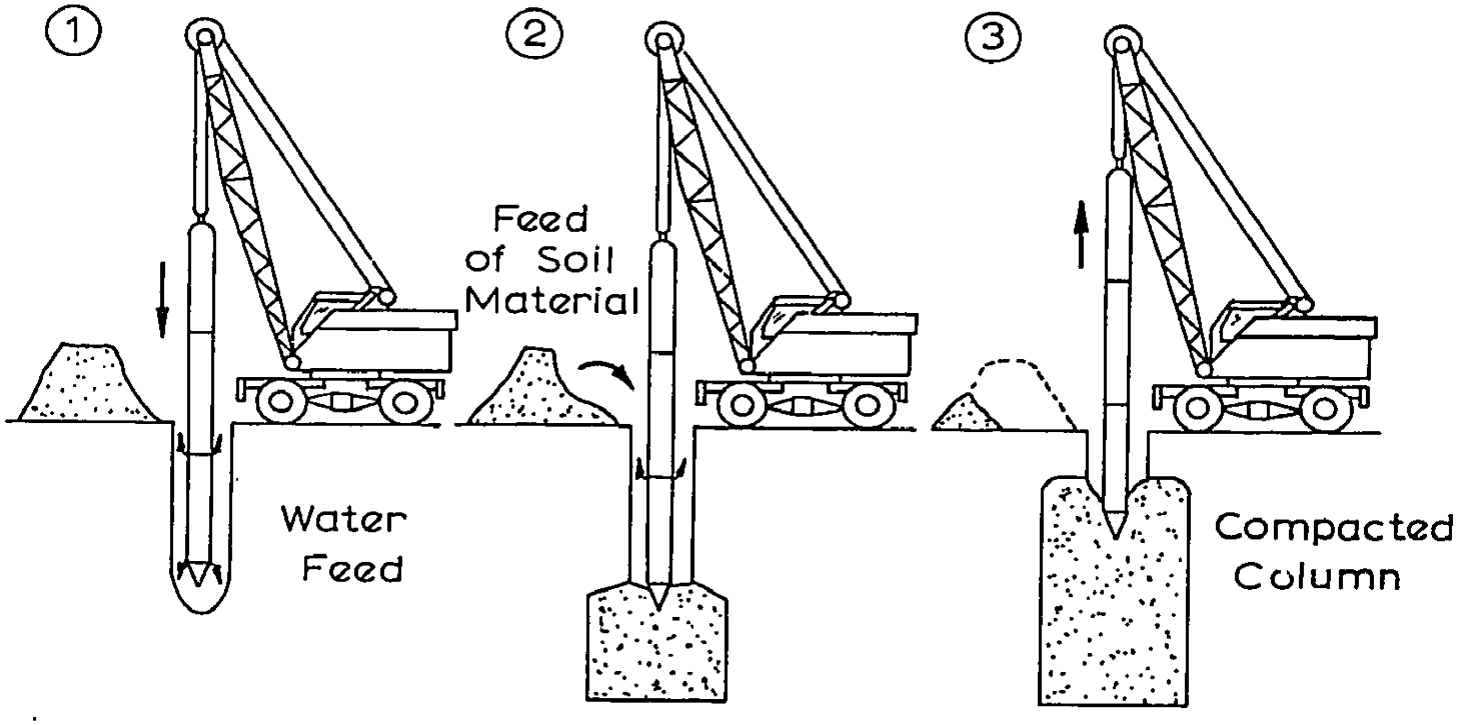

(b) Vibro - Replacement Method

FIG. 2·2 THE VIBRO - FLOTATION PROCESS

The resulting columns of compacted backfill are referred to by different authors as stone columns, granular columns or granular piles.

The vibro-replacement method is somewhat self-compensating in that the diameter of columns formed depend on the site conditions; the softer the soil the larger the diameter of the pile. The columns are usually a metre or more in diameter and are either installed in a regular pattern over a large area or used singly or in small groups to support isolated footings. They are usually spaced at 1.5 to 3 metre centres. Columns can be formed up to 30 m in length.

Improvement of the soil behaviour is due to

i. the presence of the stiffer pile
ii. the sand drain action of the pile which promotes rapid increase in strength of the clay.

The granular piles differ from sand drains because they are not formed of loose sand but of highly compacted coarse backfill.

In this thesis, consideration will be confined to the improvement of cohesive soils by the vibro-replacement method.

2.2 HISTORICAL NOTE

The stone column method is a relatively recent addition to the continually expanding group of methods of soil stabilisation. Hughes and Withers (1974) suggest that stone columns were first used in 1830 to support the ironworks at an artillery arsenal in France (Moreau et al., 1835). The method seems to have been forgotten but

was rediscovered in the 1930's with the first contract application in Nuremburg (Germany) in 1936. The development of the vibroflot was then pursued separately in Germany and the USA essentially for improvement of the vibro-compaction process. The vibro-replacement process was developed by extending the compaction process to treat silty sands and then distinctly clayey materials in Nigeria (Greenwood, 1965).

It is worthwhile noting that Moore (1944) describes the use of a hydraulic jet to form sand piles in soft clay at a site chosen for a quay for the US Navy. These piles were installed to improve the bearing capacity of the site and thus may have been the beginning of the stone column technique in America.

2.3 LITERATURE REVIEW

In the last decade the results of several load tests on treated ground have been reported. In addition, several workers have analysed the behaviour of the piles in an attempt to rationalise the design procedures. Although a rigorous solution for prediction of the behaviour of soils improved by the vibro-replacement method has not yet been reported, case studies and experience has permitted the evolution of conservative and semi-empirical design procedures.

A rational design method for the vibro-replacement process requires a rigorous theoretical analysis of the load-settlement behaviour of single isolated columns. This could then be extended to analyse soft clays reinforced by a large number of columns installed in a regular pattern. A review of the available methods of analysis

and an investigation of typical applications of the process is beneficial in determining the areas where analysis is lacking. In addition, interpretation of field loading tests designed to verify the applicability of a particular method of analysis to practical problems involving real soils, is desirable. In this review an attempt is made to categorise the contributions of researchers and practitioners into one of the above broad areas of endeavour. These are:

i. Methods for Predicting the Ultimate Load of Single Stone Columns
ii. Methods for Predicting the Settlement of Clays Reinforced with Stone Columns
iii. Some Applications of the Process
iv. Field Load Tests.

These categories are not self contained and overlap between them is inevitable.

2.3.1 Methods for Predicting the Ultimate Load of Single Stone Columns

Greenwood (1970) noted that no exact mathematical methods for estimating the bearing capacity of clay stabilised by the vibro-replacement process had been reported. He reasoned that if the column dilates and applies lateral stress to the surrounding clay which is resisted by passive pressure, then there is a triaxial stress system within the column. The column material is considered to have yielded and the vertical stress assumed to be a principal stress. It is of interest to note that the elastic solutions presented in Chapter 7 confirm this mechanism of failure. The bearing capacity can then be estimated. Greenwood adopted typical values of density, 119 lbs/cu ft

(18.68 kN/m^3); and cohesion, 500 lbs/sq ft (23.95 kN/m^2) for the clay and assumed an angle of internal friction of 35° for a column with a representative diameter of 0.9m. The bearing capacity for this typical column is about 24 tons (24.39 tonnes). When a factor of safety is allowed, Greenwood's approach compares well with the empirical method of Thorburn and MacVicar (1968) which is discussed in detail later in this section.

Hughes and Withers (1974) have presented a method for predicting the ultimate load of a stone column which was developed from the results of plasticity theory. Close agreement between the experimental results of model tests and the theory was obtained and thus this method of analysis is a significant contribution towards establishing a rational design method for this type of foundation.

The stone columns for the model tests were constructed in kaolin from Leighton Buzzard sand. Load was applied to the top of the column only and sufficient time allowed between successive increments of load for full dissipation of the excess pore pressures. Radiographic techniques were used to monitor the deformation behaviour of the columns as the load was increased to its ultimate value. A footing resting on the clay without the support of a stone column was loaded to failure and used as a comparison. The ultimate load was found to be much greater when the footing was supported by a stone column.

Typical patterns of vertical and radial deformation within the columns are reproduced in Figs. 2.3 and 2.4. These are shown for three values of vertical displacement at the top of the column. Hughes

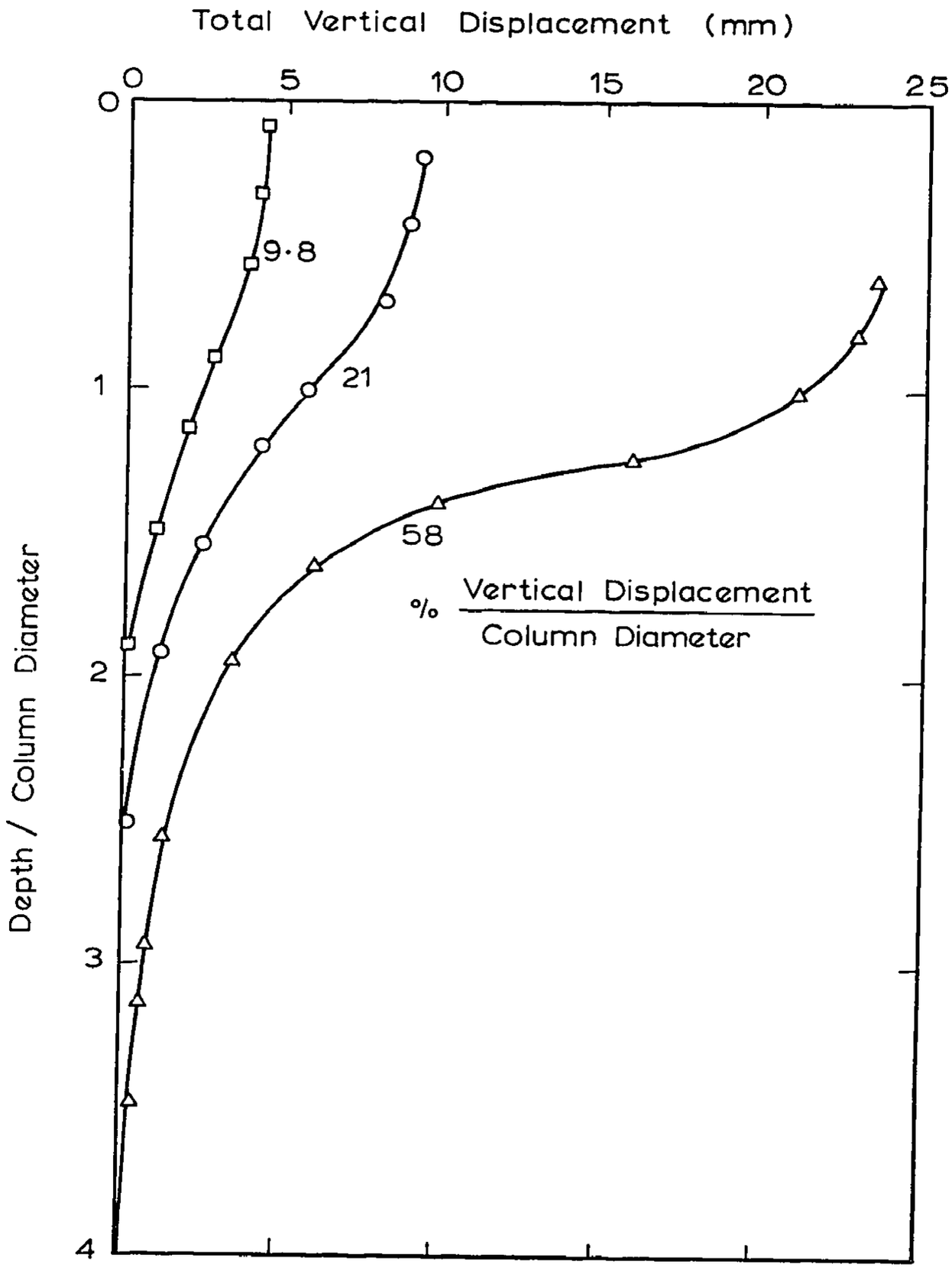

FIG. 2.3 VERTICAL DISPLACEMENT WITHIN COLUMN AGAINST DEPTH (after Hughes and Withers, 1974)

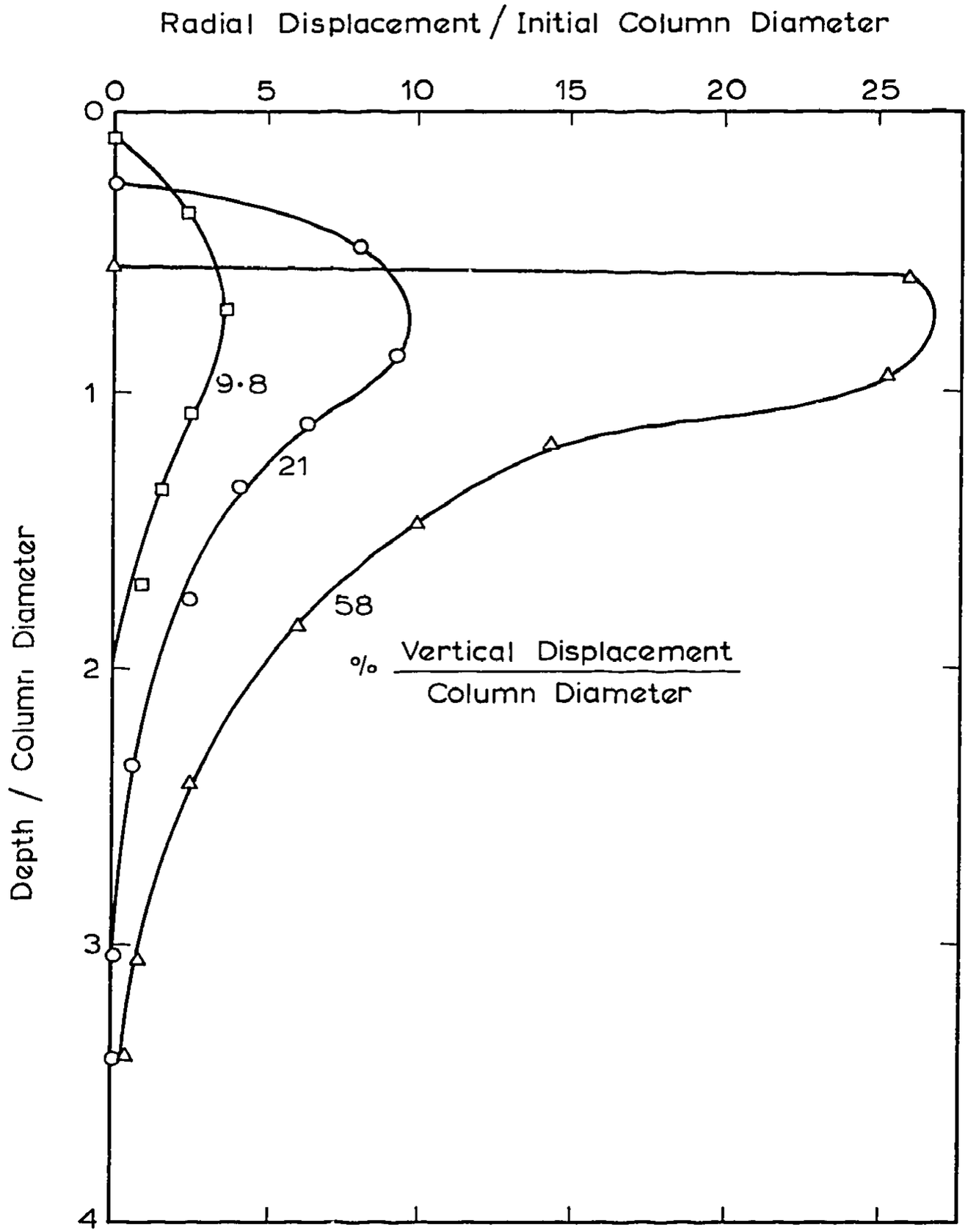

FIG. 2.4 RADIAL DISPLACEMENT AT EDGE OF COLUMN AGAINST DEPTH (after Hughes and Withers, 1974)

and Withers noted that the vertical and lateral distortion of the column diminishes rapidly with depth and that at failure significant distortion only occurred over a depth of about four diameters. Another important aspect of the deformation behaviour was that only the clay within a cylinder of about two and a half times the column diameter was significantly affected. The authors concluded from this that the columns could act independently if placed more than this distance away from each other.

The results of the experiments indicated that the ultimate strength of the column is governed by the maximum lateral resistance of the soil around the zone which bulges. This observation is used in developing the method of analysis. The lateral expansion of the pile is idealised as a cylindrical expansion into the clay. If the soil is treated as an ideal elasto-plastic material then the limiting stress is given by Gibson and Anderson (1961) as

$$\sigma_{RL} = \sigma_{RO} + c_u\{1 + \log_e \frac{E}{2c_u(1+\nu)}\} \qquad (2.1)$$

where σ_{RO} = total insitu lateral stress

E = Young's modulus

c_u = undrained cohesion

ν = Poisson's ratio

The results of quick pressuremeter tests show that equation 2.1 can be approximated by

$$\sigma_{RL} = \sigma_{RO}' + u + 4c_u \qquad (2.2)$$

where σ_{RO}' = effective insitu lateral stress

u = pore pressure.

If sand in the bulged zone of the column has yielded then

$$\sigma_v' = \{\frac{1 + \sin \phi'}{1 - \sin \phi'}\}\sigma_R' \qquad (2.3)$$

where σ_v' = vertical effective stress

ϕ' = angle of internal friction

σ_R' = lateral effective stress

The ultimate vertical stress the column can carry is then given by

$$\sigma_v' = \{\frac{1 + \sin \phi'}{1 - \sin \phi'}\} (\sigma_{RO} + 4c_u - u) \qquad (2.4)$$

To evaluate a distribution of vertical stress through the column the authors assume that the limiting value of the shear stresses along the sides of the column are equal to the undrained cohesion of the soil. Then, from vertical equilibrium, a linear distribution of vertical stress is obtained with a maximum value of σ_v' at the top ($u = 0$) to zero at some depth. This distribution then indicates that installation of the columns beyond this depth is unnecessary. Also, if the ultimate base resistance of the stone column is assumed to be $9c_u$ then this distribution in vertical stress can be used to determine the limiting length of the columns such that an end-bearing mode of failure occurs before the bulging failure.

The close agreement between the experimental results and the predicted failure load suggests that the design approach of Hughes and Withers outlined above has considerable merit. However, normally the cohesion of a clay is not constant with depth and thus the choice of c_u for use in equation 2.4 is not straightforward. Also, if the

footing does not apply load only to the top of the column but also to the surrounding soil, then the assumption that the column can be thought of as a cylinder expanding into the clay is more difficult to justify. The stresses induced in the clay due to the footing could confine the column sufficiently to alter the mechanism of failure. For example, if the footing is rigid, a punching failure through the clay may occur before the column bulges. Finally, the method of calculating the distribution of vertical stress through the column is approximate at best because when the column is failing the direction of shearing at the column-clay interface will most likely not be vertical which results in a rather different distribution of vertical stress through the pile.

Thorburn (1975) has presented an empirical design method initially recommended by Thorburn and MacVicar (1968) in which the total building loads are supported entirely by the stone columns. Thorburn considers such an approach ensures adequate factors of safety against a bearing capacity failure and provides the ground with considerable stiffness.

In Fig. 2.5 the relationship between the allowable working load, recommended for preliminary design, and the undrained shear strength of the cohesive soil, is reproduced. This relationship was obtained from the Rankine theory of passive earth pressure modified for radial deformation and from correlating field measurements of the average diameters of stone columns with the undrained shear strengths of the soils they were constructed in. This correlation only applies to stone columns formed by Cementation and Keller vibrators. Fig. 2.6 shows the allowable stress on a stone column adopted for development

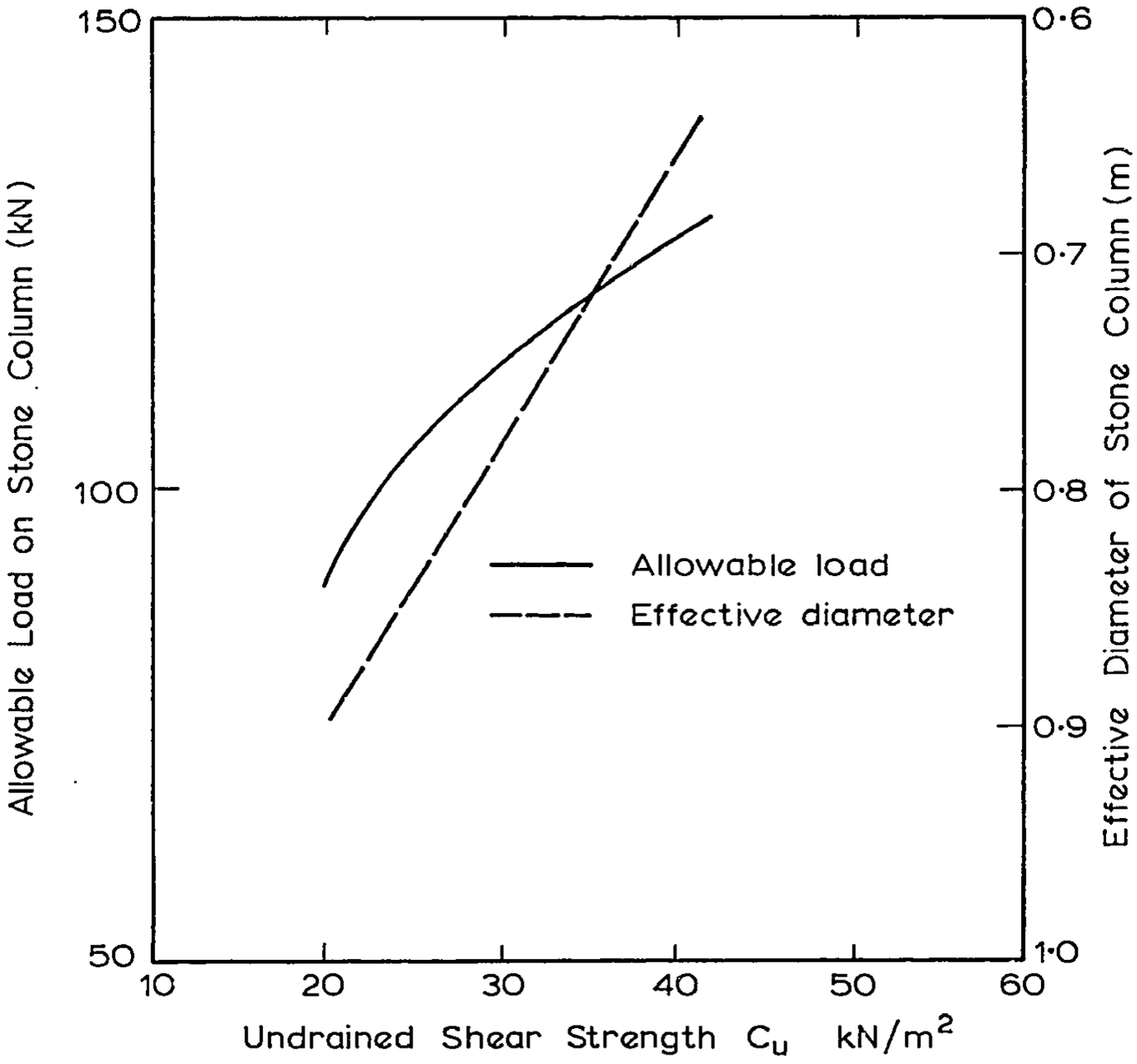

FIG. 2.5 ALLOWABLE WORKING LOAD FOR STONE COLUMN (after Thorburn, 1975)

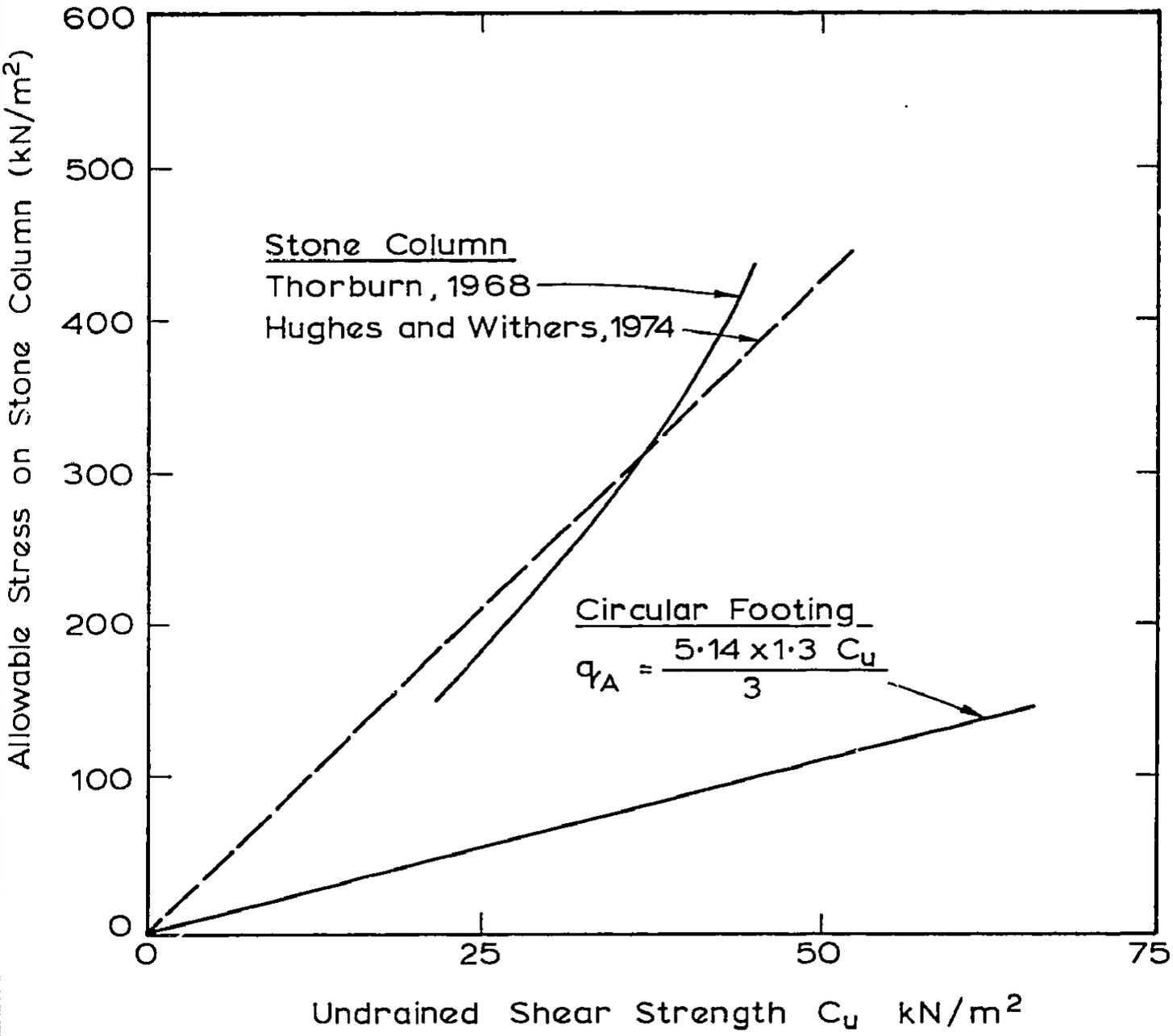

FIG.2.6 ALLOWABLE STRESS ON STONE COLUMNS

of Fig. 2.5 together with the values derived from the theory of Hughes and Withers (1974). The two resulting curves are in close agreement.

2.3.2 Methods for Predicting the Settlement of Clays Reinforced with Stone Columns

2.3.2 (i) Settlement of Isolated Columns

Mattes and Poulos (1969) have presented the results of theoretical analyses of the behaviour of single compressible piles based on linear elastic theory. Although the authors were anticipating the use of their solutions for the design of conventional pile types (steel, concrete, timber), these results are a convenient means of making preliminary settlement predictions for stone columns in the absence of field loading tests.

From the results of their analyses the following expression was derived for the settlement (S) of the top of a single compressible pile in a semi-infinite mass;

$$S = \frac{P}{E_s L} I_\rho \qquad (2.5)$$

where P = applied load

E_s = Young's modulus of soil

L = length of pile

I_ρ = displacement influence factor

In Fig. 2.7 the displacement influence factor I_ρ is plotted against the pile stiffness factor K, where

$$K = \frac{E_p}{E_s} R_A \qquad (2.6)$$

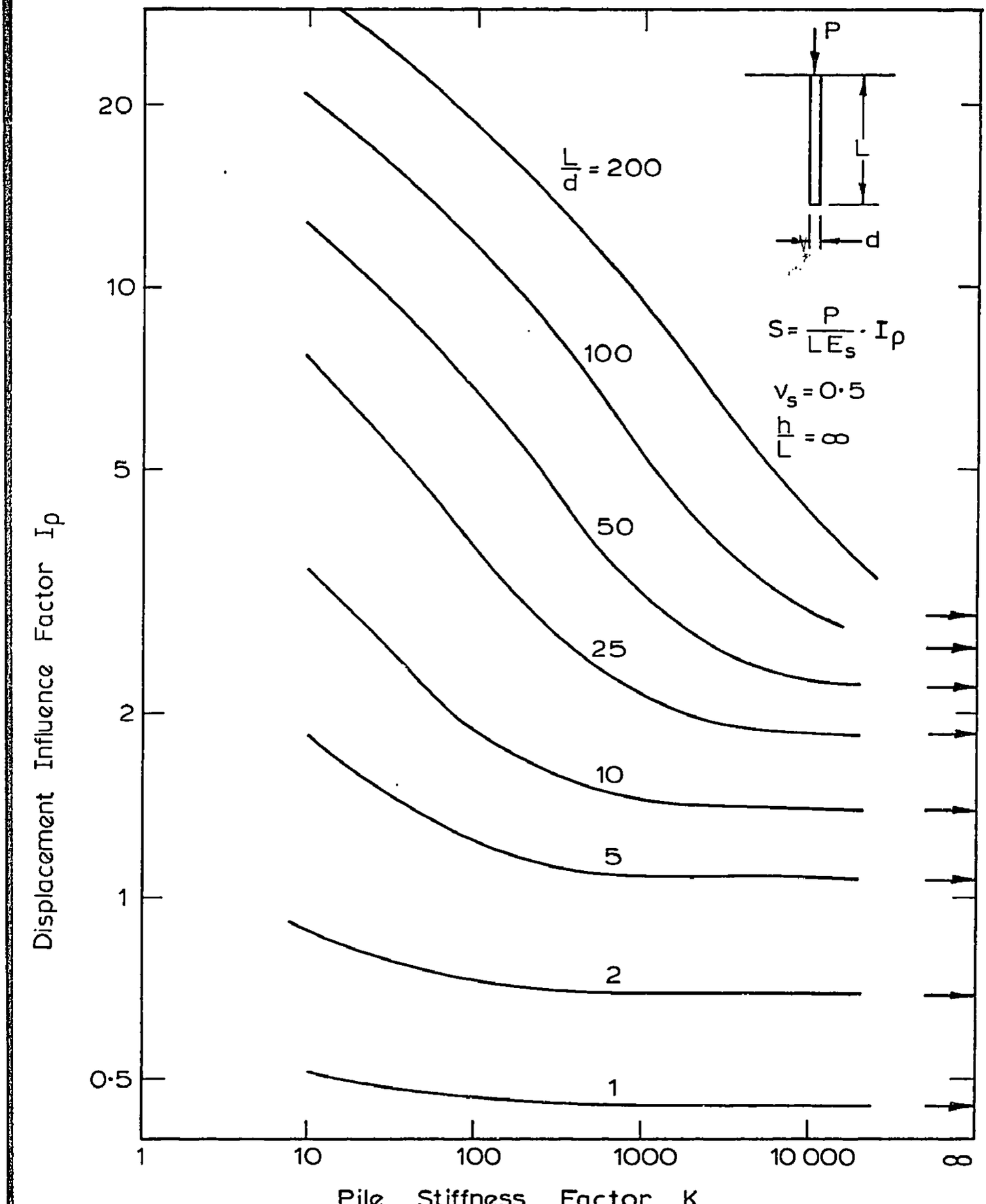

FIG. 2·7 DISPLACEMENT INFLUENCE FACTORS
(After Mattes and Poulos, 1969)

and E_p = Young's modulus of pile

R_A = ratio of area of pile section to gross cross-sectional area of pile (R_A = 1 for stone columns)

Displacement influence factors are plotted for various values of length to diameter ratio (L/d) for the piles and a Poisson's ratio of the soil, $\nu_s = 0.5$.

The immediate settlement, S_u, is calculated by putting $E_s = E_u$ (the undrained Young's modulus) and using the displacement influence factor for the undrained value of Poisson's ratio, $\nu_s = \nu_u$. The total final settlement, S_{TF} is calculated by putting $E_s = E_s'$ (the Young's modulus of the soil skeleton with respect to effective stresses) and using the displacement influence factor for the Poisson's ratio, ν_s', of the soil skeleton and the revised value of the pile stiffness factor K. The authors investigated the relative importance of the immediate settlement; these results, which are reproduced in Fig. 2.8, show that the major proportion of the total final settlement occurs as immediate settlement, although as K decreases the ratio S_u/S_{TF} decreases slightly.

Solutions were also obtained for the settlement of a pile in a finite layer of depth h underlain by a rough rigid base. It was found that for very compressible piles (K = 10) the layer depth has very little influence on the settlement of the pile. The settlement in a layer of depth h = 1.1L being only 7% less than for the same pile in a semi-infinite mass. The authors suggest that for such piles the influence factors for a pile in a semi-infinite mass be used for all layer depths. A value of K between 10 and 25 is thought to be typical of those applicable to stone columns, (Baumann and Bauer, 1974)

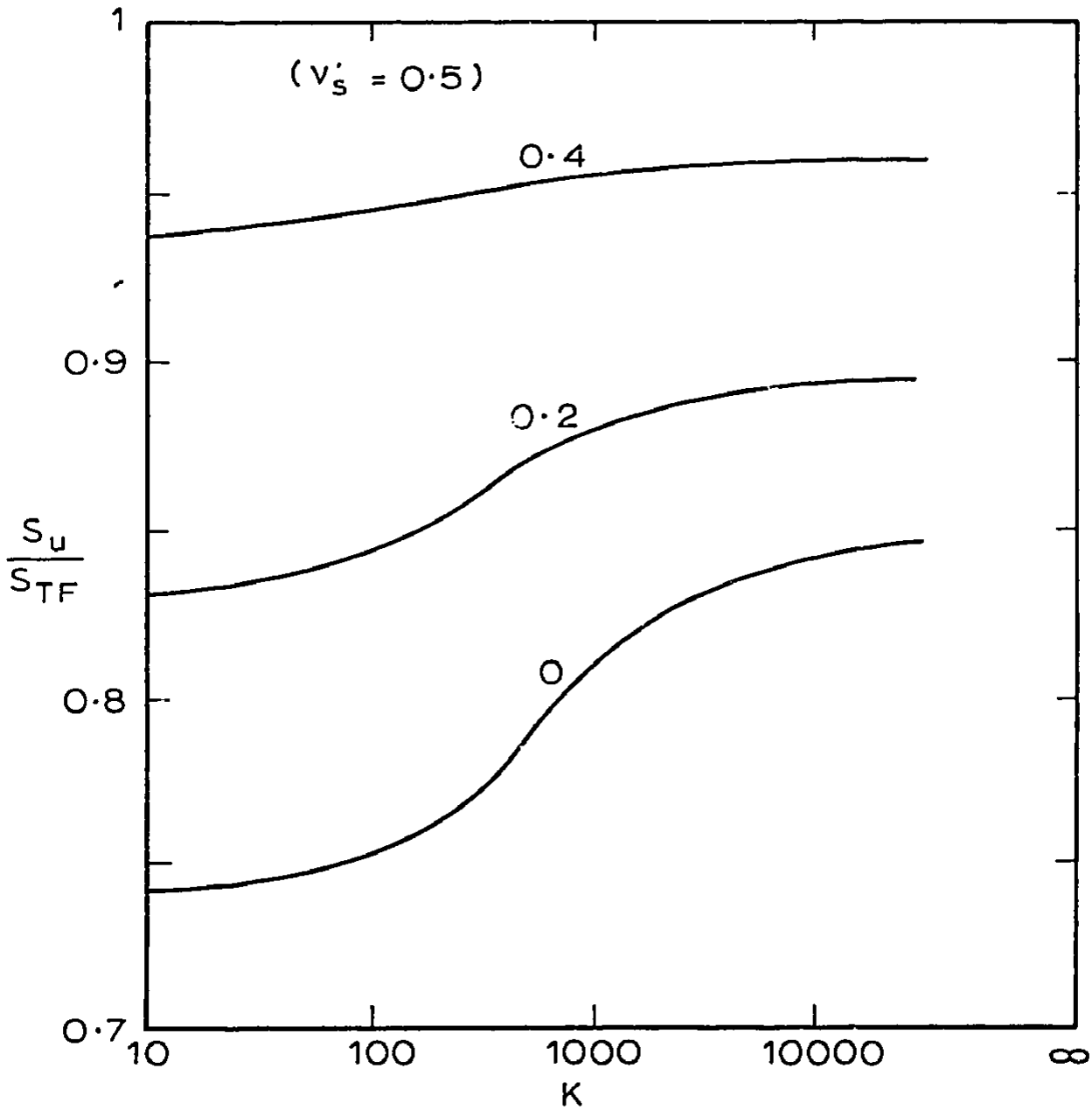

FIG. 2·8 RELATIVE IMPORTANCE OF IMMEDIATE SETTLEMENT (After Mattes and Poulos, 1969)

and thus this approach is considered sufficiently accurate for the purposes of preliminary predictions.

Hughes, Withers and Greenwood (1975) outline an approach which enables the prediction of the settlement characteristics of an isolated column. The main assumption is that the column expands radially as settlement occurs with constant volume being maintained. This assumption will lead to inaccuracies in their predictions. Before the column yields it is compressible. As yielding occurs within the column it will dilate until the critical void ratio is reached whereupon shearing will take place at constant volume.

The calculation is simplified by dividing the column into layers; the total settlement then being the sum of the contributions of each layer

$$\delta_v = \delta_1 + \delta_2 + \ldots\ldots\ldots + \delta_n \qquad (2.7a)$$

where $$\delta_n = \frac{2H_n \, \delta_{rn}}{r} \qquad (2.7b)$$

and δ_n = settlement of the layer considered

H_n = thickness of layer considered

$\frac{\delta_{rn}}{r}$ = radial strain for layer considered

The radial strain is calculated from the radial stress-strain properties of the clay which need to be established prior to the prediction. The radial stress is assumed to be K_{ps} times the vertical stress where

$$K_{ps} = \frac{1 + \sin \phi'}{1 - \sin \phi'} \qquad (2.8)$$

The authors note that these assumptions are not strictly correct but consider the inaccuracies they introduce in practice to be insignificant when the difficulties in accurately establishing the soil and stone parametersare considered.

A full scale field test on an isolated stone column indicated that the predicted settlements were too large if no side shear along the column-clay interface was allowed. Close agreement was obtained when the vertical stress in the column was calculated by subtracting the total shear along this interface from the total load above the horizon considered. The authors also suggested that the settlement characteristics cannot be accurately predicted without the radial stress-deformation data being established by use of a Cambridge-type pressuremeter (Wroth and Hughes, 1973). This is a disadvantage with this method of analysis.

2.3.2 (ii) Settlement of Ground Reinforced with Stone Columns

Greenwood (1970) noted that the estimation of settlement of the reinforced clay was empirical because rigorous solutions ensuring compatibility of column and clay deflections were not available. Curves for estimating consolidation settlements under widespread loads for uniform soft clays strengthened by stone columns are reproduced from this paper in Fig. 2.9. The shaded region represents the reductions in settlement expected when the wet process of construction is employed. These reduction in settlement could be expected when the columns rested on firm clay, sand or harder ground. They neglect immediate settlement and shear displacements. Greenwood suggests these curves should be used with caution within the range indicated.

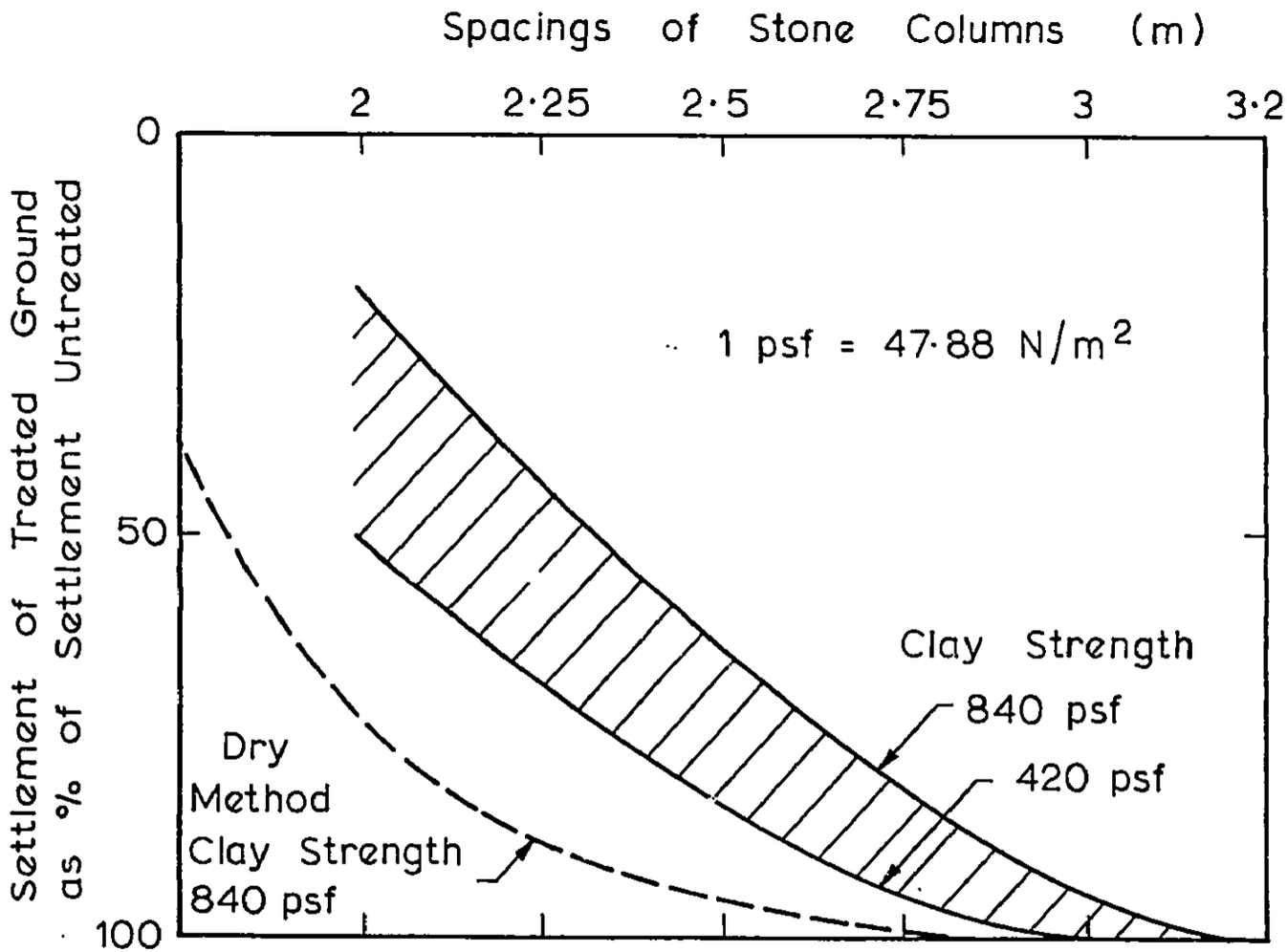

FIG. 2·9 SETTLEMENT DIAGRAM FOR STONE COLUMNS IN SOFT UNIFORM CLAY (After Greenwood, 1970)

A method for predicting the settlement of ground treated by the vibro-replacement process which uses the theory of elasticity has been developed by Baumann and Bauer (1974). The authors isolate a single column and assume the behaviour of all columns is identical. The total settlement is computed by summing the immediate (S_1) and consolidation (S_2) settlements. The immediate settlement is calculated in the following way.

The radial deformation of the column can be calculated by

$$\Delta r = \frac{\Delta\sigma}{E_c} r_o \ln \frac{a}{r_o} \qquad (2.9)$$

where $\Delta\sigma$ = lateral pressure difference between the column and clay

r_o = radius of column

E_c = Young's modulus of the stone column

$a = \sqrt{A/\pi}$

A = footing area per compaction point.

The shortening of the column is then given by

$$S_c = \frac{2\Delta\sigma}{E_c} D \ln \frac{a}{r_o} \qquad (2.10)$$

where D is the depth to which the column is compacted and the second order derivatives in equation 2.10 are neglected. The immediate settlement of the clay is

$$S_s = \frac{D}{E_s} p_s \qquad (2.11)$$

where E_s = undrained Young's modulus of the clay

p_s = stress on the clay.

If the lateral pressure increases in the column ($\Delta\sigma_c$) and the clay ($\Delta\sigma_s$) are written as

$$\Delta\sigma_c = p_c K_c \tag{2.12a}$$

$$\Delta\sigma_s = p_s K_s \tag{2.12b}$$

where p_c = stress on column

K_c = a value between the at-rest pressure and the active pressure coefficient

K_s = a value between the at-rest pressure and the passive pressure

then the lateral pressure difference between the column and clay ($\Delta\sigma$) is given by

$$\Delta\sigma = \Delta\sigma_c - \Delta\sigma_s \tag{2.13}$$

Equating the column and clay displacements and utilising equation 2.13; the ratio of pressures on the column and clay can be expressed as

$$\frac{p_c}{p_s} = \frac{(1 + 2\frac{E_s}{E_c} K_s \ln\frac{a}{r_o})}{(2\frac{E_s}{E_c} K_c \ln\frac{a}{r_o})} \tag{2.14}$$

The authors note that K_c and K_s have little influence on the value of this ratio and thus suggest that representative values be assumed. When a given size of columns and spacing is specified and the moduli of deformation determined from field or laboratory tests, the ratio of pressures can be calculated. The pressure on the clay is then de-

termined from equilibrium, ie.

$$p_o A = p_c A_c + p_s A_s \qquad (2.15)$$

where p_o = average applied stress

A_c = area of compaction column

$A_s = A - A_c$

The immediate settlement is then found from equation 2.11. The consolidation settlement is calculated using the one-dimensional settlement theory

$$S_2 = \sum_o^H \frac{\Delta\sigma_z}{E} \cdot \Delta z \qquad (2.16)$$

where E = drained Young's modulus of the clay

$\Delta\sigma_z$ = vertical stress increment at any depth z

H = total thickness of compressible layer

Δz = layer thickness

The authors suggest that the distribution of vertical stress $\Delta\sigma_z$ within the compacted zone has to be estimated by using a Boussinesq (1885) or Newmark (1942) stress distribution. They conclude that the simplifying assumptions in this analysis will lead to a solution in error but should yield the correct order of magnitude of settlement.

As this approach requires the moduli of deformation of the column and clay to be determined, it is considered that a more sophisticated method of analysis is warranted. With this data an elastic finite element analysis is relatively simple and would lead to a better prediction of settlement. The analysis of Baumann and Bauer (1974) is applicable only to rigid footings whereas in practice flexible footings

will also be encountered frequently if the treatment is employed at sites which will carry widespread loads such as storage tanks or embankments.

Hughes and Withers (1974) suggest that the settlement of large groups of stone columns is due to several interacting factors which make a prediction of settlement difficult. However, they have suggested an approach which produces an upper bound for the settlements of a rigid raft resting on soil reinforced by a large number of columns. Two assumptions are necessary. Firstly, the increased stiffness of the clay due to the bulging of the column and the effects of consolidation of the clay on the column are ignored. Secondly, the behaviour of a typical column within the group is the same as an isolated column. The stress-settlement characteristics for both the column material and the clay need to be determined (ie. oedometer test data). For a given average stress on the raft a settlement is chosen from which corresponding stresses for both the column and clay can be found. If these stresses satisfy equilibrium as expressed by equation 2.15 then the correct settlement has been chosen. If equilibrium is not satisfied then a new settlement is chosen and the process repeated. The authors have applied this approach to an example and shown that if the columns were constructed of Leighton Buzzard sand and the clay were kaolin, then the reduction in settlement of a rigid raft due to the stone columns is a function of the average stress applied to the raft; the larger the stress the less effective are the columns.

Thorburn (1975) refers to the settlement analysis proposed by Hughes and Withers (1974) and suggests that the effects of consoli-

dation on the stress-strain relationships must be taken into consideration because the short-term relationships obtained from relatively rapid plate loading tests are not applicable. Thorburn recommends that if the building loads are supported entirely by the stone columns the magnitude of settlement will be limited and the prediction of settlement becomes relatively simple. The total settlement is approximated by the final vertical strain at the tops of the columns due to the stresses imposed by the building plus the compression of the soils below the columns. Field tests have shown that the vertical displacement at the top of a densely packed clean stone column may be expected to range from 5-9mm. A conventional soil mechanics approach is recommended to provide a prediction of the compression of the soils beneath the reinforced ground to which is added a value of 5-9mm.

Datye and Nagaraju (1975) describe the use of load tests on small groups to predict the settlement of larger groups using the elastic solutions of Poulos (1968a) for incompressible piles. The authors have used the results of a load test on a group of 3 columns to calculate the settlement of a single pile and then predict the settlement of a group of seven columns using the Poulos solutions. The results from this approach are reproduced in Table 2.1. Thus, good agreement is obtained between the observed and estimated settlement for the large group, although the single column settlement is considerably overestimated.

2.3.3 Some Applications of the Process

Thorburn and MacVicar (1968) have described the utilisation

TABLE 2.1

SETTLEMENT OF STONE COLUMNS

(Based on Poulos Analysis)

Test on	Observed mm	Estimated mm
Single column	8 at 40 tonnes	26 at 50 tonnes
3 Column group	52 at 50t	52 (basis of estimation)
7 Column group	86 at 50t	96 at 50t

(after, Datye and Nagaraju, 1975)

of the vibro-replacement process for economic low rise housing development on gap sites in Glascow. Gap sites are those formerly occupied by buildings which have been demolished or those under-developed because of poor ground conditions. Cost comparisons revealed that piled foundations would be uneconomical. As it was essential that no damage be caused to surrounding buildings due to the vibrations of the vibroflot, a series of tests were performed to ascertain the possibility of this occurring. A Cambridge Vibrograph was mounted on a concrete slab cast on top of an external stone footing of a four storey masonry building. The results of these tests are reproduced in Table 2.2. These results suggested that the process could be used without concern for damage to nearby buildings. A study of the time-settlement behaviour of buildings founded on the stabilised soil was considered essential. The results of settlement records taken at two sites are reported. These show that the building performed satisfactorily with no surface cracks being visible.

The unexpected ineffectiveness of stone columns in reducing

TABLE 2.2

Test No.	Distance of Vibrator from concrete slab (ft)	Maximum Amplitude (ins)	Depth of Vibrator below ground surface (ft)	Stage of formation of column
1	30	1×10^{-4}	12	I
2	20	$(2 \pm 1) \times 10^{-4}$	12	I
3	15	$(2 \pm 1) \times 10^{-4}$	12	I
4	10	$(8 \pm 1) \times 10^{-4}$	12	I
5	15	$(2 \pm 1) \times 10^{-4}$	12	II
6	10	$(8 \pm 1) \times 10^{-4}$	12	II

1in = 25.4mm

Stage I: Initial penetration of vibrator

Stage II: Compacting column

(after, Thorburn and MacVicar, 1968)

the settlements of a trial embankment built on soft clay has been described by McKenna, Eyre and Wolstenholme (1975). The site for the trial embankment consisted of a uniform alluvium 27.5m in depth. The columns were constructed of crushed limestone nominally 38mm single size on a triangular grid at 2.4m spacing. They were 11.3m long and 0.9m in diameter. Comparisons between the treated and untreated ground showed that the columns had no apparent effect on the performance of the embankment; the settlement of the stone column area, in both amount and rate of settlement, was identical to that of the untreated area.

The authors postulate that the stone columns were ineffective for two reasons. Firstly, the grading of the crushed limestone was too coarse to act as a filter, and as a result the voids in the piles pro-

bably became filled with clay slurry preventing the sand drain action of the piles. Secondly, the inability of the piles to reduce settlements could have been due to the backfill being so coarse that it was not restrained by the surrounding soft soil. However, this size is within the range (20-70mm) recommended by Greenwood (1970).

Greenwood (1976) disagrees with these postulations. With the continuous water circulation while the column is being backfilled and rammed into place Greenwood suggests that water sorting of the displaced clay occurs leaving predominantly silty sand in the void spaces. Although this has a moderately low permeability it is much more permeable than the insitu clay. Secondly, regarding the displacement of the stone into the surrounding clay; three observations are cited which dispute this. A theoretical approach proposed by Raffle and Greenwood (1961) based on the Kozeny-Carman equations predict a penetration of the clay into the stone much less than that required to cause the observed volume of settlement. In addition it is noted that the lateral stresses due to the embankment are much less than those imposed by the vibroflot during column construction. Thus, the external stresses should not induce further penetration of the clay into the stone. Finally, observations of excavated columns do not support the suggestion that significant penetration of the clay occurs. Greenwood submits the alternative explanation that slight remoulding around the periphery of the column would be sufficient to allow a punching failure of the column acting as a stiff pile. The relative shearing movement would cause warping of the clay laminations which may contribute to the cesstation of drainage into the columns.

Two successful applications of the vibro-replacement process

have been reported by Rathgeb and Kutzner (1975). The first site considered was treated to increase the bearing capacity and reduce the deformability of the foundation soil for a large power station. The structural characteristics of power stations usually make deep foundations uneconomical or undesirable with the possible exception of very heavy boilers and stacks. The treatment was extended to the soil between conventional piles supporting the boilers and stacks; this increased the proportion of the pile loads taken up by friction in the upper part of the piles resulting in a reduction in the load carried by the base.

The second application has proved itself a technical and economic success. Stability analyses of an embankment resting on a very soft clay layer with organic enclosures gave factors of safety of less than unity. The vibro-replacement process was applied to the clay beneath the toe of the embankment to improve the shear strength of the clay layer. The columns can be thought of as 'shear pins'. The authors have described the use of a slip circle analysis to design the layout of the columns in which allowance is made for the variation in shear strength of the column and clay materials.

The site considered for the construction of a sewage treatment plant consisting of predominantly deep, soft cohesive soils in an area of highest seismic susceptibility is discussed by Engelhardt and Golding (1975). The results of a series of large scale field tests designed to determine the resistance of the reinforced ground to strong shaking are reported. The likelihood of liquefaction of sand lenses in the native soil was also investigated using standard penetration tests. The authors conclude that by installing stone columns sand lenses in the

cohesive subsoil are densified sufficiently with respect to their liquefaction potential and the reinforced ground developed a shear strength which could safely resist horizontal forces resulting from a ground acceleration of 0.25g while providing an adequate vertical load-settlement relationship.

Seed and Booker (1976) have also considered the use of gravel or rock drains for stabilising soil deposits susceptible to liquefaction. The one dimensional theory of pore water pressure generation and dissipation developed by Seed et al., (1975) is generalised to three dimensions and used to analyse the granular columns under a variety of earthquake conditions. The results of these analyses are summarised by a series of charts which provide a convenient basis for evaluating the possible effectiveness of a gravel drain system.

An interesting extension of the process to the treatment of unconsolidated domestic refuse or other random fill has been mentioned by Watt, de Boer and Greenwood (1967). The authors cite an example of a site in Dublin for a nest of ten fertiliser silos of total capacity 20,000 tons (20,320 tonnes). Stone columns were constructed through domestic refuse (ashes, bottles, cans, etc.) and clay fill to a depth of 24 ft. (7.32m) where firm gravel stratum was found. The silos were constructed on a reinforced concrete raft approximately 156 x 66 ft. (47.55 x 20.12m) and 4 ft. (1.22m) thick. Interim measurements, at the time of publication, showed maximum settlements of less than 1 in. (25.4mm) had occurred with the silos half full.

An adaptation of the stone column method of construction

has been described by Datye and Nagaraju (1976, 1977a) in which pre-assembled, precompressed granular columns confined in tensile reinforcing rings or spirals with longitudinal reinforcement are used to improve the load carrying capacity of the stone column. This is achieved by reducing the bulging at the top of the column where low soil strength and rigidity is commonly found due to lack of overburden pressure. Reinforcement can be reduced or eliminated in the lower portion of the column.

An advantage of this method of construction is that standard equipment normally used for sand drain installation can be employed and thus the use of special equipment such as vibroflots can be avoided. Laboratory research indicates a potential for the use of such piles as flexible load bearing piles. Also, if used at sites subjected to seismic loading, these piles help overcome the conflicting requirements of flexibility to withstand deformations induced by soil movements and stiffness to reduce settlements under vertical load. However, the results of field tests are needed to confirm these predictions.

2.3.4 Field Load Tests

Watson and Thorburn (1966) summarise the results of load tests on a 25 ft. (7.62m) square slab resting on the surface of a site before and after it has been stabilised by the vibro-replacement process. The borings showed that the site consisted of about 12 ft. (3.66m) of uncompacted fly ash material overlying superficial deposits of soft silty clays, peat and glacial till. The kentledge employed were large steel ingots placed carefully in position to give as uni-

formly distributed load as possible. The authors summarise the results of the tests thus:

(a) Untreated Natural Ground:

Total Settlement at centre of slab, loading intensity 1 ton/sq.ft. 12 in.

(b) Stone Skeletons at 7.5 ft. centres:

Total Settlement at centre of slab, loading intensity 0.5 ton/sq.ft. 1.25 in.

Total Settlement at centre of slab, loading intensity 1 ton/sq.ft. 4.375 in.

1 in. = 25.4 mm

1 ton/sq.ft. = 107.252 kN/m^2

The results of three 24 in. (.61m) diameter plate loading tests are also reported in which the constant rate of penetration method was employed. Two tests were performed before stabilisation. The test after stabilisation was performed midway between stone columns spaced at 7 ft. 6 in. (2.29m) centres in a triangular pattern. The load-settlement curves from these tests are reproduced in Fig. 2.10. These tests verify the substantial improvement in the load-settlement behaviour of ground stabilised by the vibro-replacement process.

Results of loading tests on completed storage tanks at three sites are presented by Watt et al., (1967). These are considered in detail in Chapter 5. However at one site, Newport (England), which consisted of 30 ft. (9.14m) of natural soft clays overlying firm clays and marls, a reinforced concrete test plate 15 ft. (4.57m) square was loaded to failure. Granular columns were installed in two areas in a triangular grid at 4.5 ft. (1.37m) and 6.5 ft. (1.98m) spacings res-

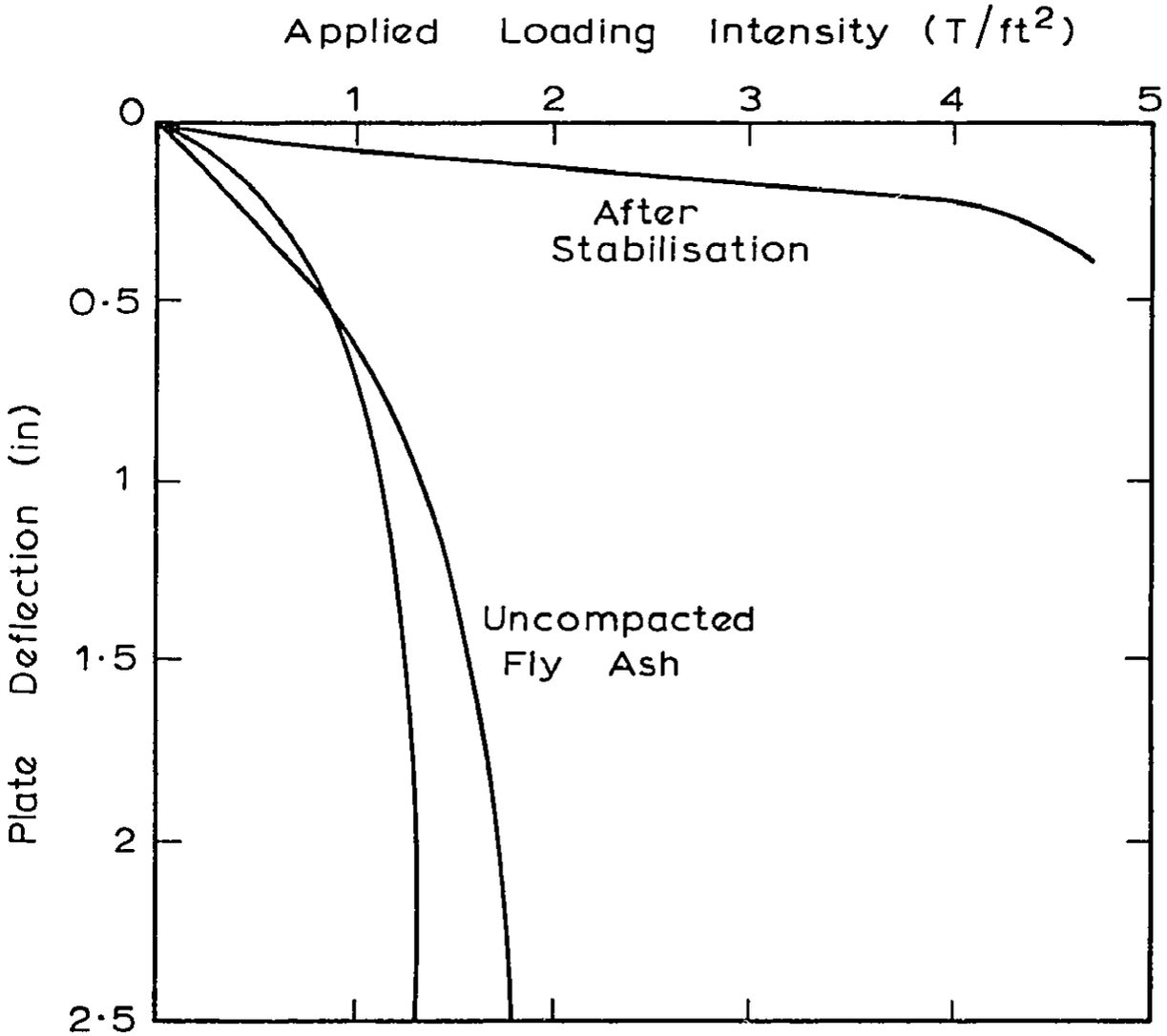

FIG. 2·10 RESULTS OF PLATE LOADING TESTS
(After Watson and Thorburn, 1966) 1in = 2·54cm
1 T / ft² = 107·25 kN/m²

pectively. Columns were taken into the firm clay to a depth of approximately 35 ft. (10.67m). A carpet of slag 3 ft. (.91m) thick was rolled in layers over the site. The test plate was loaded in these two areas in increments of 0.25 tons/sq.ft. (26.81 kN/m^2) per day. The results are reproduced in Fig. 2.11. These indicate a marked improvement in the bearing capacity of the stabilised ground with closer spacing of the piles.

Baumann and Bauer (1974) discuss the results of four footing load tests carried out at a site for a student residence in Konstanz, Germany. Three bore logs revealed that immediately below ground surface sandy silt with some organic content was encountered below which a layer of silty gravelly sand followed with a maximum thickness of 1.7m. A varved marine clay deposit followed to a depth of 40m below ground surface. Vibro-replacement was considered 40% cheaper than the most economical pile foundation. A fill was placed over the site and mechanical improvement to an average depth of 5.5m was undertaken.

The loading tests were carried out under drained conditions; the load being kept constant until the settlement had ceased. The first test was performed on the marine clay before stabilisation. The remaining three tests were carried out after stabilisation. The second footing was placed on the surface of the fill material, the third on the marine clay at the same elevation as the first test. The fourth footing was located on the organic sandy silt. The footings were placed on the surfaces of the deposits, that is, they were not embedded. At approximately half the ultimate bearing capacity the load was reduced to zero and then increased to failure. The layout of the footing tests is shown in Fig. 2.12. The results are reproduced in Fig. 2.13. Al-

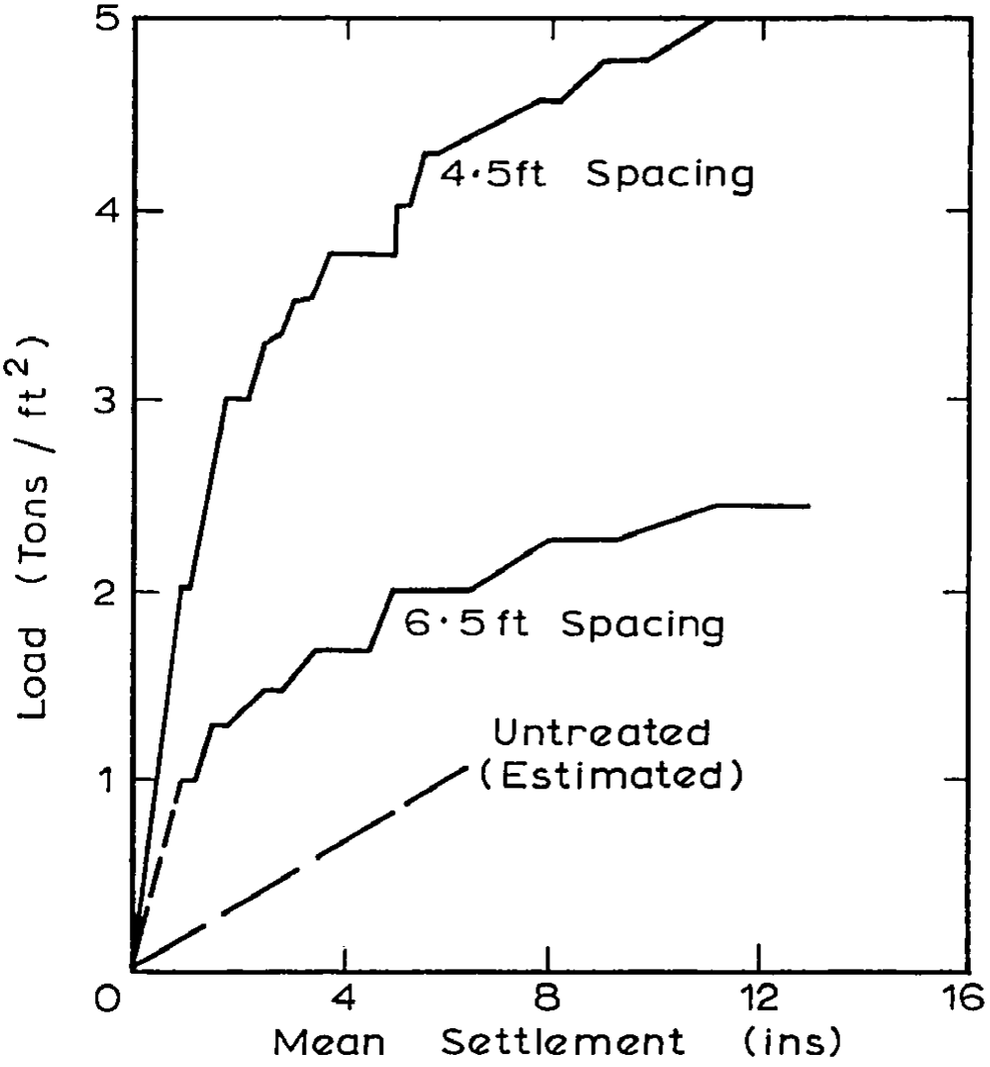

FIG. 2·11 LOAD TEST AT NEWPORT
(After Watt et al, 1967) 1 T/ft² = 107·252 kN/m²
1 in = 2·54 cm

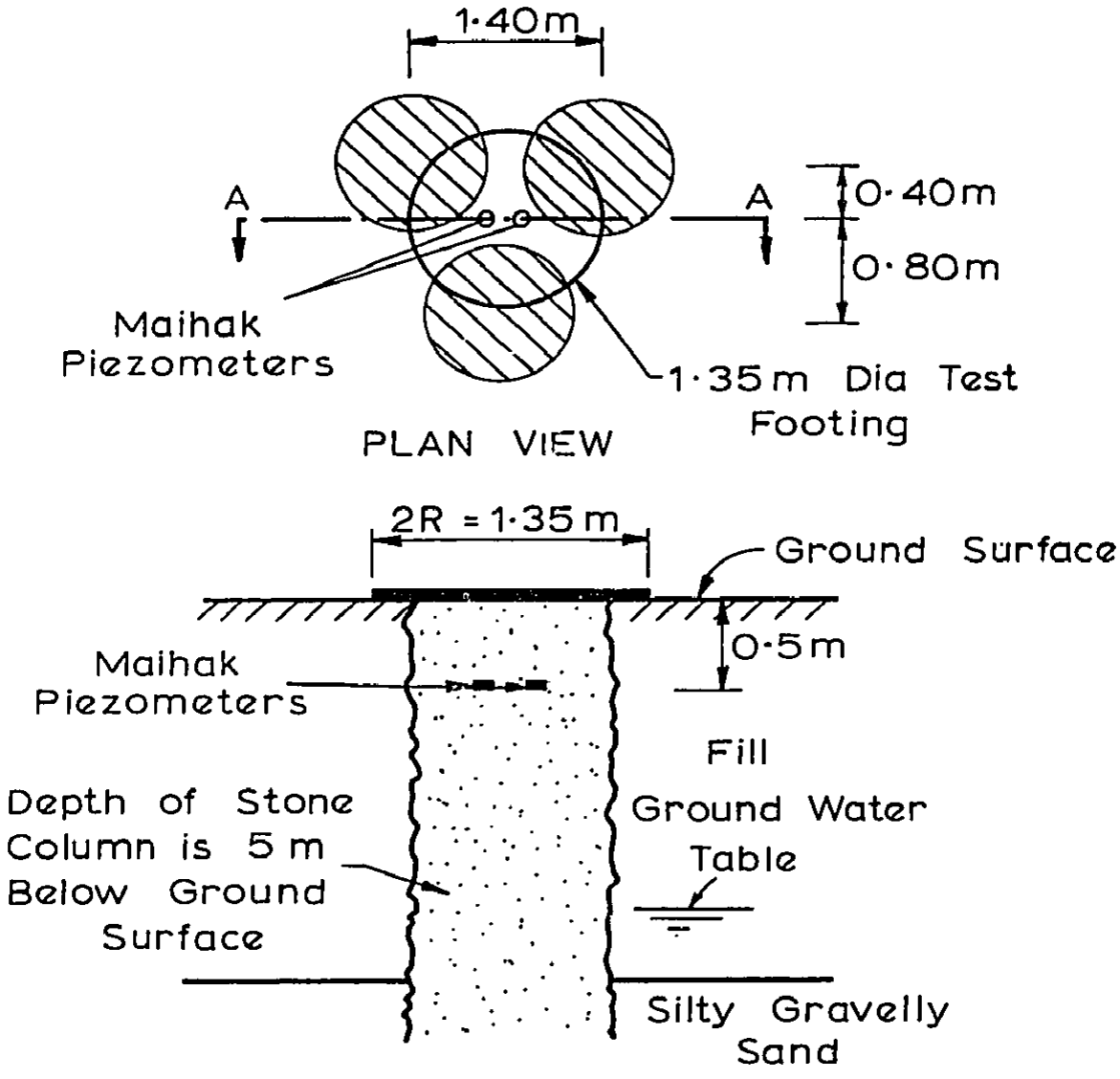

FIG. 2·12 LAYOUT OF FOOTING LOAD TEST
(After Baumann and Bauer, 1974)

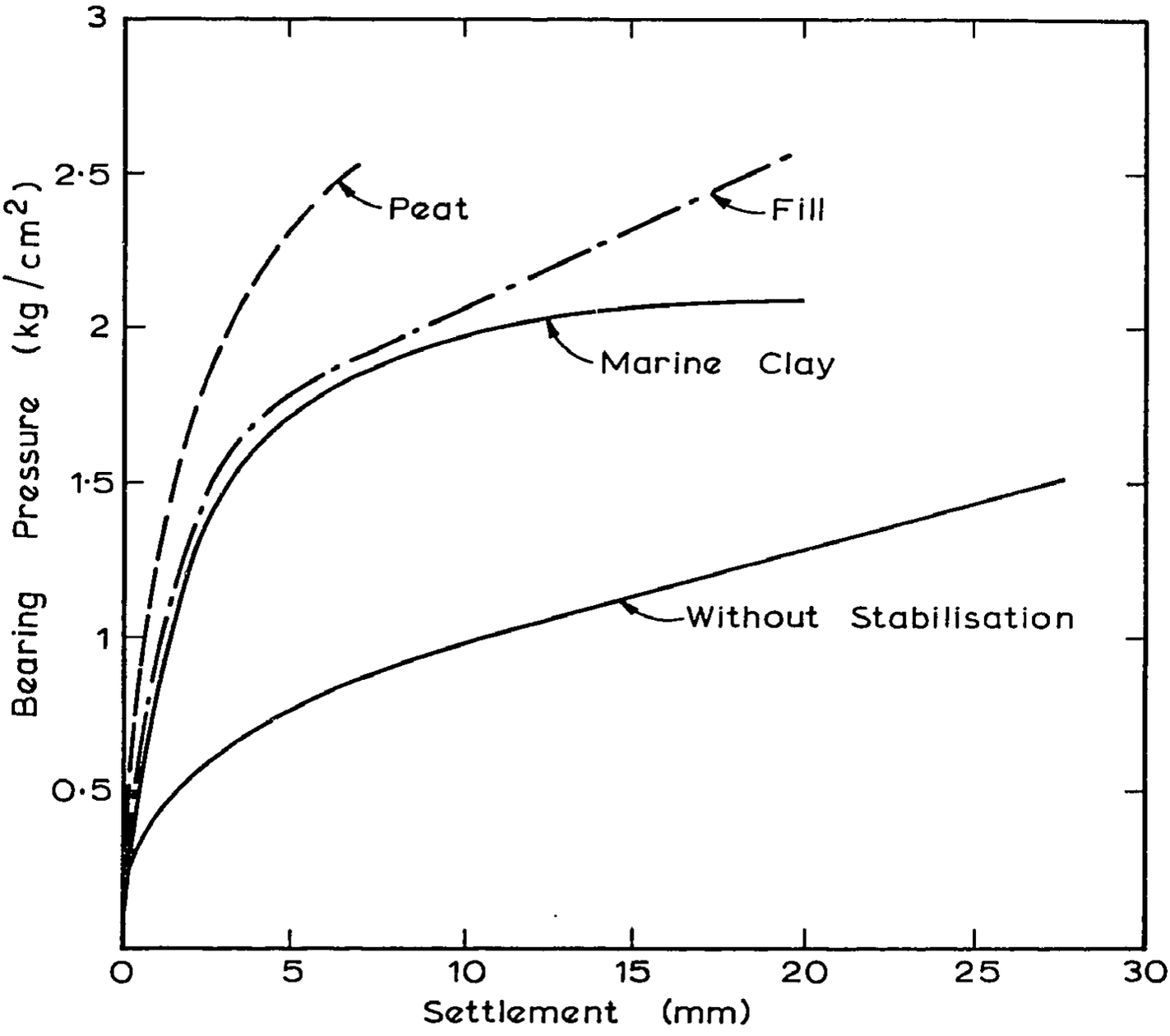

FIG. 2·13 RESULTS OF LOAD TESTS
(After Baumann and Bauer, 1974)

though the bearing capacity of an isolated footing resting on the stabilised ground is not significantly improved, the settlements are reduced markedly.

In the third test two Maihak vibrating-wire piezometers were installed 50 cm. below the test footing and between the granular columns as shown in Fig. 2.12. The average excess pore pressures measured by these two piezometers is plotted in Fig. 2.14. These results verify that the rapid dissipation of excess pore water pressures envisaged due to a sand drain action of the columns is valid. However, the authors note that the rate of dissipation in the underlying untreated zone was not measured and will be somewhat slower than in the treated zone.

In addition, settlement records for the student residence over a 2.5 year period after completion of construction are presented. Settlement records over a seven year period for similar high rise buildings founded on the stabilised soil indicated a total settlement of 15-20cm and differential settlements of the order of 10cm would be expected if vibro-replacement was not undertaken. The expected rate of settlement behaviour would be as follows; 30% of the total settlement completed at the end of the construction period, 50% after 1 year and 90% after 4 years with no further settlement being observed after seven years. The stabilised ground on which the student residence was constructed compressed 6.5cm; 5cm taking place during the construction period. The marine clay underlying the columns compressed by 1.6cm at the end of the construction period with an additional 1.4cm after 2.5 years. Therefore, the total settlement of the site was about 10cm. The maximum differential settlements were approximately 3cm. This

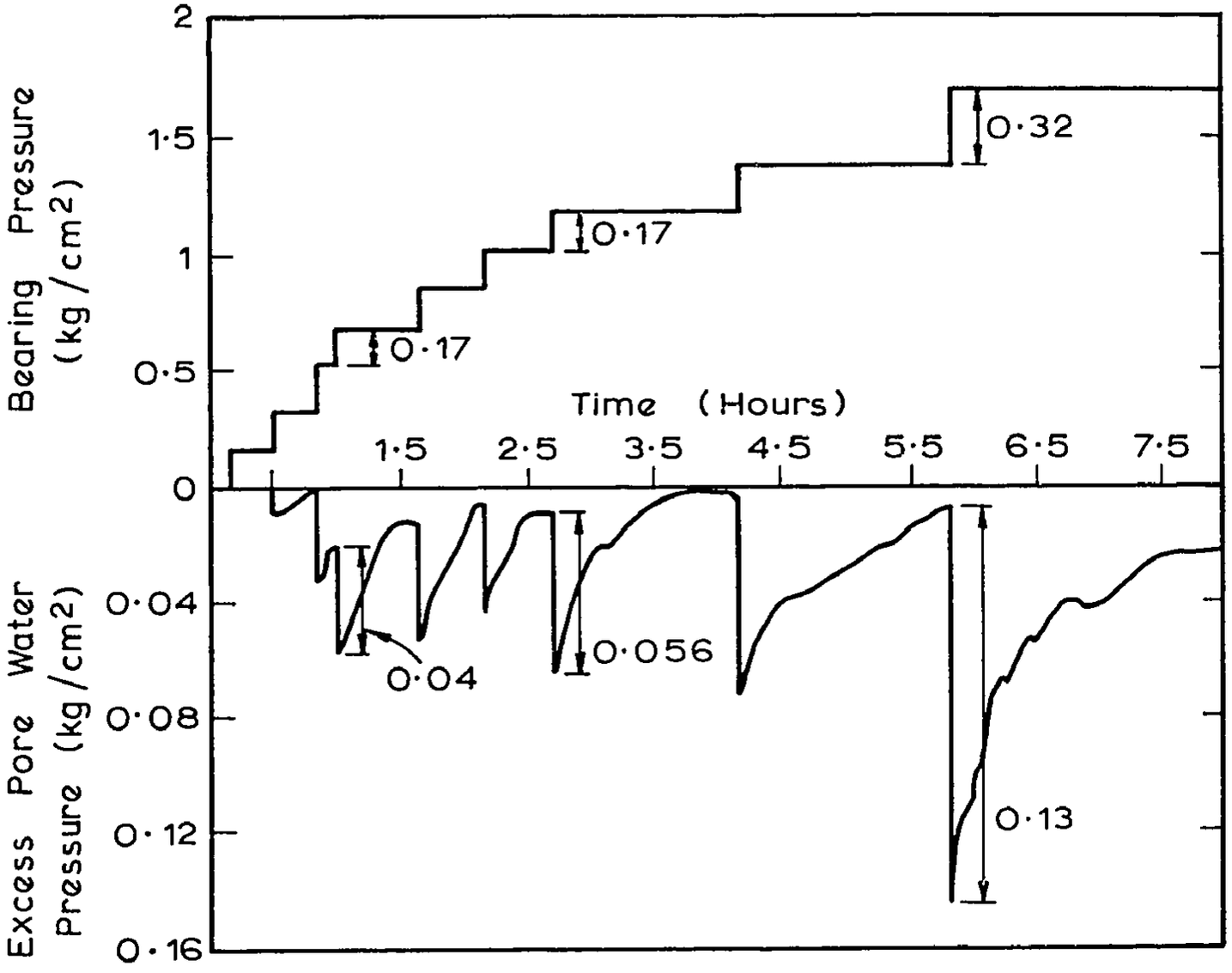

FIG. 2·14 RATE OF DISSIPATION OF EXCESS PORE PRESSURE UNDER TEST FOOTING (After Baumann and Bauer, 1974)

experimental programme has verified the predicted improvement in the load-settlement behaviour of the reinforced ground. The settlement characteristics of the site were improved considerably due to stabilisation, especially when the differential settlements and the rate of settlement are considered.

Hughes et al., (1975) have reported in detail the results of a field loading test on an isolated column. A thousand similar columns were installed, at the site of the test, for the foundations of two 31m diameter oil storage tanks. The test was conducted to verify the theory proposed by Hughes and Withers (1974) which has been reviewed in Section 2.3.1.

The column strength was predicted using the lowest value of measured passive restraint over the critical length of the column; the minimum length where a bulging failure of the pile and a base failure occur simultaneously. An angle of internal friction of 38° was assumed for the column. The column was loaded by a concentric circular plate marginally smaller than the top of the column. The test was completed in half an hour and thus was assumed to be under undrained conditions. The ultimate load appeared to be 30% higher than the theory predicted with the column being much stiffer than expected. After examination of the test column the initial assumed diameter was considered too small. The authors note that the predicted load for a given failure stress varies as the square of the diameter, emphasising the importance of an accurate initial estimate. When the settlement and failure load were recalculated using a better estimate of the actual diameter of the column and allowing for shear transfer along the column-clay interface, very close agreement between the predictions

and the results of the field tests were obtained.

The authors conclude that the close agreement indicates that the shear transfer assumed along the column-clay interface is valid. The authors note that the value of the Cambridge type pressuremeters is demonstrated and suggest that

> "the column load-settlement relationship cannot be established without the radial stress-deformation data from a Cambridge type pressuremeter."

Having now reviewed much of the relevant literature concerning the vibro-replacement process, the following chapters will endeavour to present rational methods of analysis for single isolated columns, small groups of columns and large arrays of stone columns. These methods will be applied to some problems of interest. Some of the material reviewed in this chapter will again be referred to in the following chapters.

CHAPTER THREE

FINITE ELEMENT ANALYSES

3.1 INTRODUCTION

In order to investigate the factors which influence the load-settlement behaviour of granular piles, the method of analysis must take account of the modes of failure within the pile-soil system. The pile's load carrying capacity generally decreases as the rate of load application increases, with a minimum value occurring when the load is applied rapidly enough to cause the soil to deform under undrained conditions. The three modes of failure most likely to occur in the granular pile-soil system for this condition are

(a) interface slip between the granular pile and soil

(b) failure under undrained conditions within the soil mass

(c) failure under drained conditions within the granular pile.

As the deformation moduli and strength properties within the pile and soil masses are likely to be non-homogeneous, an analytical solution is only possible if radical simplifications are made. The finite element method offers itself as the most convenient numerical method of solution to this problem. In this chapter two finite element analyses for predicting the load settlement behaviour of a single pile are described. Both analyses overcome the need to introduce special joint elements at the pile-soil interface (Ellison et al., 1971; Goodman et al., 1968) when considering pile-soil slip.

The first analysis treats the pile and soil as separated bodies, equilibrium and displacement compatability at the pile-soil interface is then imposed to obtain a solution for the settlement of the pile. This analysis takes account of only the first two modes

of failure with a simple bi-linear model being adopted for the stress-strain relationship for the soil. Therefore, it is presented as a method for analysing a single conventional pile where slip is the dominant mechanism of failure. The effects of installation of a conventional pile on its load-settlement behaviour has been investigated (Balaam et al., 1975) using this analysis. This analysis can be extended to take account of failure within the pile with both the pile and soil being treated as elasto-plastic materials. However, as a tangent stiffness approach is used, this analysis would become computationally inefficient.

Therefore, a second analysis was developed in which an initial stress approach is used and the necessity of separating the pile and soil to analyse slip at the interface is avoided. The pile and soil are treated as elasto-plastic materials which do not necessarily obey an associated flow law. The soil is taken to be purely cohesive whereas the pile is assumed to be a purely frictional dilatant material. Dual nodes are introduced into the finite element mesh along the pile-soil interface so that the possibility of slip can be incorporated into the elasto-plastic formulation. The pile-soil interface is initially considered to have a finite adhesive strength. The analysis is then extended to take account of a dilatant interface whose strength is either adhesive-frictional or purely fr[illegible].

Finally, a numerical scheme is described which enables finite element analyses to be performed in a manner which is more economical in terms of computer storage and time. The results of an investigation into the relative merits of isoparametric and constant

strain triangular finite elements for elastic and elasto-plastic axisymmetric analyses are also presented.

3.2 FINITE ELEMENT ANALYSIS OF A SINGLE CONVENTIONAL PILE

In this section a finite element analysis is presented for a single pile in which slip at the pile-soil interface and yield within the soil mass is taken into account. A purely adhesive interface strength is assumed and a simple bi-linear model adopted for the stress-strain relationship for the soil. The bi-linear model is considered sufficiently sophisticated for the analysis of conventional piles as slip at the interface is the dominant mechanism of failure with only a relatively small bulb of soil yielding around the pile. The pile is treated as a linearly elastic material throughout the range of applied load.

3.2.1 Elastic Analysis

An axially loaded floating pile of length L, diameter d and cross-sectional area A_p is considered. The soil and pile are assumed to be ideal elastic materials with Young's moduli and Poisson's ratios E_s, ν_s and E_p, ν_p respectively. The soil and pile are treated as separate bodies as shown in Fig. 3.1. The nodes at the pile-soil interface exert normal and tangential forces upon each other (except for the node at the centre of the base where only a vertical force is assumed to exist).

The interface nodal deflections for the soil $\{\rho_s\}$ may be expressed as

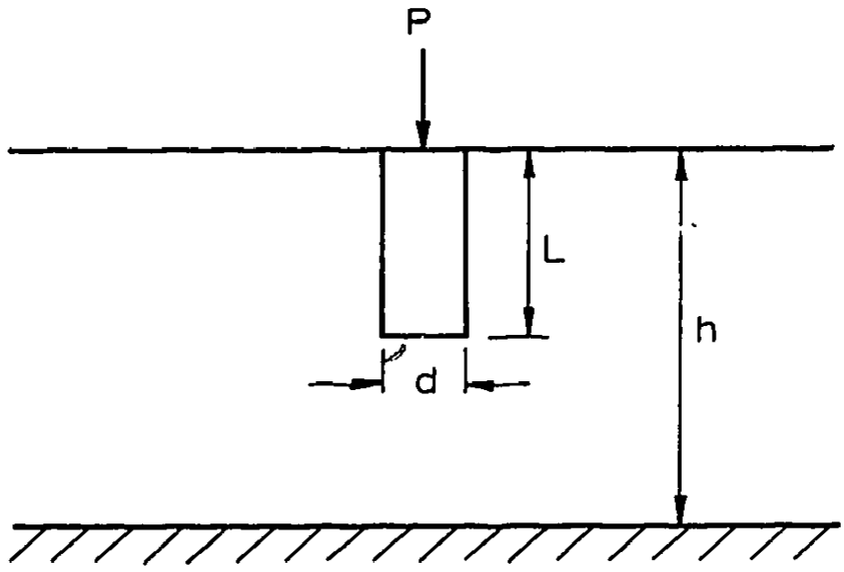

(a) Definition of Pile Geometry

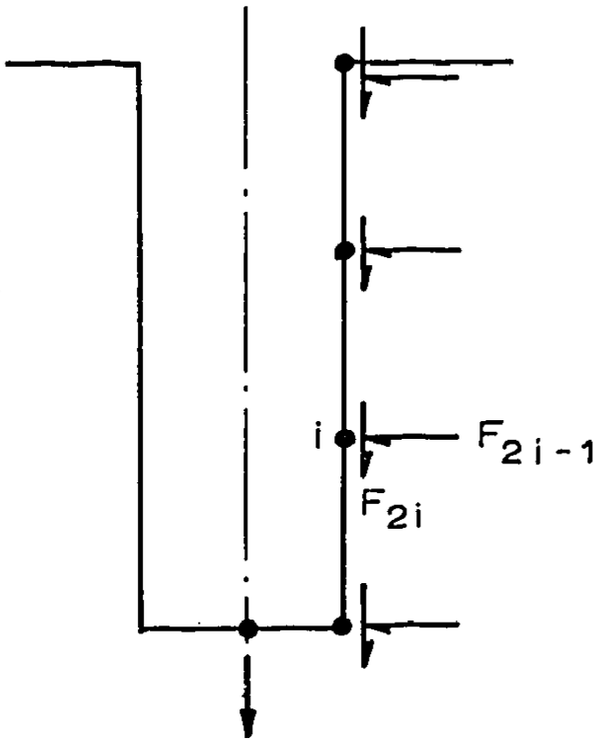

(b) Nodal Forces on Soil

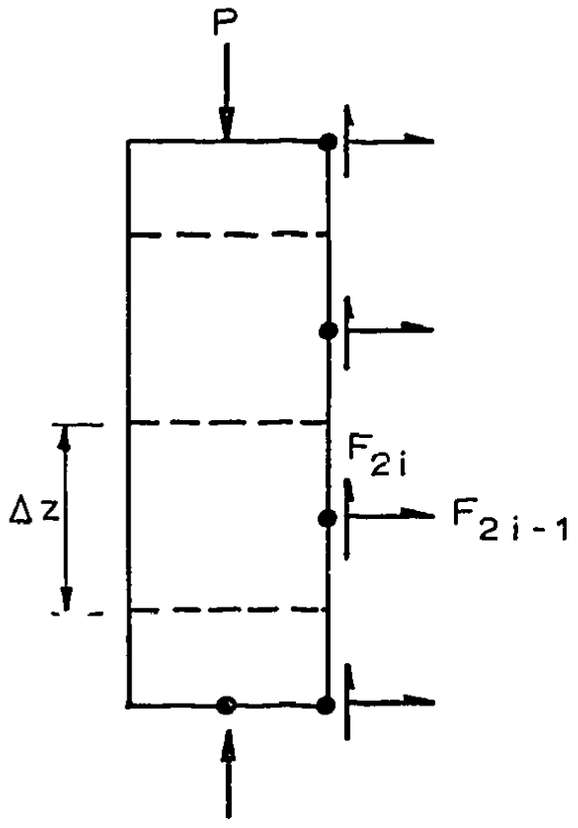

(c) Nodal Forces on Pile

FIG. 3.1

$$\{\rho_s\} = [I_s]\{F\} \qquad (3.1)$$

where $[I_s]$ = elastic displacement influence matrix

$\{F\}$ = the vector of nodal forces at the interface

The matrix $[I_s]$ is generated by repetitive solution of the finite element equation

$$[K_s]\{\delta_s\} = -\{t\} \qquad (3.2)$$

where $[K_s]$ = soil stiffness matrix

$\{\delta_s\}$ = vector of soil displacements throughout the finite element mesh

$\{t\}$ = load vector containing zeros except for a unit force applied at the node and in the direction corresponding to the degree of freedom being considered.

The same procedure is repeated for the pile although a modification is necessary as the pile stiffness matrix $[K_p]$ is singular. This singularity occurs because when the pile is considered separate from the soil there is no vertical boundary restraint and so the deflections of the pile can only be determined to within an arbitrary vertical displacement. To overcome this difficulty the value of the vertical deflection at an interior node of the pile is specified. The value of this deflection is later determined from the condition of equilibrium (ie. no nodal force induced at this node) and compatibility at the pile-soil interface. The relevant nodal deflections for the pile may be written as

$$\{\rho_p\} = [I_p]\{F'\} \tag{3.3}$$

where $\{\rho_p\}$ = vector of pile displacements comprising the displacements at the pile-soil interface and the displacement at the node loaded by the point load P

$\{F'\}$ = modified nodal force vector with the addition of the point load P and the prescribed displacement Δ_o at an interior node of the pile.

The matrix $[I_p]$ is generated in the same manner as $[I_s]$, the relevant equation being

$$[K_p]\{\delta_p\} = \{g\} - \Delta_o\{p\} \tag{3.4}$$

where $\{\delta_p\}$ = pile displacements throughout the finite element mesh

$\{g\}$ = load vector corresponding to a unit nodal force applied at the node loaded by the point load P or along the pile-soil interface in the direction corresponding to the degree of freedom being considered

$\{p\}$ = the column of $[K_p]$ corresponding to the node with the prescribed displacement Δ_o

Equation 3.1 can be rewritten in terms of the modified nodal force vector $\{F'\}$ thus

$$\{\rho_s'\} = [I_s'] \{F'\} \tag{3.5}$$

where $[I_s']$ is the augmented soil influence matrix, obtained by adding a row and two columns of zeros to $[I_s]$ and $\{\rho_s'\}$ is the augmented soil displacement vector obtained by adding the displacement under the point load P.

The relative slip between the pile and soil may be expressed as

$$[I_p - I_s'] \{F'\} = \{\rho_{rs}\} \tag{3.6}$$

where $\{\rho_{rs}\}$ = vector of relative slip of the pile and soil. As $\{\rho_{rs}\}$ is zero for the elastic analysis, compatibility at the pile-soil interface is imposed when

$$[I_p - I_s'] \{F'\} = \{\underline{0}\} \tag{3.7}$$

Using the equilibrium condition

$$\sum_{j=1}^{n} F_{2j} = P \tag{3.8}$$

where n is the number of nodes along the pile-soil interface; a vector of nodal forces $\{F\}$ and the unknown displacement Δ_o may be obtained for a unit applied load P. Thus the displacements within the soil and pile masses may be found by solution of equations 3.2 and 3.4, where the load vectors $\{t\}$ and $\{g\}$ now comprise the actual nodal forces acting at the pile-soil interface.

This formulation in terms of the nodal forces at the pile-soil interface offers several advantages over a conventional analysis

in which the pile and soil are analysed together in a single finite element analysis. Firstly, since the pile and soil are treated separately it is not necessary to treat elements of vastly different stiffnesses in the one finite element analysis, and this greatly reduces the risk of serious round-off error in the solution process. Secondly, for a given geometry, $[I_p]/E_p$, $[I_s]/E_s$ depend only on ν_p, ν_s respectively and thus these influence factors may be used to obtain the solution for any ratio of E_p/E_s. Finally, and most importantly; having formulated the elastic analysis in terms of the nodal forces at the pile-soil interface, the analysis of the pile-soil slip can be developed without need to introduce a special joint element at the interface. It should be emphasised at this point that except for these computational advantages the method is entirely equivalent to a conventional finite element analysis and the solutions obtained by this elastic analysis will be precisely the same except for roundoff.

For a pile in a homogeneous soil layer, comparisons have been carried out between solutions obtained from the above finite element analysis and those obtained using the method described by Mattes and Poulos (1969). In the finite element analysis, the pile was divided vertically into five layers with each layer consisting of four constant strain triangular elements while the soil was divided into 160 elements. The outer boundary was located at 35 pile diameters from the pile axis and assumed to be stress free. The pile was taken to have a dimensionless length L/d = 10 Poisson's ratio $\nu_p = 0.3$ and $E_p/E_s = 1000$ and was situated in a homogeneous soil layer of depth h = 2L and Poisson's ratio $\nu_s = 0.48$, underlain by a rough rigid base. The elastic solution for deflection of the pile

head given by the finite element analysis was found to be 2% less than the value given by Mattes and Poulos. Moving the boundary into 10 diameters from the pile axis (but still using the same number of elements) increased the discrepancy to 3.5%. Decreasing the number of elements in the pile to 10 and the soil elements to 120, but retaining the free boundary at 35 pile diameters, gave a pile head settlement 3.6% less than the Mattes and Poulos value. In addition, a comparison between the present finite element analysis and a corresponding conventional elastic finite element analysis, showed almost exact agreement between the two solutions. This suggests that both the finite element analysis or the analysis of Mattes and Poulos can be used with confidence to compute the settlement of a single pile.

3.2.2 Analysis Taking Slip Between the Pile and Soil into Account

The elastic analysis is valid only while the shear stresses developed along the pile-soil interface are less than the finite adhesive strength between the two bodies, c_a. As the load P is increased, the tangential nodal forces increase linearly until the most heavily loaded node reaches its limiting value. When pile-soil slip occurs at a node, if the interface strength is assumed to be purely adhesive, it can support no further increase in load and any additional load is supported by the remaining elastic nodes. Referring to Fig. 3.1(b) the tangential nodal force at the ith node has a maximum value of

$$F_{2i(max)} = \pi d \, \Delta z \, c_a \qquad (3.9)$$

The applied load at which each node reaches its limiting

value is evaluated by an incremental solution of equation 3.6 which may be written as

$$[I_p - I_s'] \{\Delta F'\} = \{\Delta \rho_{rs}\} \tag{3.10}$$

Thus, for all elastic nodes $\Delta \rho_{rs_{2i}} = 0$ while for those nodes that have slipped $\Delta F'_{2i} = 0$. Load is applied until the forces at all nodes including the base nodes have reached their limiting values. In this analysis, it is assumed that base failure will occur for a purely cohesive soil with cohesion c_u, when

$$\sum_{i=1}^{m} F_{bi} = A_p . c_u . N_c \tag{3.11}$$

where m is the number of nodes along the base and N_c is the bearing capacity factor used here to be 9. The ultimate load P_u of the pile is then given by

$$P_u = A_p . N_c . c_u + \pi d L c_a \tag{3.12}$$

The analysis of pile-soil slip developed in this section differs from one in which special joint elements are used, in that it substitutes the solution of the relatively small set of equations 3.10 for a complete finite element analysis of the pile-joint-soil system.

3.2.3 Modified Analysis to Take Soil Failure into Account

The analysis presented in the previous section describing the load-settlement relationship for the pile does not allow for the development of yielding within the soil mass. Therefore, throughout

the range of applied load it is assumed that the soil and pile are linearly elastic materials. In this modified analysis the non-linear behaviour of the soil is taken into account. Furthermore, in this analysis the ultimate base load is not specified as in equation 3.11.

Failure within the soil mass is defined by the Tresca yield criterion which may be written as

$$\frac{\sigma_1 - \sigma_3}{2} = c_u \qquad (3.13)$$

where σ_1, σ_3 are the major and minor principal stresses within a soil element and c_u is the shear strength.

A simple bi-linear model is adopted as the stress-strain relationship for the soil. D'Appolonia and Lambe (1970) used this model to study the load deformation behaviour of structures on clay. In this model, yielded elements are assumed to have a reduced modulus E_y which is related to the linear elastic modulus E_s. A convenient reduction is

$$E_y = .01\ E_s \qquad (3.14)$$

When an element yields the reduction in Young's modulus results in the Bulk modulus K_B being reduced also, where

$$K_B = \frac{E}{3(1-2\nu)} \qquad (3.15)$$

and E, ν are the Young's modulus and Poisson's ratio. However, if the

elasticity matrix is written in terms of the Shear and Bulk moduli (Appendix 3A), when an element yields the Bulk modulus can be kept constant but the Shear modulus reduced. This approach has been suggested by Christian (1971). In the analysis of conventional piles the number of elements which yield is small in comparison to the total number of elements used to represent the continuum. Where large numbers of elements yield as is the case for surface footings, such procedures may be employed to model the compressibility of the soil mass more closely although the treatment of the soil as an ideal elasto-plastic material may be warranted.

The loads at which the nodal forces at the pile-soil interface reach their limiting values are initially calculated by solution of equation 3.10. At each load, the incremental displacements due to the previous load increment are determined by

$$[K_s] \{\Delta\delta_s\} = -\{\Delta t\} \qquad (3.16)$$

where $\{\Delta\delta_s\}$ is the vector of incremental soil displacements, and $\{\Delta t\}$ is the vector of incremental nodal forces.

The increments in stresses are calculated for each element and the total stress state determined. If all the elements are elastic, equation 3.10 is applicable for further increments in load. If yielding occurs within the soil mass during an increment in load, a new displacement influence matrix $[I_s"]$ is assembled. $[I_s"]$ is generated by repetitive solution of the equation

$$[K_s'] \{\delta_s\} = -\{t\} \qquad (3.17)$$

where the vectors $\{\delta_s\}$ and $\{t\}$ are defined in the same way as for equation 3.2 and where $[K_s']$ is the new soil stiffness matrix for the soil mass with the zones of local yield.

The loads at which the remaining nodal forces reach their limiting values are now calculated by solution of

$$[I_p - I_s''] \{\Delta F'\} = \{\Delta \rho_{rs}\} \quad (3.18)$$

The incremental displacements within the soil mass are calculated from

$$[K_s'] \{\Delta \delta_s\} = -\{\Delta t\} \quad (3.19)$$

If further yielding occurs a new soil stiffness matrix and influence matrix must be assembled and the equation governing the load-deflection mechanism of the pile altered.

A comparison between load-settlement curves to failure from the present analysis and that of Mattes and Poulos is given in Fig. 3.2. For this comparison, when full shaft resistance was mobilised, the load was increased to its ultimate value given by equation 3.12 and the corresponding deflection calculated. The pile was assumed to be in saturated clay, and the adhesion c_a was taken equal to the cohesion c_u.

The agreement is generally quite good, although at loads approaching failure, the settlements given by the finite element analysis are somewhat greater; however as mentioned by Mattes and Poulos, their post-slip settlements are likely to be too small since they are still based on the use of elastic theory.

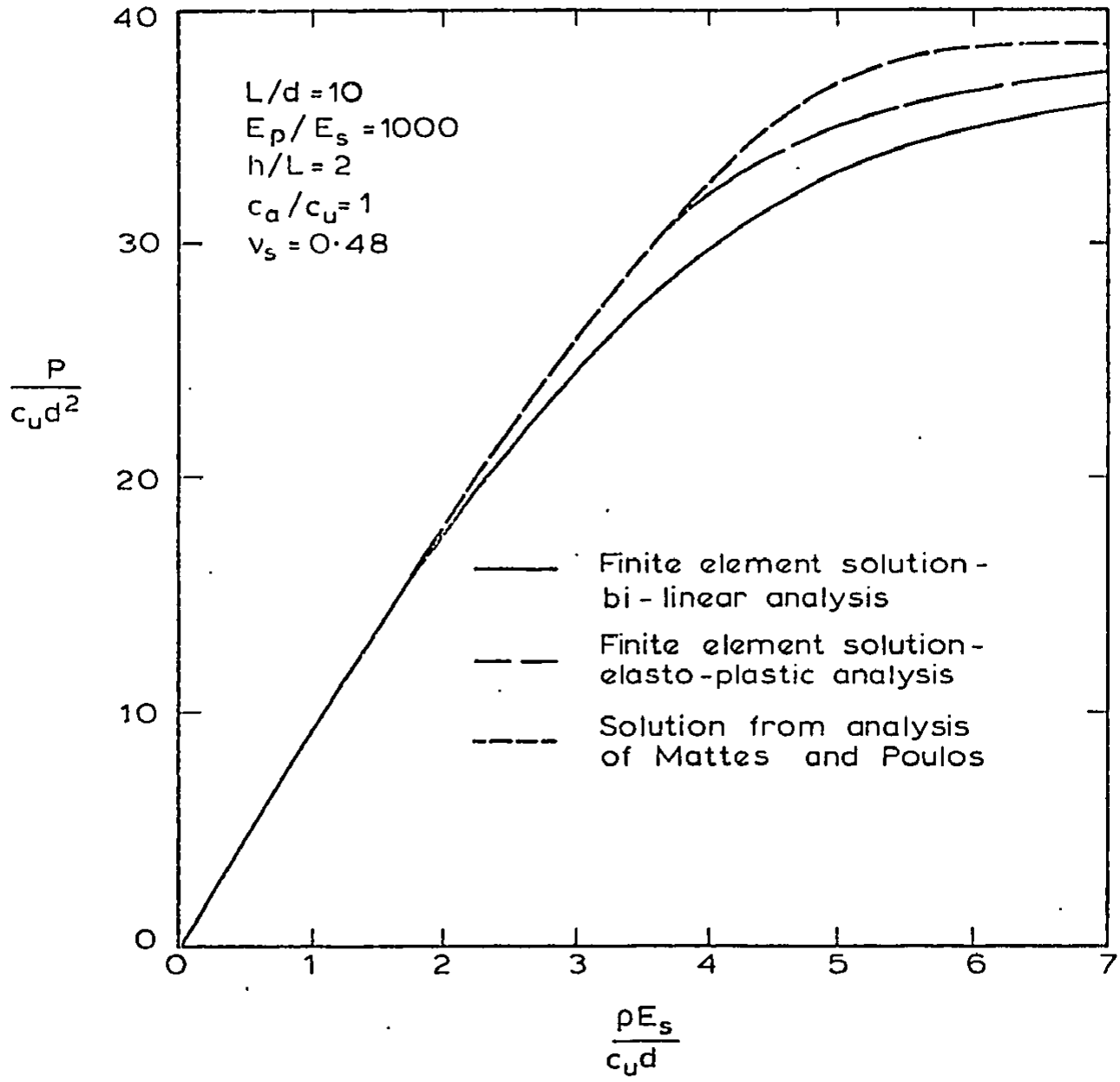

FIG. 3.2 COMPARISONS BETWEEN LOAD - SETTLEMENT CURVES TO FAILURE FOR PILE IN A HOMOGENEOUS LAYER

While the finite element analysis described above appears to be suitable for conventional piles, it becomes extremely cumbersome if extended to allow for consideration of failure within the pile itself. In addition, if a more realistic stress-strain model is adopted for the granular material constituting the pile, (e.g. elastic-plastic) in preference to a simple bi-linear or multi-linear model, then the tangent stiffness approach is computationally inefficient. For these reasons, an alternative approach is presented in which the initial stress method is used and three modes of failure are taken into account. This analysis is described in the following section.

3.3 FINITE ELEMENT ANALYSIS OF A SINGLE GRANULAR PILE

In order to predict the load-settlement behaviour of a granular pile the analysis must be capable of allowing for yield of the pile material. A finite element analysis is described in this section in which three modes of failure are taken into account

(a) slip at the pile-soil interface

(b) failure within the soil mass

(c) failure within the pile.

The pile and soil are treated as elasto-plastic materials which do not necessarily obey an associated flow law. Dual nodes are introduced into the finite element mesh along the pile-soil interface so that the possibility of slip can be incorporated into the elasto-plastic formulation. This enables an initial stress approach to be used and avoids the necessity of treating the pile and soil as separate bodies as was the case in the previous analysis. This approach has been used (Rowe et al , 1976) to analyse a variety of soil struc-

ture interaction problems. An adhesive pile-soil interface strength is initially considered and then the analysis extended to take account of a dilatant interface whose strength is either adhesive-frictional or purely frictional.

3.3.1 Elasto-Plastic Behaviour

The failure of soils under plane strain and triaxial conditions can often be described by the Coulomb failure law. There are several possible generalisations of this law to deal with three dimensional conditions; e.g. the extended Von Mises, the extended Tresca and the Mohr-Coulomb failure criteria. However, experimental evidence (Kirkpatrick, 1957) suggests that the behaviour of real soils is most closely approximated by the Mohr-Coulomb criterion.

Under three dimensional conditions it is convenient to represent the state of stress of an element by a point $(\sigma_1, \sigma_2, \sigma_3)$ in principal stress space. The yield surface for a purely frictional material obeying the Mohr-Coulomb criterion is then a hexagonal pyramid with its apex at the origin, while the yield surface for a purely cohesive material is a regular hexagonal cylinder. These yield surfaces which represent the assumed failure behaviour of the pile and soil, when the pile undergoes undrained loading, are shown in Fig. 3.3.

In general the equation of the yield surface of the material may be written in the form

$$f(\{\sigma\}) = 0 \qquad (3.20)$$

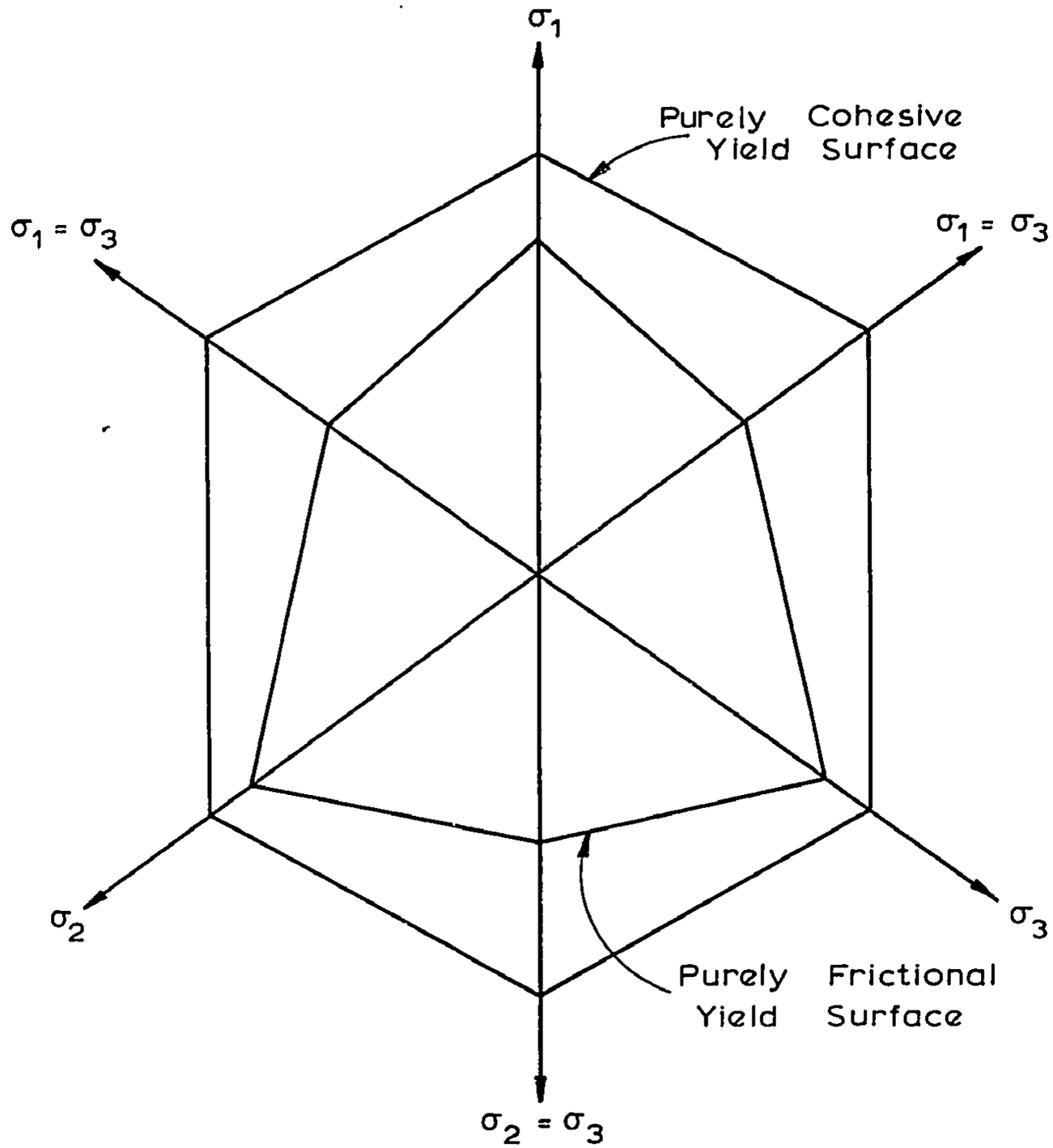

FIG. 3.3 MOHR - COULOMB FAILURE SURFACES

Thus for a cohesive frictional soil with cohesion c' and friction angle ϕ' obeying a Mohr-Coulomb yield criterion under conditions of axial symmetry the equation of the yield surface takes the form

$$\frac{\sigma_{max} + c' \cot \phi'}{\sigma_{min} + c' \cot \phi'} = N_{\phi} = \frac{1 + \sin \phi'}{1 - \sin \phi'} \tag{3.21}$$

where σ_{max}, σ_{int}, σ_{min}, are the maximum, intermediate and minimum values of the three principal stresses.

An element having a stress state lying within the yield surface will deform elastically while an element having a stress state lying on the yield surface will deform plastically. The total strain rate $\{\dot{\varepsilon}\}$ can then be thought of as consisting of an elastic component $\{\dot{\varepsilon}_E\}$ and a plastic component $\{\dot{\varepsilon}_p\}$

$$\{\dot{\varepsilon}\} = \{\dot{\varepsilon}_E\} + \{\dot{\varepsilon}_p\} \tag{3.22a}$$

$$\text{where} \quad \{\dot{\varepsilon}_E\} = [D_E]^{-1}\{\dot{\sigma}\} \tag{3.22b}$$

and $[D_E]$ is the matrix of elastic constants.

The plastic deformation of the soil is described by the flow rule of the material; in general this may be written in the form

$$\{\dot{\varepsilon}_p\} = \lambda\{a\} \tag{3.23}$$

where $\{a\}$ is a known function of the current stress state. The quantity λ is a one-signed proportionality factor indicating that no viscous effects are present and that unrestricted flow may occur under conditions

of constant stress, provided the rate of plastic work remains positive.

Many investigators have assumed an associated flow rule so that

$$\{\dot{\varepsilon}_p\} = \lambda\{b\} \tag{3.24}$$

where $$\{b\} = \partial f/\partial\{\sigma\} \tag{3.25}$$

This predicts a rate of dilatancy far greater than that found in practice except for saturated clays under undrained conditions. To overcome this difficulty, Davis (1968) has postulated a class of materials with non-associated flow rules which are characterised by a dilatancy angle ψ. Davis restricted his attention to two dimensional situations although it is possible to extend his approach to three dimensional situations. In this analysis it is assumed that

$$\frac{\dot{\varepsilon}_{min}}{\dot{\varepsilon}_{max}} = -N_\psi = -\frac{1 + \sin\psi}{1 - \sin\psi} \tag{3.26a}$$

and $$\dot{\varepsilon}_{int} = 0 \tag{3.26b}$$

where $\dot{\varepsilon}_{max}$, $\dot{\varepsilon}_{int}$, $\dot{\varepsilon}_{min}$ are the strain rates corresponding to the stresses σ_{max}, σ_{int}, σ_{min}. Thus if $\psi = \phi'$ the material has an associated flow rule and dilates at a maximum rate whereas if $\psi = 0$, the material deforms at constant volume.

3.3.2 Finite Element Analysis

The equations of the previous section can be combined (Ring,

1975) to give an incremental stress strain law

$$\{\dot{\sigma}\} = [D_{EP}]\ \{\dot{\varepsilon}\} \tag{3.27a}$$

$$\text{where}\quad [D_{EP}] = [D_E] - \frac{[D_E]\{a\}\{b\}^T[D_E]}{\{a\}^T[D_E]\{b\}} \tag{3.27b}$$

The finite element method is then used to obtain a numerical solution to a given problem. This leads to a set of equations

$$[K_{EP}]\ \{\Delta\delta\} = \{\Delta F_B\} \tag{3.28}$$

where in the usual notation

$[K_{EP}]$ = $\int [B]^T [D_{EP}]\ [B]\ d\ Vol$, the elasto-plastic stiffness matrix

$\{\Delta\delta\}$ = the increments in nodal displacements

$\{\Delta F_B\}$ = the increment in nodal forces due to the applied boundary tractions.

Equation 3.28 represents a non-linear set of equations for the unknown increments in nodal deflections. A convenient method of solving these equations is the initial stress approach (Zienkiewicz et al., 1969). Equation 3.28 is then solved iteratively using the following scheme

$$[K_E]\ \{\Delta\delta^{(n+1)}\} = \{\Delta F_B\} + [K_c^{(n)}]\ \{\Delta\delta^{(n)}\} \tag{3.29a}$$

where $[K_E]$ is the elastic stiffness matrix and

$$[K_c] = [K_E] - [K_{EP}] \tag{3.29b}$$

and the superscript n indicates the 'nth' approximation.

3.3.3 Analysis Taking Account of Slip

In order to incorporate the possibility of slip into the elasto-plastic formulation, dual nodes are introduced along the pile-soil interface as shown in Fig. 3.4 and it is assumed that there is a finite adhesive strength between the two bodies, c_a.

Initially, the increments in nodal forces at a dual node were evaluated by incorporating springs between these nodes in both the vertical and horizontal directions. This is analogous to the introduction of special joint elements at the pile-soil interface. These springs are assigned stiffnesses K_V and K_H respectively. Referring to Fig. 3.5, the increments in nodal forces is given by

$$\begin{bmatrix} \Delta F_{N1} \\ \Delta F_{N2} \\ \Delta F_{T1} \\ \Delta F_{T2} \end{bmatrix} = \begin{bmatrix} K_H & -K_H & 0 & 0 \\ -K_H & K_H & 0 & 0 \\ 0 & 0 & K_V & -K_V \\ 0 & 0 & -K_V & K_V \end{bmatrix} \begin{bmatrix} \Delta u_{N1} \\ \Delta u_{N2} \\ \Delta u_{V1} \\ \Delta u_{V2} \end{bmatrix} \qquad (3.30a)$$

where the terms in this equation are defined in Fig. 3.5. This can be rewritten as

$$\{\Delta F\}_s = [k_s]\ \{\Delta u\}_s \qquad (3.30b)$$

Displacement compatibility at the pile-soil interface is imposed by assigning the springs very large stiffnesses. These stiffness matrices for the springs are added to the stiffness matrix $[K_E]$ which is assembled

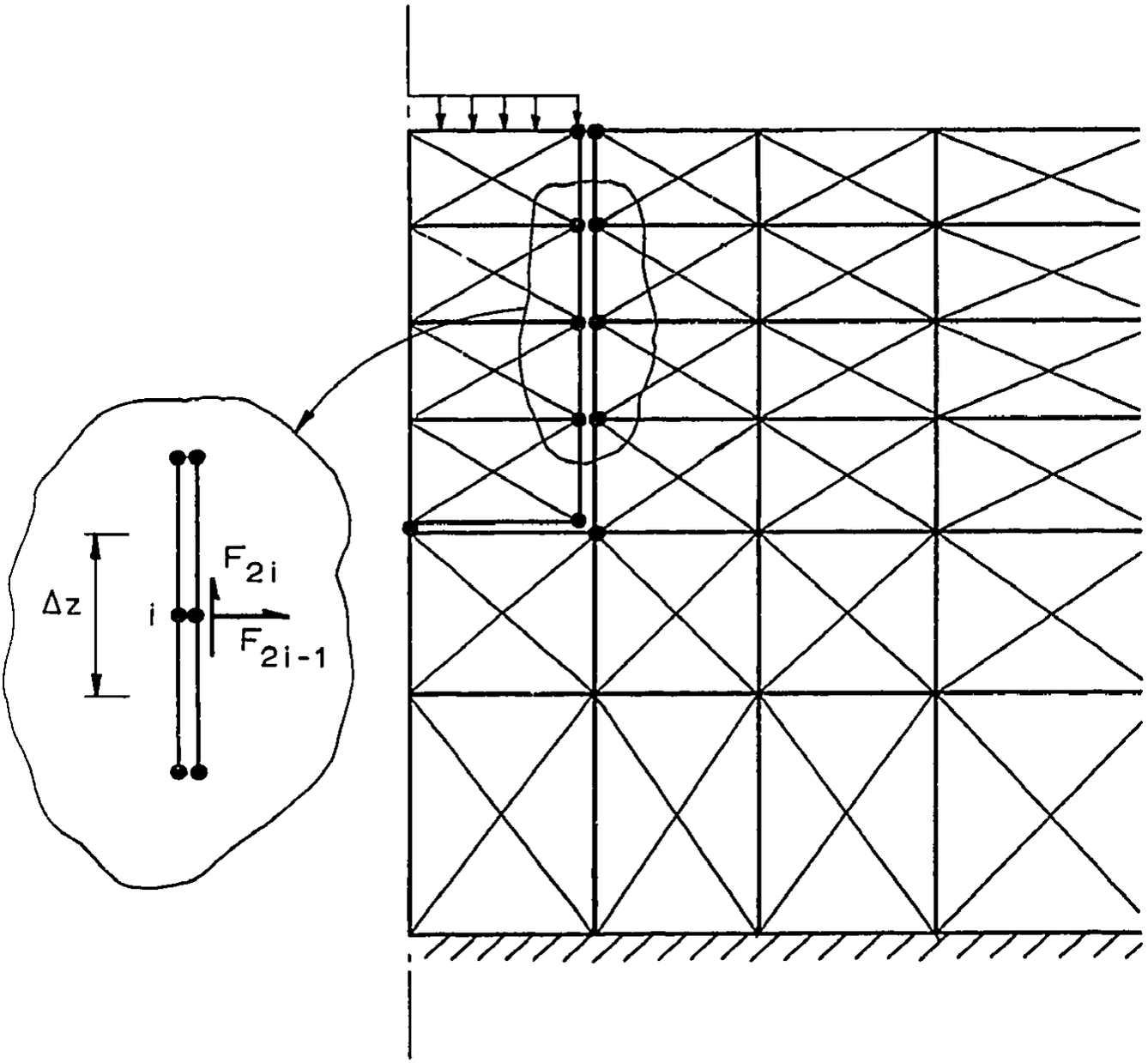

FIG. 3.4 DUAL NODES IN FINITE ELEMENT MESH

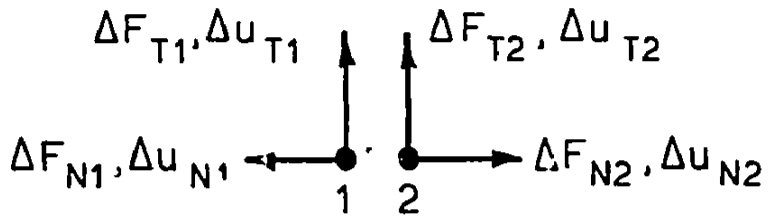

(a) Definition of Incremental Forces and Deflections at a Dual Node

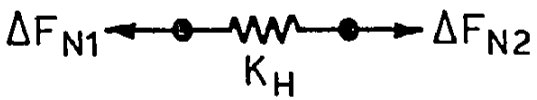

(b) Horizontal Springs

(c) Vertical Springs

FIG. 3.5 INCORPORATION OF SPRINGS AT A DUAL NODE

with the dual nodes included in the mesh, ie.

$$[K_{DN}] = [K_E] + \sum_{i=1}^{N_d} [k_s] \tag{3.31}$$

where $[K_{DN}]$ = stiffness matrix for the continuum with springs at the dual nodes included in the mesh

N_d = the number of dual nodes included in the mesh.

The solution for the purely elastic case can be written in the form

$$[K_{DN}] \{\Delta\delta\} = \{\Delta F_E\} \tag{3.32}$$

where $\{\Delta\delta\}$ = increment in nodal displacements throughout the mesh

$\{\Delta F_E\}$ = increment in nodal forces due to the external applied load.

The increments in nodal forces at a dual node are evaluated by solution of equations 3.30. The solution procedure continues until an increment in applied load results in an increment in nodal force at a dual node ΔF_{DN_i} exceeding the allowable value ΔF_{DN_a}. When this occurs equation 3.32 is resolved so that

$$\Delta F_{DN_i} = \Delta F_{DN_a} \tag{3.33}$$

When using the initial stress approach this modification takes the form of a correction added to the right hand side of equation 3.32. Equation 3.32 is replaced by

$$[K_{DN}] \{\Delta\delta\} = \{\Delta F_E\} + \{\Delta c\} \tag{3.34}$$

where $\{\Delta c\}$ = vector of corrections.

It was found extremely difficult to obtain a convergent solution to this set of equations and thus a "variable stiffness" technique in which the stiffness matrix is reassembled when slip occurs would need to be employed. To overcome this an alternative approach is described below. This analysis resembles the use of springs in that the dual nodes are retained at the pile-soil interface. However, it differs in that the nodal forces at these dual nodes $\{\Delta F_{DN}\}$, rather than their deflections, are treated as unknowns.

The solution for the purely elastic case can be written in the form

$$[K_E]\ \{\Delta\delta\} = \{\Delta F_E\} + \{\Delta F_{DN}\} \qquad (3.35)$$

where $\{\Delta F_{DN}\}$ = vector of incremental nodal forces at the dual nodes

This can be solved and rewritten in the following form

$$\{\Delta\delta\} = \{\Delta\rho_E\} + [H]\ \{\Delta F_{DN}\} \qquad (3.36)$$

where $[H]$ = elastic influence matrix

$\{\Delta\rho_E\}$ = vector of incremental deflections due to the external load.

The first column of the matrix [H] is obtained by applying unit nodal forces in the vertical direction at each of the nodes which constitute the first "dual node" being considered. These unit nodal forces are applied in opposite directions. A solution is then obtained for the displacements throughout the mesh due to these forces. This solution

vector becomes the first column of the matrix [H]. This process is then repeated but with the forces being applied in the horizontal direction. The new solution vector is then the second column of the matrix. The matrix [H] is assembled when each of the 'dual nodes' has been treated in the above manner.

The incremental relative slip at the dual nodes is given by

$$\{\Delta\rho_I\} = \{\Delta s\} + [I]\ \{\Delta F_{DN}\} \qquad (3.37)$$

where $\{\Delta\rho_{rs}\}$ = vector of incremental relative slip at the dual nodes

$[I]$ = elastic influence matrix; this is obtained from [H] by subtracting the rows of the matrix corresponding to the displacement of the two nodes constituting a 'dual node'

$\{\Delta s\}$ = vector of incremental relative displacement due to the external load; this is obtained from $\{\Delta\rho_E\}$ by subtracting the displacements at the dual nodes.

To determine the initial elastic solution in which no slip has occurred, the vector $\{\Delta s\}$ is evaluated for the applied increment in external load. Initially when no slip has occurred the relative slip at the dual nodes is zero and the nodal forces are unknown, ie.

$$\{\Delta\rho_{rs}\} = \{\underline{0}\} \qquad (3.38)$$

A vector of nodal forces $\{\Delta F_{DN}\}$ can then be found by solution of equation 3.37, ie.

$$[I]\ \{\Delta F_{DN}\} = -\{\Delta s\} \tag{3.39}$$

Substitution into equation 3.36 gives the incremental deflections throughout the mesh.

The solution procedure continues until an increment in applied load results in an increment in nodal force ΔF_{DN_i}, which exceeds the allowable increment, ΔF_{DN_a}. When this occurs equation 3.39 is modified and resolved so that equation 3.33 is satisfied. This results in a redistribution of load onto the remaining non-slipped dual nodes. Equation 3.39 is then modified again so that for additional increments in applied load the slipped nodes take no further increase in load. Thus when slip occurs at a dual node the nodal force ΔF_{DN_i} is now known and the relative slip $\Delta \rho_{rs_i}$ becomes an unknown.

As the applied load is increased and yielding occurs within the pile or clay equation 3.35 is no longer applicable and is replaced by

$$[K_{EP}]\ \{\Delta\delta\} = \{\Delta F_E\} + \{\Delta F_{DN}\} \tag{3.40}$$

To facilitate the use of the initial stress method of solution and to avoid the necessity of assembling new [H] and [I] matrices and up-dating them to their current status within each iteration, equation 3.40 is written in the following form.

$$[K_E]\ \{\Delta\delta^{(n+1)}\} = (\{\Delta F_E\} + [K_c^{(n)}]\ \{\Delta\delta^{(n)}\}) + \{\Delta F_{DN}^{(n)}\} \tag{3.41}$$

where the corrections $[K_c^{(n)}]\ \{\Delta\delta^{(n)}\}$ which appear on the right hand side are treated as an additional external loading.

In finding a converged solution to equation 3.41 the iterative scheme outlined below is employed. A new vector of incremental deflections $\{\Delta\rho_E^{(n+1)}\}$ due to the external load is found by solution of

$$[K_E]\ \{\Delta\rho_E^{(n+1)}\} = \{\Delta F_E\} + [K_c^{(n)}]\ \{\Delta\delta^{(n)}\} \qquad (3.42)$$

The vector of incremental relative displacements at the dual nodes $\{\Delta s^{(n+1)}\}$ is obtained from $\{\Delta\rho_E^{(n+1)}\}$. This is updated by setting to zero the $\Delta s_i^{(n+1)}$ corresponding to the nodes that have slipped, and a new set of incremental nodal forces $\{\Delta F_{DN}^{(n+1)}\}$ is found by solution of

$$[I]\ \{\Delta F_{DN}^{(n+1)}\} = -\{\Delta s^{(n+1)}\} \qquad (3.43)$$

If an increment in nodal force $\Delta F_{DN_i}^{(n+1)}$ exceeds the allowable increment ΔF_{DN_a}, equation 3.43 is modified so that resolving gives

$$\Delta F_{DN_i}^{(n+1)} = \Delta F_{DN_a} \qquad (3.44)$$

Equation 3.43 is then modified again so that the slipped node or nodes take no further increase in load. In order to achieve this, the influence matrix [I] is adjusted by setting the ith row and column to zero and placing a one on the leading diagonal. The new solution set $\{\Delta\delta^{(n+1)}\}$ is found by substitution of $\{\Delta F_{DN}^{(n+1)}\}$ into

$$\{\Delta\delta^{(n+1)}\} = [H]\ \{\Delta F_{DN}^{(n+1)}\} + \{\Delta\rho_E^{(n+1)}\} \qquad (3.45)$$

Noting that equation 3.41 is obtained by substituting equation 3.42 into equation 3.45, where [H] is the subset of $[K_E]^{-1}$ corresponding to the dual nodes, it can be seen that neither $[K_E]$ nor [H] requires modification due to slip or yield. If convergence is not achieved, a new vector of corrections $[K_c^{(n+1)}]\ \{\Delta\delta^{(n+1)}\}$ is evaluated and the process repeated.

The solution method is economical because it retains the advantages of the initial stress method, in that the matrices [H], [I] need only be assembled once. Any subsequent changes due to slip are allowed for by removal of rows and columns from the original [I] matrix. Changes in both interfacial and continuum behaviour due to yielding within the pile and soil masses are taken into account by treating the vector of corrections $[K_c^{(n)}]\ \{\Delta\delta^{(n)}\}$ as an additional external load within the iterative scheme. In addition the method avoids the convergence difficulties associated with the use of joint elements.

3.3.4 Analysis of an Adhesive-Frictional; Dilatant Interface

In this section the analysis is extended so that the interface strength can be either adhesive, adhesive-frictional or purely frictional. In addition, the analysis is generalised so that the interface can dilate when slip occurs. Referring to Fig. 3.6 and assuming that the slip between the pile and soil is governed by a Mohr-Coulomb law, then

(a) The pile and soil adhere completely if

$$|F_{T1}| < F_{ca} + F_{N1} \tan \phi_a \qquad (3.46)$$

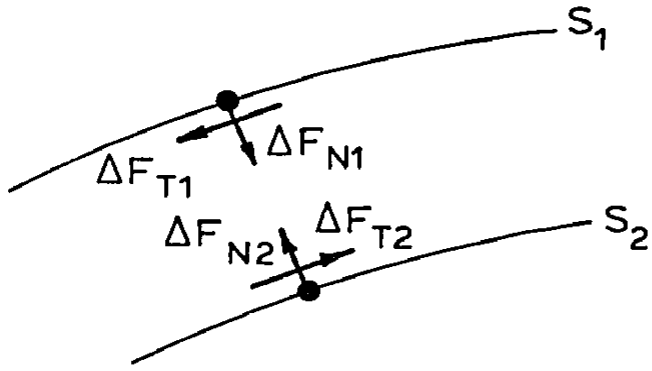

(a) Incremental Nodal Forces at a Dual Node

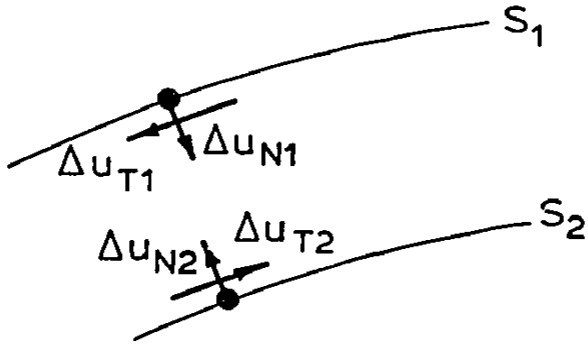

(b) Incremental Nodal Deflections at a Dual Node

FIG. 3.6

where F_{ca} is the adhesive strength and F_{T1}, F_{N1} are the tangential and normal nodal forces respectively and ϕ_a is the angle of friction governing slip at the interface.

(b) Slip occurs at the pile-soil interface when

$$|F_{T1}| = F_{ca} + F_{N1} \tan \phi_a \tag{3.47}$$

(c) When slip occurs F_{T1} must remain on the yield surface for further increments in applied load ie.

$$|\Delta F_{T1}| \cos \phi_a - \Delta F_{N1} \sin \phi_a = 0 \tag{3.48}$$

If slip has occurred the increments in normal and tangential displacements at a dual node $(\Delta u_{N1}, \Delta u_{T1})$, $(\Delta u_{N2}, \Delta u_{T2})$ satisfy

$$\Delta u_{N1} = \Delta u_{N2} \tag{3.49a}$$

$$\Delta u_{T1} = \Delta u_{T2} \tag{3.49b}$$

When slip occurs, if the interface does not dilate then for further increments in applied load

$$\Delta u_{N1} = \Delta u_{N2} \tag{3.50}$$

To incorporate a simple dilatancy behaviour into the analysis, equation 3.50 is replaced by

$$\tan \psi_a = \frac{\Delta u_{N2} - \Delta u_{N1}}{\Delta u_{T2} - \Delta u_{T1}} \tag{3.51}$$

where ψ_a is the angle governing the dilatant behaviour at the pile-soil interface. Thus if $\psi_a = 0$ the interface is non-dilatant whereas if $\psi_a = \phi_a$ maximum dilatancy occurs.

When slip occurs equations 3.48 and 3.51 must be satisfied for further increments in applied load. In this section the set of axes which are normal and tangential to the pile-soil interface are defined as the N-T axes. If the deflections and nodal forces are referred to an alternate set of axes the same solution procedure outlined in the previous section can be retained. These alternate axes are the η-ξ axes for nodal forces and the U-V axes for deflections where the rotation matrices are given by

$$\begin{bmatrix} \Delta u_{V1} \\ \Delta u_{U1} \end{bmatrix} = \begin{bmatrix} \cos \psi_a & - \sin \psi_a \\ \sin \psi_a & \cos \psi_a \end{bmatrix} \begin{bmatrix} \Delta u_{T1} \\ \Delta u_{N1} \end{bmatrix} \tag{3.52a}$$

$$\begin{bmatrix} \Delta F_{\xi 1} \\ \Delta F_{\eta 1} \end{bmatrix} = \begin{bmatrix} \cos \phi_a & - \sin \phi_a \\ \sin \phi_a & \cos \phi_a \end{bmatrix} \begin{bmatrix} \Delta F_{T1} \\ \Delta F_{N1} \end{bmatrix} \tag{3.52b}$$

This rotation of axes results in the nodal forces in the ξ-direction being analogous to the nodal forces in the T-direction in the previous analysis for the purely adhesive interface. Thus, the same solution procedure can be retained if a force in the ξ-direction is treated in the same manner as a force in the T-direction in the previous analysis. The maximum allowable force in the ξ-direction, ΔF_{DN_a}, is given by equation 3.47 as

$$F_{DN_a} = F_{ca} \cos \phi_a \tag{3.53}$$

Global rotation matrices [A] and [B] are assembled such that

$$\{\Delta F_{DN}\}_{\eta\xi} = [A]\ \{\Delta F_{DN}\} \tag{3.54}$$

where $\{\Delta F_{DN}\}_{\eta\xi}$ = vector of nodal forces at the dual nodes with the η-ξ axes as the reference set of axes

and $$\{\Delta \rho_{rs}\}_{UV} = [B]\ \{\Delta \rho_{rs}\} \tag{3.55}$$

where $\{\Delta \rho_{rs}\}_{UV}$ = vector of incremental relative slip at the dual nodes with the UV axes as the reference set of axes.

Equation 3.37 is rewritten thus

$$\{\Delta \rho_{rs}\}_{UV} = \{\Delta s\}_{UV} + [B][I][A]^T\{\Delta F_{DN}\}_{\eta\xi} \tag{3.56}$$

where $\{\Delta s\}_{UV}$ = vector of incremental relative displacement due to the external load with the UV axes as the reference set of axes.

Initially when no slip has occurred the relative slip at the dual nodes is zero, ie.

$$\{\Delta \rho_{rs}\}_{UV} = \{\underline{0}\} \tag{3.57}$$

A vector of nodal forces $\{\Delta F_{DN}\}_{\eta\xi}$ can be found by solution of equation 3.56, ie.

$$[B][I][A]^T\{\Delta F_{DN}\}_{\eta\xi} = -\{\Delta s\}_{UV} \tag{3.58}$$

The vector of nodal forces $\{\Delta F_{DN}\}$ is found by solution of equation 3.54 and substitution into equation 3.36 gives the incremental deflections throughout the mesh. The solution procedure continues until an increment in applied load results in an increment in nodal force in the ξ-direction, $\Delta F_{\xi i}$, which exceeds the allowable value, ΔF_{DN_a}. When this occurs, equation 3.58 is modified and re-solved so that

$$\Delta F_{\xi i} = \Delta F_{DN_a} \tag{3.59}$$

Equation 3.58 is then modified again so that for additional increments in applied load the slipped nodes take no further increase in load in the ξ-direction.

As the applied load is increased and yielding occurs within the pile or soil the only alteration to the analysis presented in the previous section for a purely adhesive interface is that equation 3.43 is replaced by

$$[B][I][A]^T\{\Delta F_{DN}^{(n+1)}\}_{\eta\xi} = -\{\Delta s^{(n+1)}\}_{\eta\xi} \tag{3.60}$$

A new set of nodal forces $\{\Delta F_{DN}^{(n+1)}\}$ can be found from this set of nodal forces with respect to the η-ξ axes, $\{\Delta F_{DN}^{(n+1)}\}_{\eta\xi}$, by solution of equation 3.54. With this set of nodal forces $\{\Delta F_{DN}^{(n+1)}\}$, a new solution set $\{\Delta\delta^{(n+1)}\}$ is found by substitution into equation 3.45. If convergence is not achieved, a new set of corrections $[K_c^{(n+1)}]$ $\{\Delta\delta^{(n+1)}\}$ is evaluated. A converged solution is then obtained using the iterative scheme outlined in the previous section.

3.4 AN ECONOMICAL METHOD FOR PERFORMING ELASTO-PLASTIC FINITE ELEMENT ANALYSES

In an elasto-plastic finite element analysis considerable computational effort is required for

(a) the assembly of the stiffness matrix

(b) the solution of the set of equations relating the unknown deflections to the nodal forces.

In this section a method is described which enables the size of the equation set used in an analysis to be reduced. This therefore results in considerable economy. Also, both elastic or elasto-plastic analyses can be performed on computers where the solution of the complete equation set is cumbersome because it exceeds the storage capacity of the machine.

For elasto-plastic analyses this method is most efficient when the plastic zone is within the immediate vicinity of the loaded area and at the ultimate load, a large portion of the continuum is still elastic.

3.4.1 Method of Analysis

3.4.1 (i) Separation of Finite Element Meshes into Blocks

A typical plot of the plastic zone beneath a strip footing loaded to failure is shown in Fig. 3.7(a). The continuum can therefore be separated into two blocks as in Fig. 3.7(b). Block A includes all the elements that have yielded when the collapse load is reached. As a result of the discrete finite element representation of the continuum

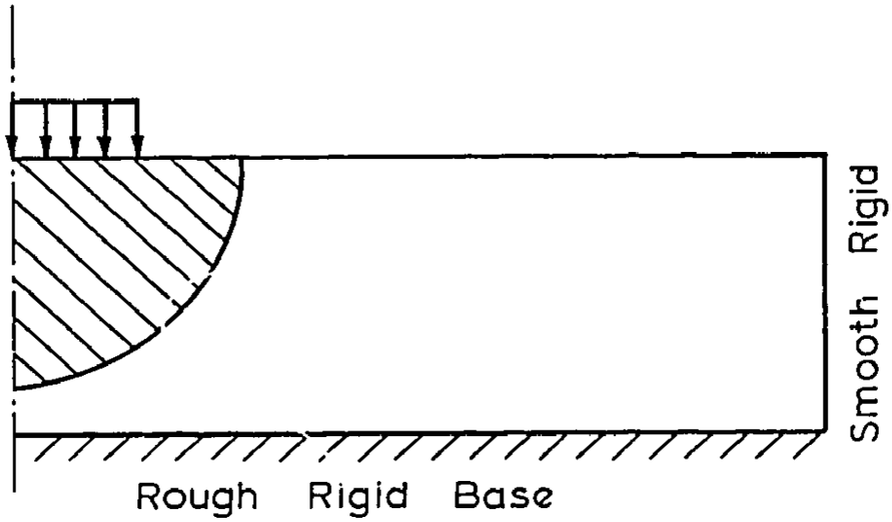

(a) Typical Plot of Yielded Zone at Ultimate Load

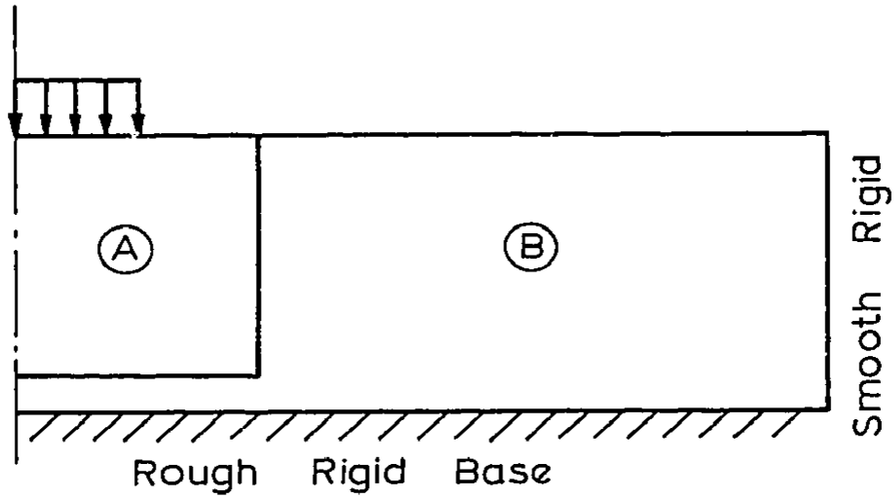

(b) Non - Linear Block A and Elastic Block B

FIG. 3.7 DIVISION OF CONTINUUM INTO AN ELASTIC BLOCK (B) AND A NON - LINEAR BLOCK (A)

the interaction between the two blocks manifests itself in the nodal forces developed at the nodes along the interface. Block B contains only elements which remain elastic even at the ultimate load; thus its response is elastic throughout the loading history.

Initially when no yielding has occurred the elastic displacements throughout the continuum can be obtained by solution of the standard finite element equation

$$[K_E]\ \{\delta\} = \{F\} \tag{3.61}$$

In this method of solution the size of this equation set is reduced by analysing Block A separately. Equation 3.61 then reduces to

$$\begin{bmatrix} a & b \\ b^T & c \end{bmatrix} \begin{bmatrix} \underline{\delta}_I \\ \underline{\delta}_A \end{bmatrix} = \begin{bmatrix} \underline{F}_I \\ \underline{G} \end{bmatrix} \tag{3.62}$$

where $\{\delta_I\}$ = vector of deflections for nodes along the interface of Blocks A and B

$\{\delta_A\}$ = vector of deflections for nodes within Block A

$\{F_I\}$ = vector of nodal forces along the interface of Blocks A and B

$\{G\}$ = vector of nodal forces due to the applied tractions.

The nodal forces at the interface $\{F_I\}$ depend on the elastic response of Block B. This response is determined before commencing an analysis by assembling the stiffness matrix for Block B and generating an influence matrix such that

$$\{\delta_I\} = -[I]\ \{F_I\} \tag{3.63}$$

where $[I]$ = elastic influence matrix for Block B

Equation 3.63 is inverted giving

$$\{F_I\} = -[I]^{-1}\{\delta_I\} \tag{3.64a}$$

or

$$\{F_I\} = -[J]\ \{\delta_I\} \tag{3.64b}$$

Equation 3.64b can be rewritten as

$$\begin{bmatrix} -J & 0 \\ 0 & 0 \end{bmatrix} \begin{bmatrix} \underline{\delta}_I \\ \underline{\delta}_A \end{bmatrix} = \begin{bmatrix} \underline{F}_I \\ \underline{0} \end{bmatrix} \tag{3.65}$$

Substituting the above into equation 3.62 gives

$$\begin{bmatrix} a+J & b \\ b^T & c \end{bmatrix} \begin{bmatrix} \underline{\delta}_I \\ \underline{\delta}_A \end{bmatrix} = \begin{bmatrix} \underline{0} \\ \underline{G} \end{bmatrix} \tag{3.66}$$

Now the size of the elastic stiffness matrix for the continuum is determined only by the number of nodes in Block A. However, the bandwidth is the maximum bandwidth of equations 3.62 or 3.65. Thus, care must be exercised when separating the continuum into blocks in order that the subsequent economy achieved by reducing the equation set is not undermined by increasing the bandwidth. Also, for elasto-plastic analyses the division must be such that all the elements within Block B remain elastic throughout the loading history.

3.4.1 (ii) A Particular Boundary Condition

In Fig. 3.8 if Block B is separated from the continuum, the boundary conditions are such that it is displacement defined in the vertical direction only. When generating the influence matrix [I], unit forces are applied at the interface in the vertical and horizontal directions. In order that this influence matrix can be generated, a node away from the interface is pinned in the horizontal direction. Thus the deflections at the interface can be written as

$$\{\delta_I\} = -[I^*]\{F_I\} + \Delta_o\{e\} \tag{3.67}$$

where $[I^*]$ = elastic influence matrix for Block B with a node pinned in the horizontal direction

Δ_o = unknown displacement in the horizontal direction at the pinned node

$\{e\}$ = vector containing unity for displacements in the horizontal direction and zero for displacements in the vertical direction.

Horizontal equilibrium of Block B can be expressed as

$$\{e\}^T\{F_I\} = \{\underline{0}\} \tag{3.68}$$

Multiplying 3.67 by $[I^*]^{-1}$ gives

$$[I^*]^{-1}\{\delta_I\} = -\{F_I\} + [I^*]^{-1}\{e\}\,\Delta_o \tag{3.69a}$$

ie. $$\{e\}^T[I^*]^{-1}\{\delta_I\} = -\{e\}^T\{F_I\} + \{e\}^T[I^*]^{-1}\{e\}\,\Delta_o \tag{3.69b}$$

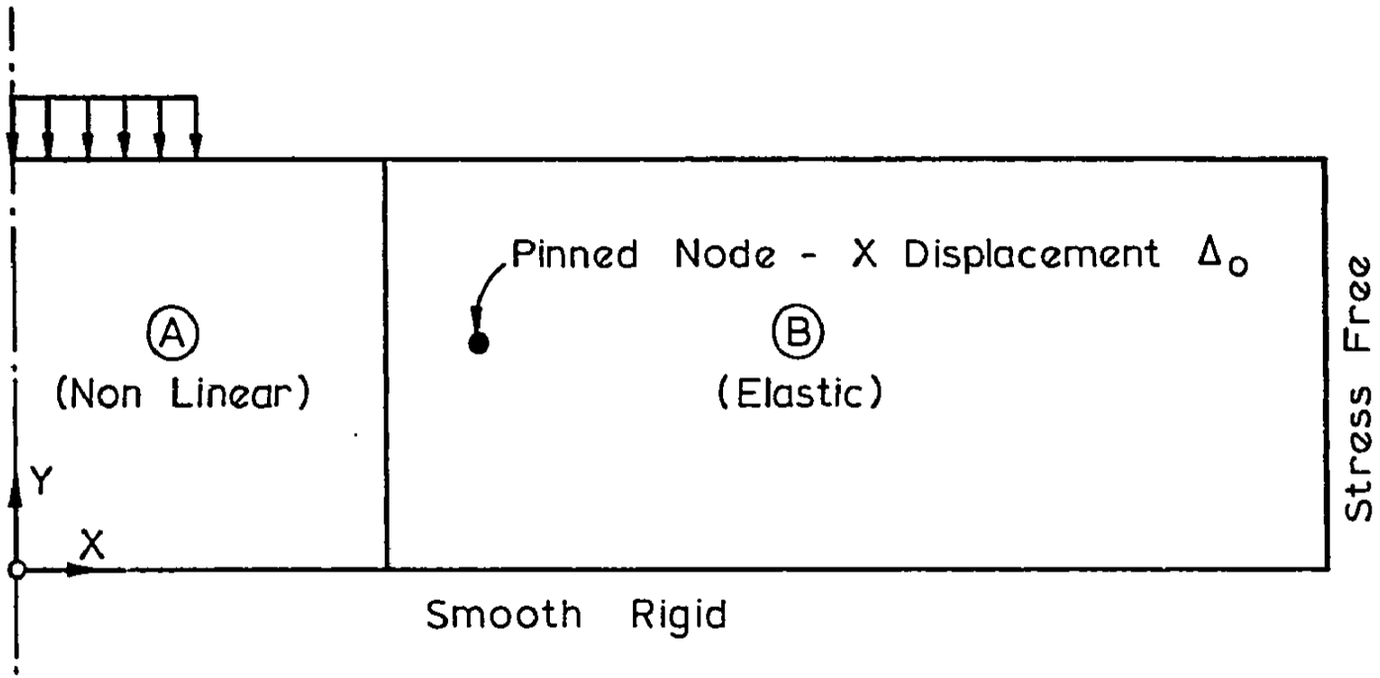

FIG. 3.8 PLANE STRAIN FOOTING PROBLEM - BOUNDARY CONDITION PROBLEMS

Substituting equation 3.68 into equation 3.69b gives the unknown displacement Δ_o as

$$\Delta_o = \frac{\{e\}^T [I^*]^{-1} \{\delta_I\}}{\{e\}^T [I^*]^{-1} \{e\}^T} \tag{3.70}$$

Substituting this unknown displacement into equation 3.69a and re-arranging gives

$$\{F_I\} = -\left[[I^*]^{-1} - \frac{[I^*]^{-1}\{e\}\{e\}^T[I^*]^{-1}}{\{e\}^T [I^*]^{-1} \{e\}}\right] \{\delta_I\} \tag{3.71a}$$

ie. $$\{F_I\} = -[J] \{\delta_I\} \tag{3.71b}$$

Thus, the relationship between the interface deflections and forces has been obtained.

3.4.2 Application of the Method to Elastic and Elasto-Plastic Analyses

The procedure for application of this method is now described in detail.

Three elastic analyses of a homogeneous continuum of depth h, subjected to a uniform circular loading of radius a (Fig. 3.9) were performed using the constant strain triangular finite element mesh shown in Fig. 3.10. This mesh has 232 degrees of freedom and a half-bandwidth of 24. Therefore, the size of the stiffness matrix required to analyse this mesh is (232, 24). In the first analysis the stiffness matrix for the entire mesh was assembled and an elastic solution obtained in the standard manner.

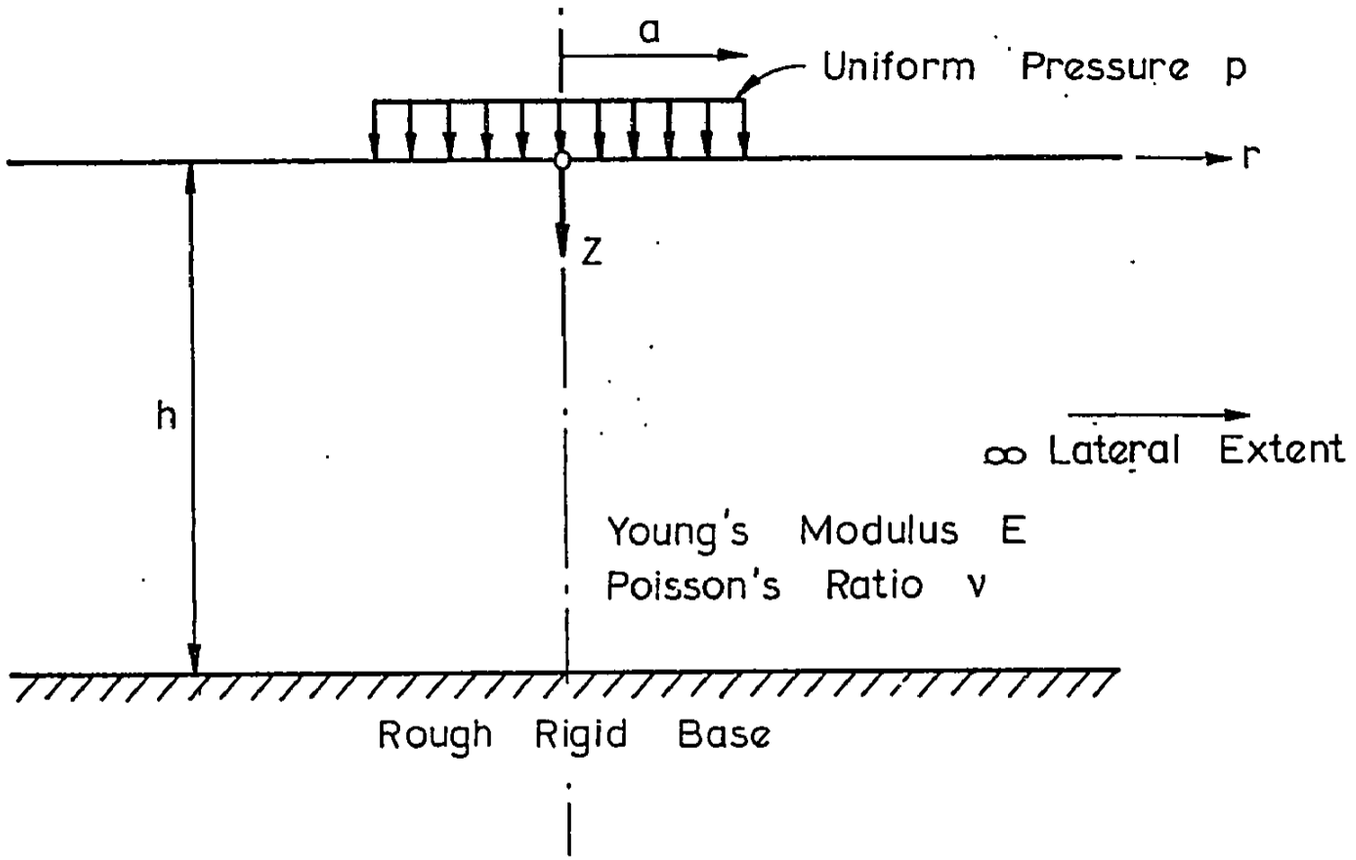

FIG.3.9 DEFINITION OF AXI - SYMMETRIC PROBLEM

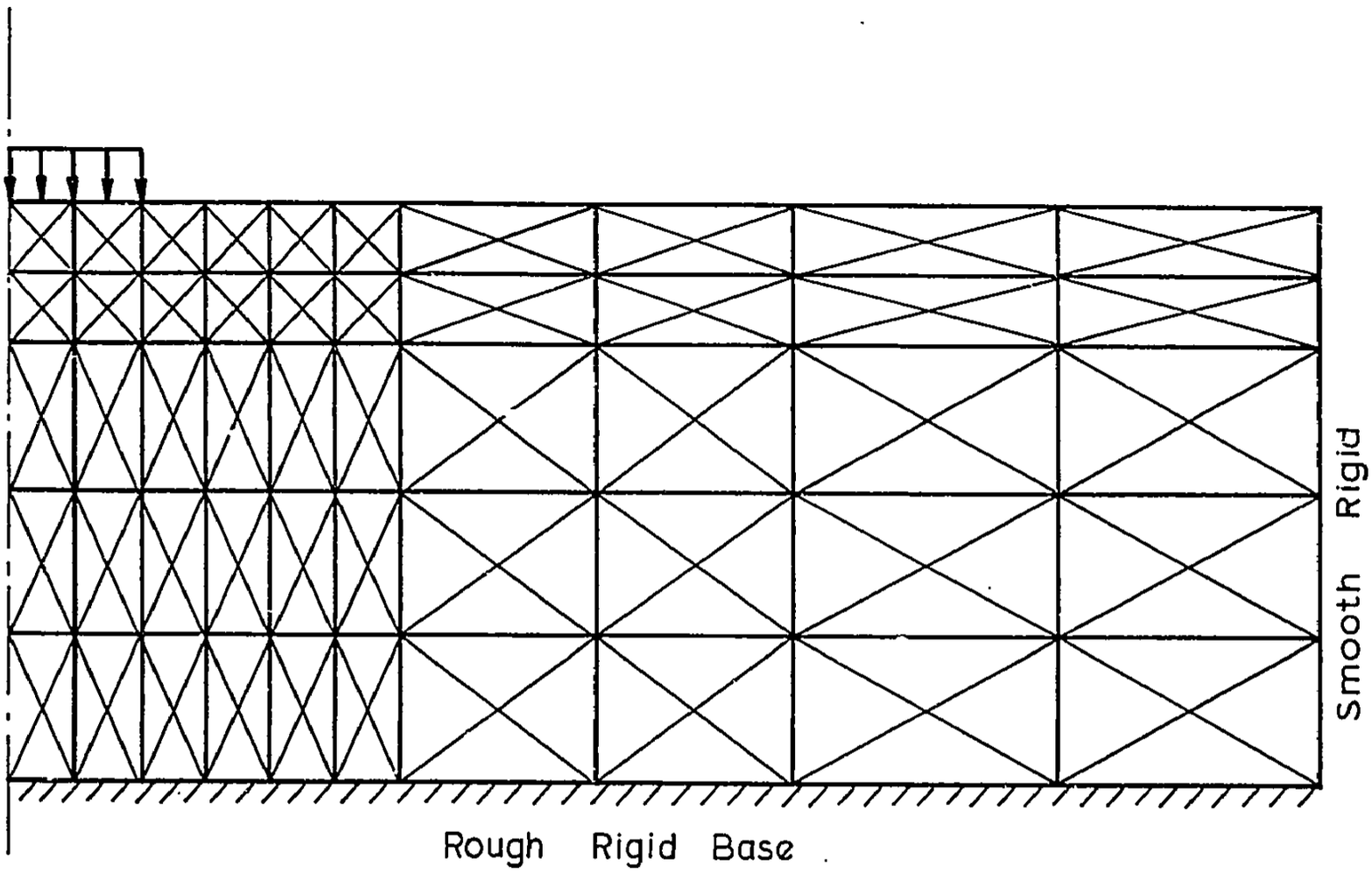

FIG. 3.10 ELASTIC AXI - SYMMETRIC ANALYSIS No.1 - COMPLETE F.E. MESH

In the second analysis the continuum was separated into two blocks (Fig. 3.11) with each block being analysed separately. For this analysis the stiffness matrix for Block B is assembled (182, 24) and an influence matrix [J] is generated. The stiffness matrix for Block B is then assembled and the terms in the matrix [J] added to it. The size of this stiffness matrix is (78, 24).

The third analysis would be applicable when a computer's storage capacity is very small. In this analysis the continuum was divided into more than two blocks (Fig. 3.12). The procedure then is as follows; the stiffness matrix for Block C (78, 24) is assembled and an influence matrix $[J_2]$ generated. This influence matrix is the elastic response of Block C on Block B. Then the stiffness matrix for Block B (100, 24) is assembled and the terms in the matrix $[J_2]$ added to it. An influence matrix $[J_1]$ is generated for the elastic response of Blocks B and C on Block A. Matrices $[J_1]$ and [J] are therefore identical. Finally, the stiffness matrix for Block A (78, 24) is assembled and the terms in matrix $[J_1]$ added to it.

The results of these three analyses, which are identical, are shown in Figs. 3.13 and 3.14. Both the surface displacement profile and the stresses along the centreline are in close agreement with Giroud's (1972) and Milovic's (1970) solutions respectively.

To illustrate what is anticipated to be the method's most common application, plane strain elasto-plastic analyses of a strip footing loaded to failure were performed using the finite element mesh shown in Fig. 3.15. The initial stress method of solution is employed. A Mohr Coulomb yield criterion was adopted and the material

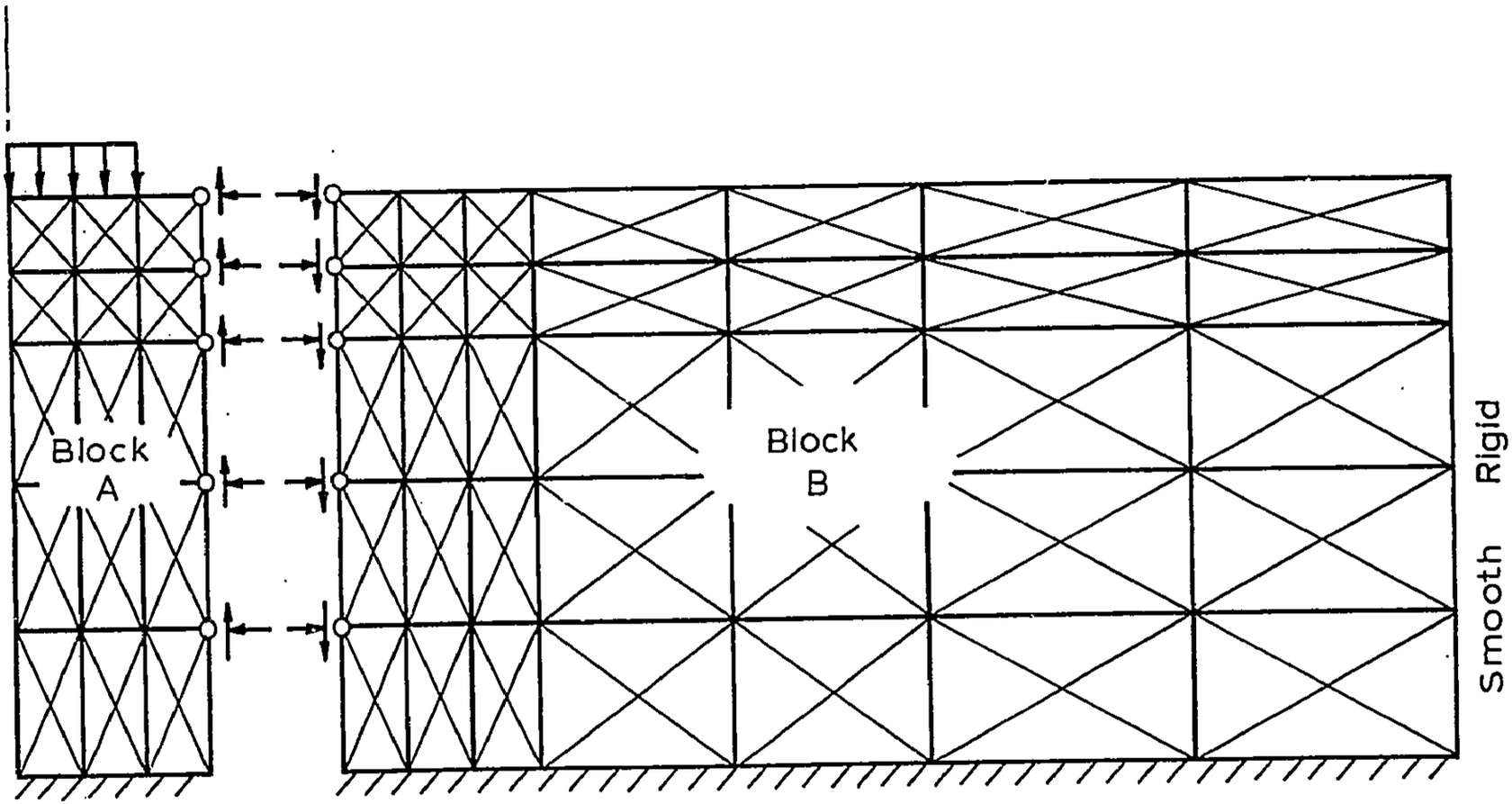

FIG. 3.11 ANALYSIS No. 2 : BLOCKS A & B ANALYSED SEPARATELY

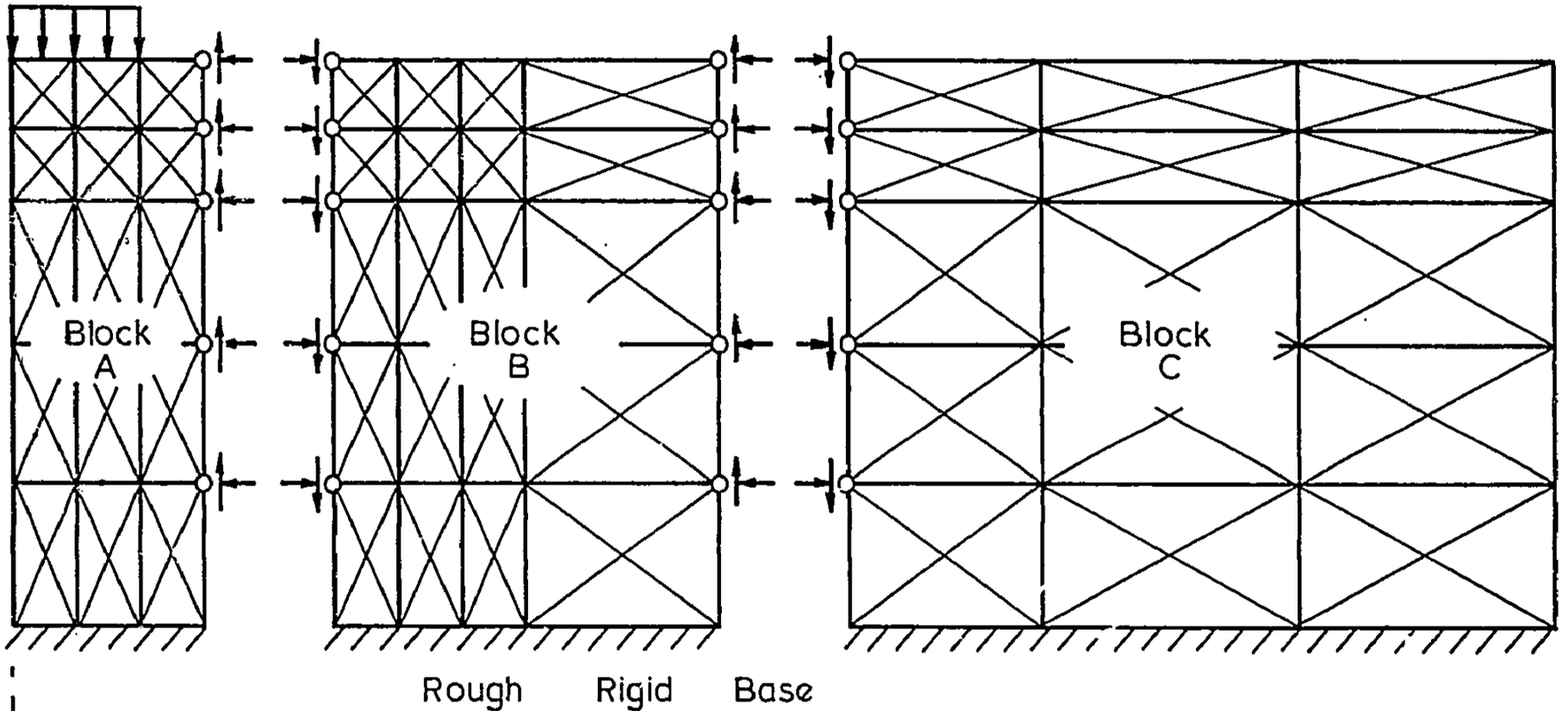

FIG. 3.12 ANALYSIS No. 3 : BLOCKS A, B & C ANALYSED SEPARATELY

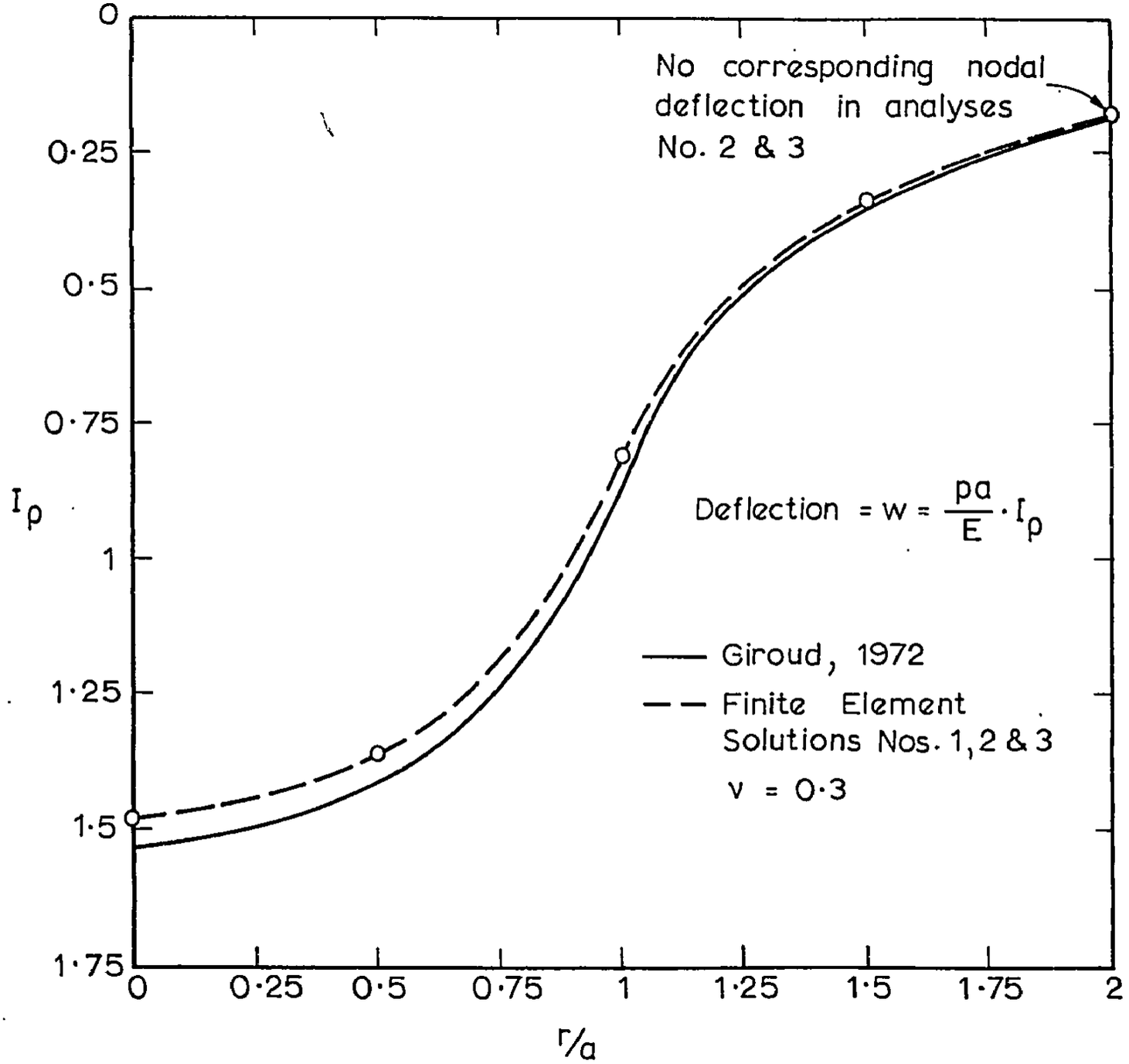

FIG.3.13 COMPARISON OF SURFACE DISPLACEMENTS

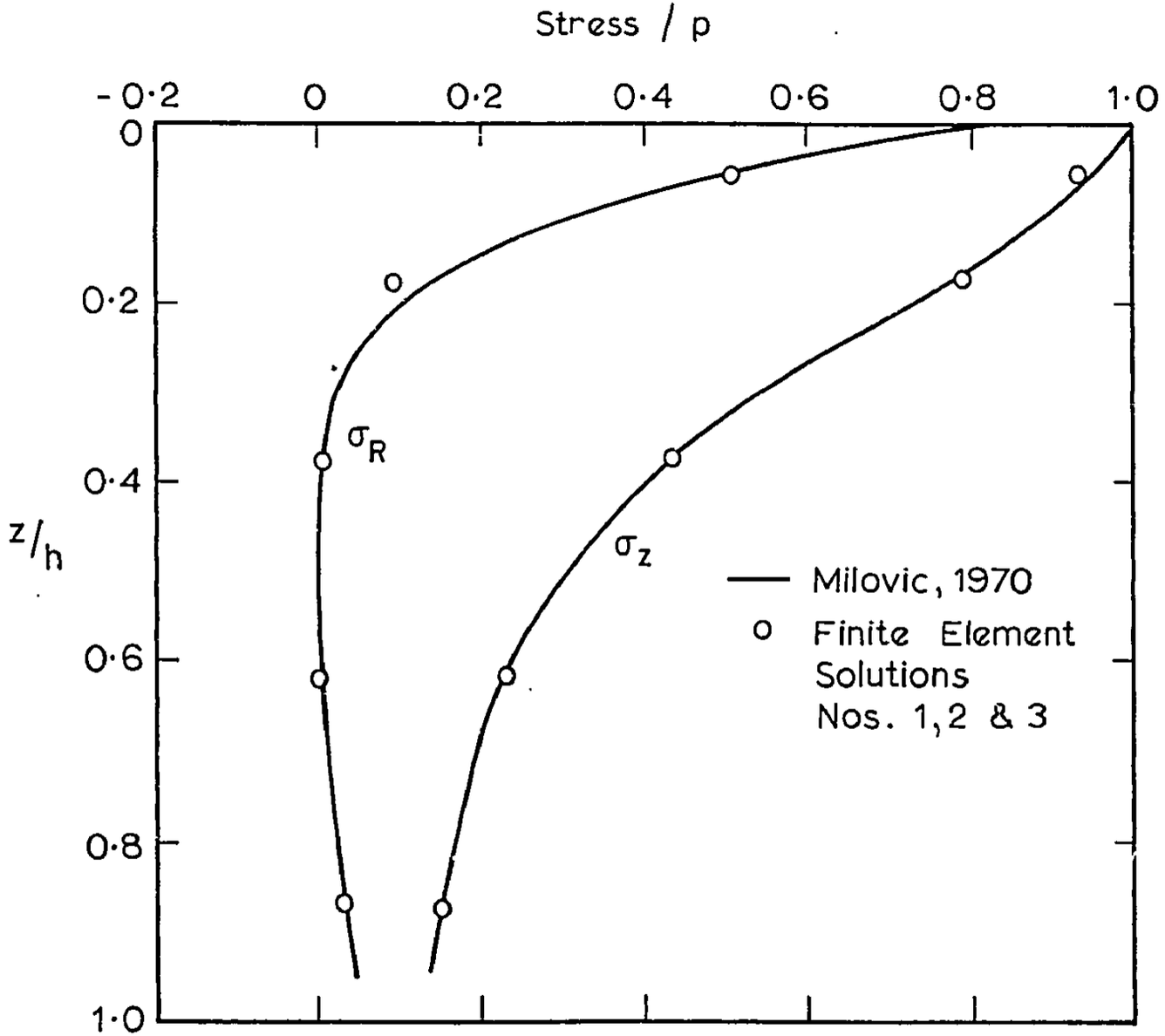

FIG. 3.14 VERTICAL AND RADIAL STRESSES ALONG CENTRELINE FOR CIRCULAR UNIFORM PRESSURE

FIG. 3.15 ELASTO - PLASTIC PLANE STRAIN ANALYSIS No. 1
COMPLETE F.E. MESH

taken to be purely cohesive with cohesion c_u and a Poisson's ratio $\nu = 0.48$ which approximates incompressible behaviour. The parameters chosen correspond to undrained loading of a fully saturated homogeneous soil layer.

Three analyses were performed. In the first analysis the complete mesh was used and the pressure p increased to a value of $p/c_u = 5.2$. The extent of the yielded zone for this value of pressure is shown diagrammatically in Fig. 3.16. The second analysis was performed using the portion of the mesh from the centreline to cut AA (Fig. 3.16). This is referred to as Block A. The 'elastic' response of the remainder of the mesh from AA to the outer boundary (Block B) was generated using the method described above. It is evident that the response of Block B is not elastic throughout the loading history as elements yield beyond the cut AA. The third analysis was performed with Block A extending from the centreline to cut BB, the elastic response of Block B (BB to outer boundary) being generated before commencement of the analysis. The same load increments and convergence criterion were used for the three analyses so that valid comparisons of computer times could be made.

The results of these three analyses are shown in Fig. 3.17. The results of the second analysis are erroneous because the initial division of the mesh is such that the response of Block B is not elastic throughout the loading history resulting in a stiffer response of the continuum when elements 'yield' in Block B. Care must be exercised when the initial division of the mesh is made. It is the author's experience that if elements yield along the division of the mesh the analysis should be repeated with a larger portion of the mesh included

Analysis 1 : Complete Mesh
Analysis 2 : Mesh ℄ Cut AA
Analysis 3 : Mesh ℄ Cut BB

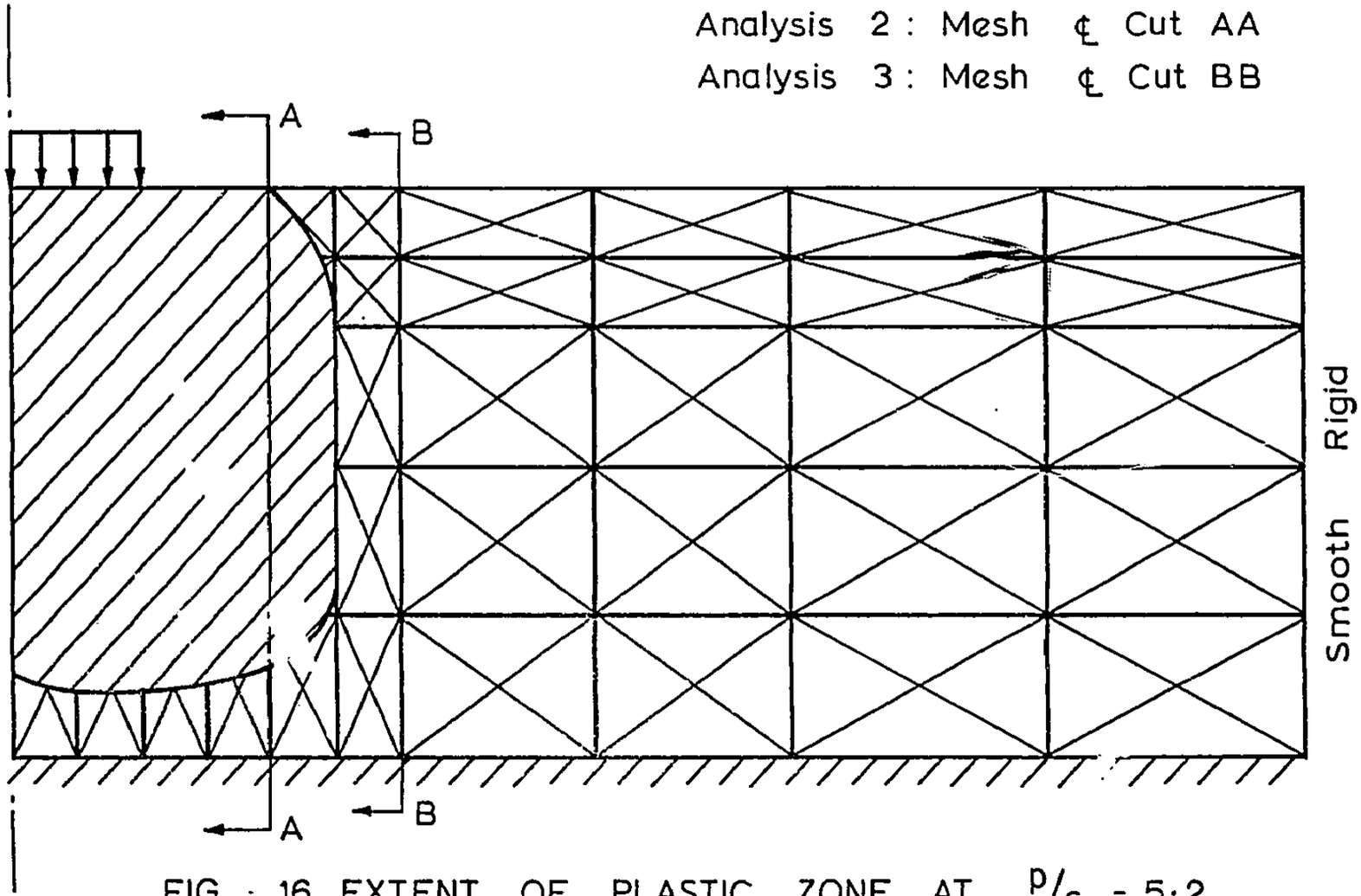

FIG. 16 EXTENT OF PLASTIC ZONE AT $p/c_u = 5{\cdot}2$

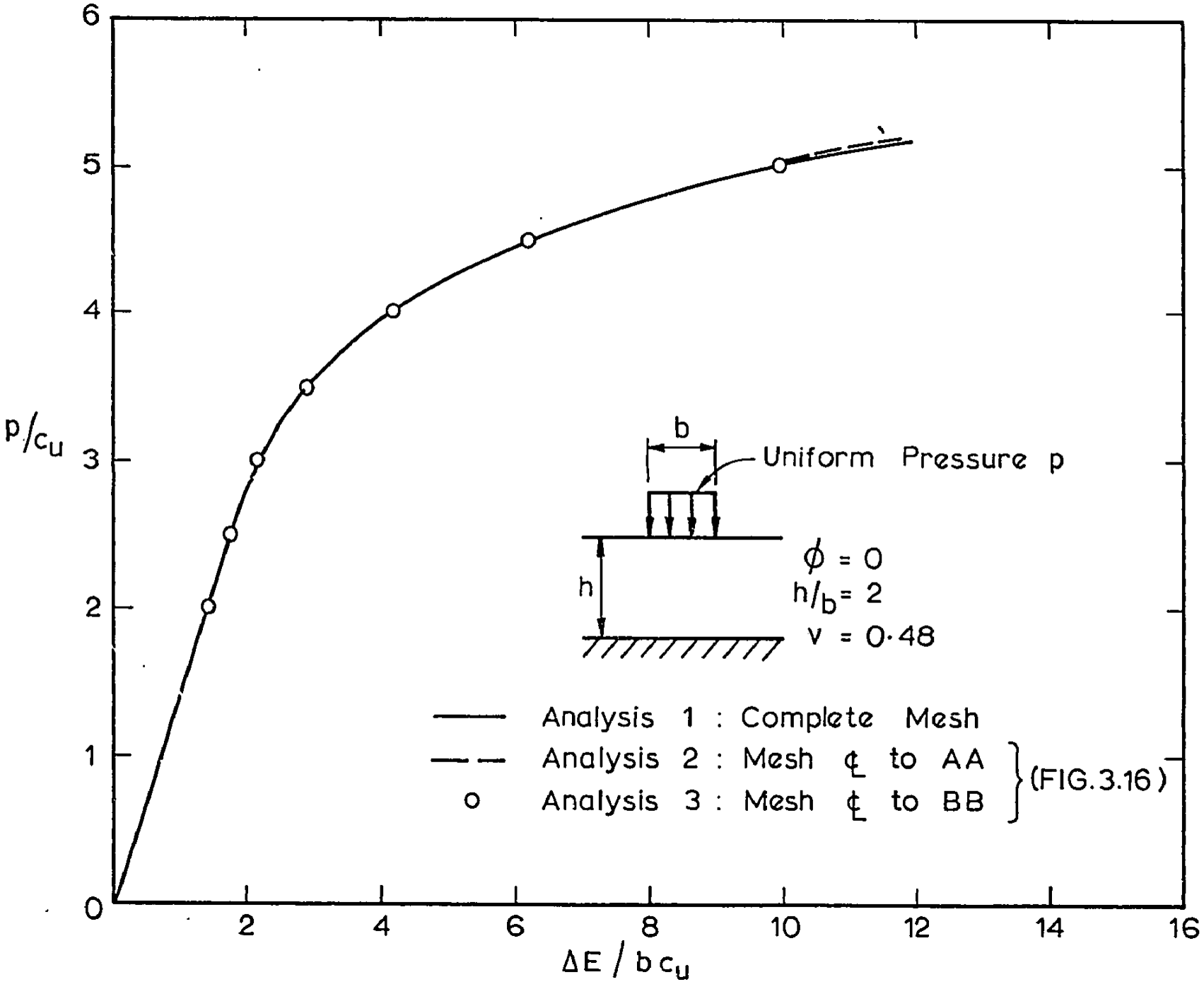

FIG. 3.17 RESULTS OF THREE ELASTO - PLASTIC ANALYSES

in Block A.

The results from analyses 1 and 3 are identical, with analysis 3 taking 80% of the computer time required for analysis 1. However, the economy in computer time is a function of the number of nodes in Block B compared with the total number of nodes in the complete mesh. Thus, larger savings are most likely in many analyses.

Although the implementation of the method described in this section is straightforward, it

(a) permits finite element analyses of problems on minicomputers which would otherwise be cumbersome or impossible

(b) leads to considerable economy in computer time for elasto-plastic analyses.

In this section surface footings were considered for convenience. However, the conclusions are also relevant for single pile analyses and the method has been used for elasto-plastic analyses of single granular piles. The results of these analyses are presented in Chapter 4.

3.5 THE CHOICE OF ELEMENT

Finite element solutions to elastic and elasto-plastic analyses of granular pile behaviour are presented in this thesis. These solutions were obtained using either constant strain triangular elements

or rectangular isoparametric elements of quadratic order. In this section, the results of an investigation into the relative merits of these two element types are presented. Comparisons are made between solutions to elastic and elasto-plastic axisymmetric analyses obtained using the two element types. The conclusions are also considered relevant to plane strain analyses.

3.5.1 Rectangular Isoparametric and Constant Strain Triangular Elements

The constant strain triangular element is the simplest of the two dimensional elements. As the name implies, the polynomial chosen for the displacement function results in a constant strain (ie. stress) state throughout the element.

Isoparametric elements are now widely used and many examples of successful applications are found in the finite element literature (Clough, 1969; Zienkiewicz, 1971). The elements are formulated using an intrinsic co-ordinate system ξ,η defined by element geometry, not by the elements orientation in the global co-ordinate system. The name 'isoparametric' stems from the use of the same interpolation function to define the displacements within the element as is used to map the local co-ordinates to the global co-ordinate system. Rectangular elements of quadratic order (ie. displacement function parabolic) were chosen for this comparison. These elements may have curved sides and thus provide a better fit to a curved boundary than constant strain elements. A rectangular quadratic element and its parent element are shown in Fig. 3.18. Using the notation of Zienkiewicz (1971), the mapping functions for this element are given by

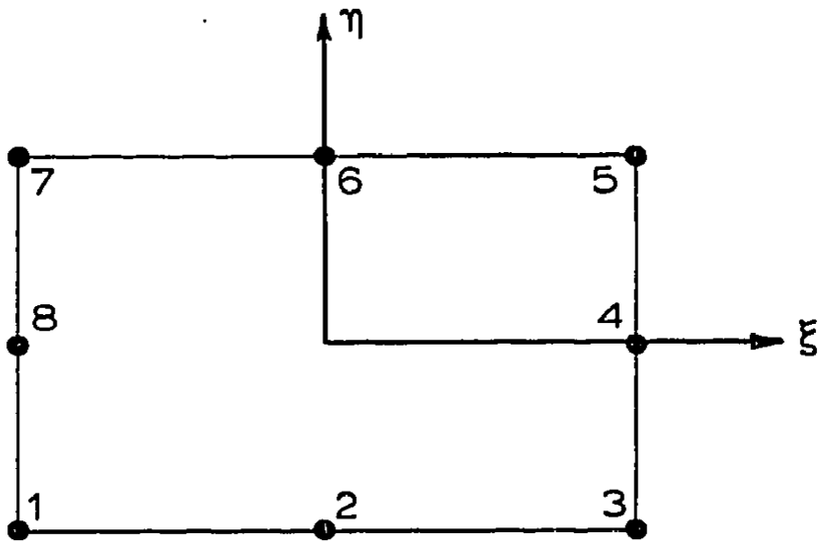

(a) Parent Element - Local Co-ordinates

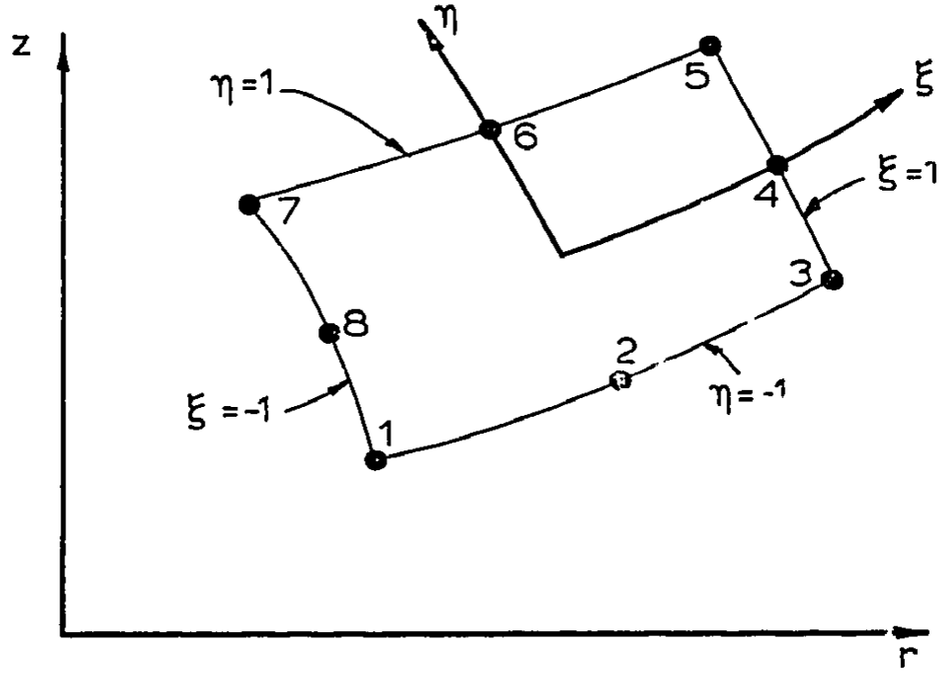

(b) Isoparametric Element - Global Co-ordinates

FIG. 3.18 QUADRATIC PARENT AND ISOPARAMETRIC ELEMENT

$$r = \sum_{i=1}^{8} N_i r_i \tag{3.72a}$$

$$z = \sum_{i=1}^{8} N_i z_i \tag{3.72b}$$

where $N_i = \frac{1}{4}(1 + \xi\xi_i)(1 + \eta\eta_i)(\xi\xi_i + \eta\eta_i - 1)$

$$\text{for } i = 1, 3, 5, 7 \tag{3.72c}$$

$$N_i = \frac{1}{2}(1 - \xi^2)(1 + \eta\eta_i) \quad \text{for } i = 2, 6 \tag{3.72d}$$

$$N_i = \frac{1}{2}(1 + \xi\xi_i)(1 - \eta^2) \quad \text{for } i = 4, 8 \tag{3.72e}$$

and for i running from 1 to 8 the consecutive values for ξ_i and η_i are

$$\xi_i = -1, 0, 1, 1, 1, 0, -1, -1 \tag{3.72f}$$

$$\eta_i = -1, -1, -1, 0, 1, 1, 1, 0$$

Having adopted this interpolation scheme, the formulation of the element stiffness matrices is relatively straightforward. This formulation is well documented by many authors (Zienkiewicz, 1971; Cook, 1974) and so no derivation of the governing equations is given here. The stiffness matrix is assembled by numerical integration using the Gaussian quadrature formula. For rectangular elements of quadratic order, the isoparametric element requires four sampling points with the stiffness of each element being the sum of the stiffnesses at each of these points. These sampling points are referred to as Gauss points.

When the applied load does not take the form of point loads acting at the nodes but rather a traction acting along part of a boun-

dary, the corresponding nodal forces are calculated by equating the work done by the traction to that done by the nodal forces. The expressions for the nodal forces are given in Appendix 3B for axisymmetric analyses using either constant strain or isoparametric elements of quadratic order.

3.5.2 Elastic Analyses - The Two Elements Compared

Elastic analyses of a homogeneous continuum of depth h, subjected to a uniform circular loading of radius a, were performed using successively finer isoparametric and constant strain finite element meshes. This allowed a comparison of the relative performance of the two element types in the elastic range. The outer boundary was located at a distance 20a from the centreline and taken to be smooth rigid. The Poisson's ratio of the material was taken to be equal to 0.15 and h/a = 5.

In Fig. 3.19 the results of the analyses using isoparametric elements are shown. Commencing with a mesh which consisted of 2 elements and 13 nodes, the subdivision of the continuum was made successively finer. The dimensionless parameter, I_ρ, is plotted against the number of nodes in a mesh. These results illustrate that the solution for the central elastic deflection converges rapidly to a solution 2.5% smaller than that given by Giroud (1972) for a continuum of infinite lateral extent. The meshes consisting of 29 and 73 nodes give values of I_ρ which differ by only .014. However, the stress distributions are significantly improved by the addition of more nodes. The distributions in vertical and radial stresses at a radius of .085a obtained from the meshes consisting of 45 nodes (mesh IS1) and 73 nodes

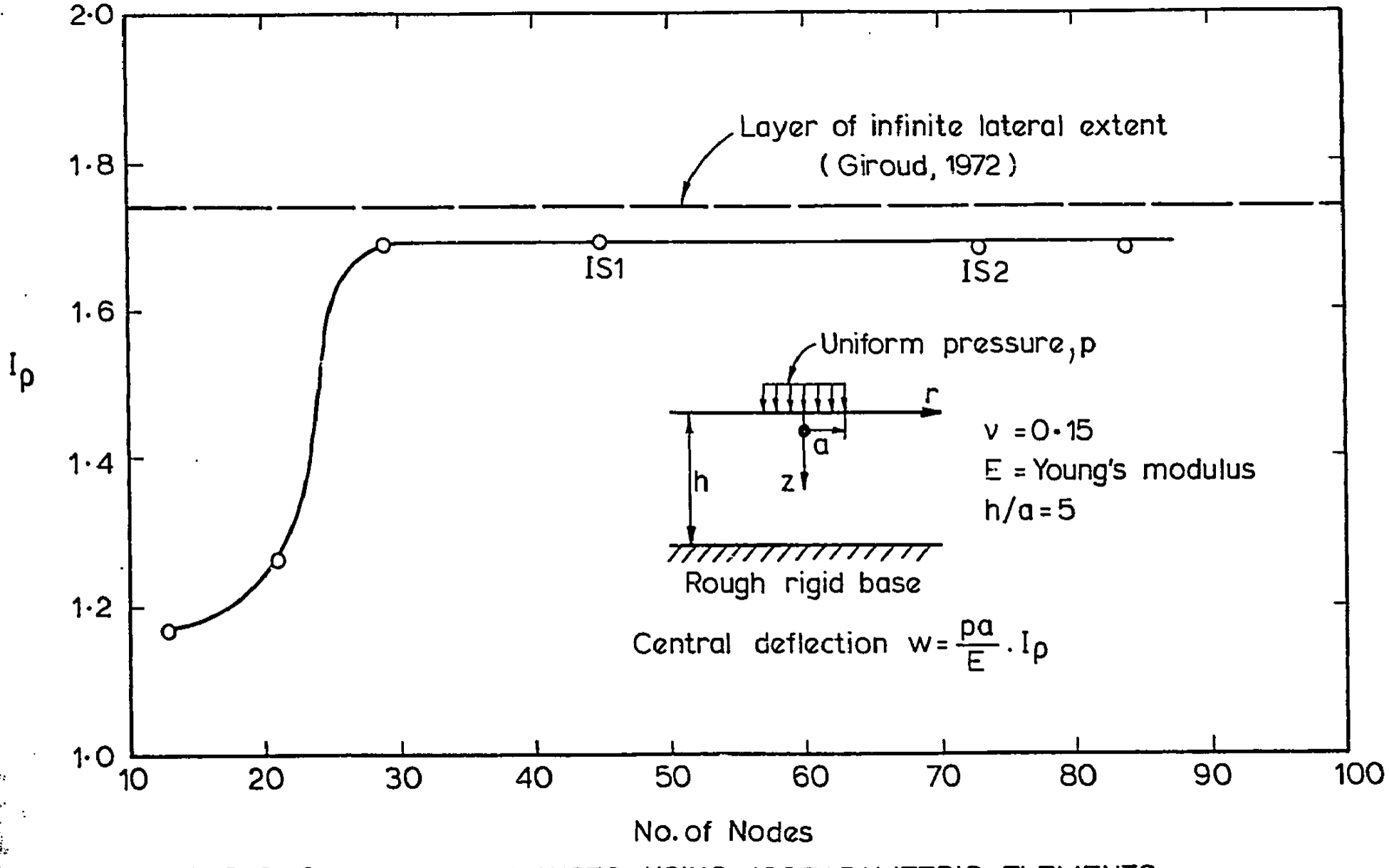

FIG. 3.19 ELASTIC ANALYSES USING ISOPARAMETRIC ELEMENTS

(mesh IS2) are shown in Fig. 3.20. Although the vertical stress distribution from mesh IS1 is in reasonable agreement with the results of Milovic (1970), the radial stress distribution is significantly different. The stress distributions for mesh IS2 closely reproduce those of Milovic. This mesh, which is reproduced in Fig. 3.21, is considered to be representative of the coarsest subdivision of the continuum into isoparametric elements which yields accurate results.

The same procedure was adopted with the constant strain triangular elements. Commencing with a mesh consisting of 32 elements and 23 nodes, the number of nodes and elements were successively increased. In Fig. 3.22 the results of these analyses are plotted along with those from Fig. 3.19. The stress distributions from the meshes consisting of 111 nodes (mesh CS1) and 137 nodes (mesh CS2) are shown in Fig. 3.23. The value of I_ρ is improved slightly by the addition of the extra nodes but the stress distributions from the two meshes are virtually identical. Mesh CS1 which is reproduced in Fig. 3.24 is thus considered to be representative of the coarsest subdivision of the continuum into constant strain elements which yields accurate results. This mesh produces a value of I_ρ 4.5% smaller than that given by Giroud.

The results of this investigation suggest that for elastic analyses the number of nodes, and thus the size of the stiffness matrix, can be greatly reduced by employing isoparametric elements. To illustrate this, the size of the stiffness matrix for mesh IS2 is (146, 28) whereas for mesh CS1 it is (222, 28), ie. 50% larger. However, accurate results can be achieved using both element types judi-

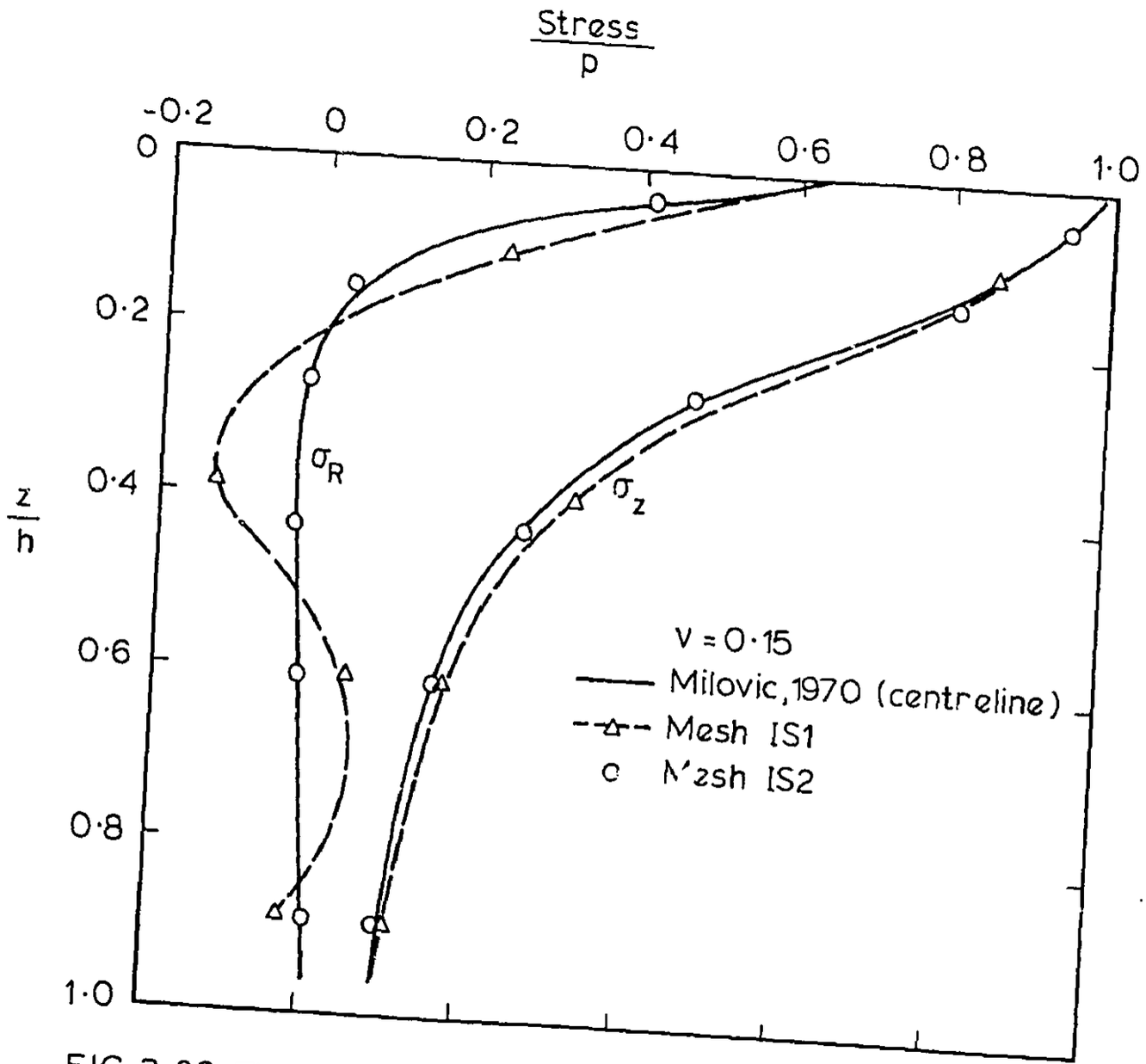

FIG.3.20 ELASTIC STRESS DISTRIBUTIONS - MESHES IS1, IS2

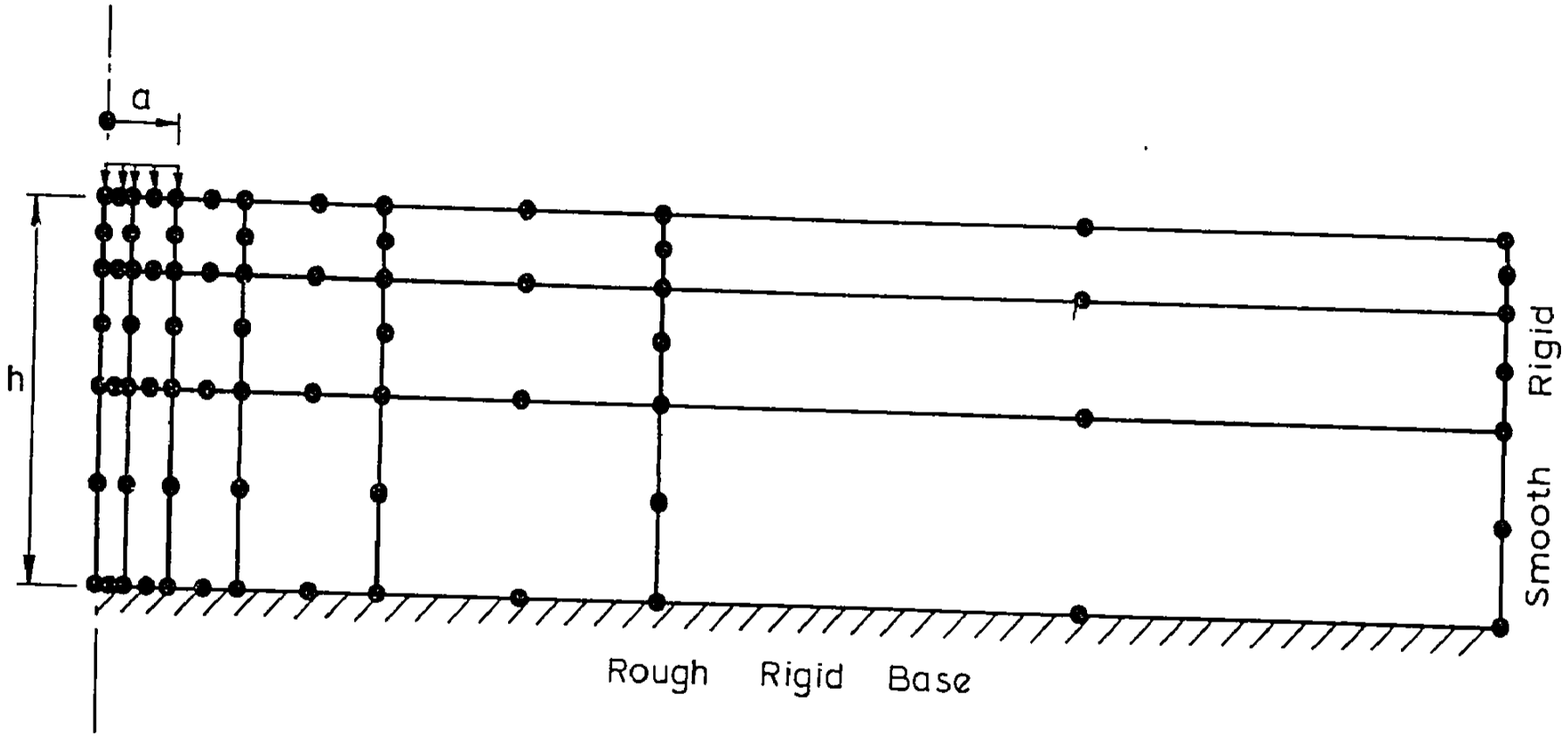

FIG. 3.21 ISOPARAMETRIC MESH IS2 - 73 NODES

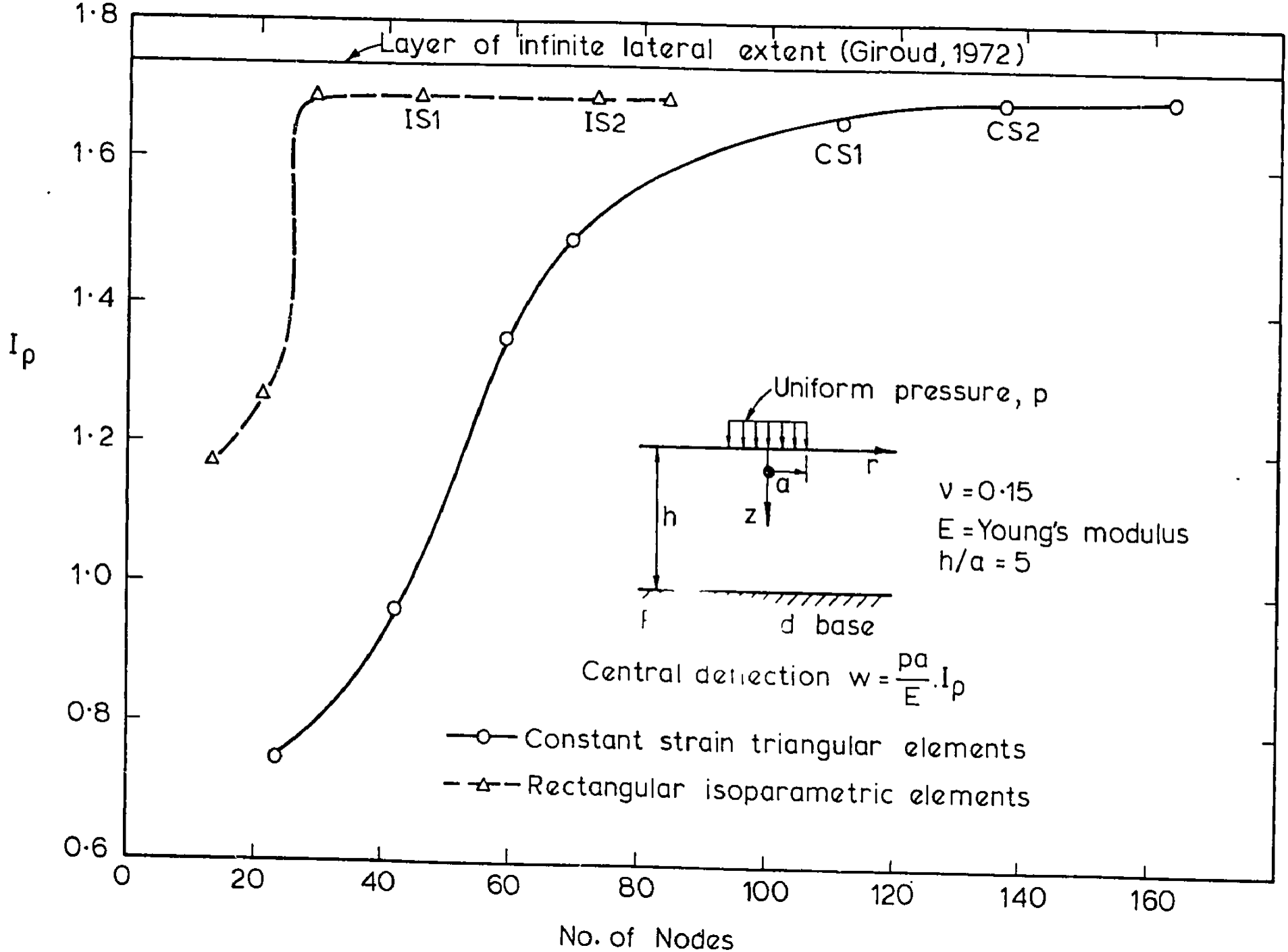

FIG. 3.22 COMPARISON BETWEEN RESULTS USING CONSTANT STRAIN AND ISOPARAMETRIC ELEMENTS

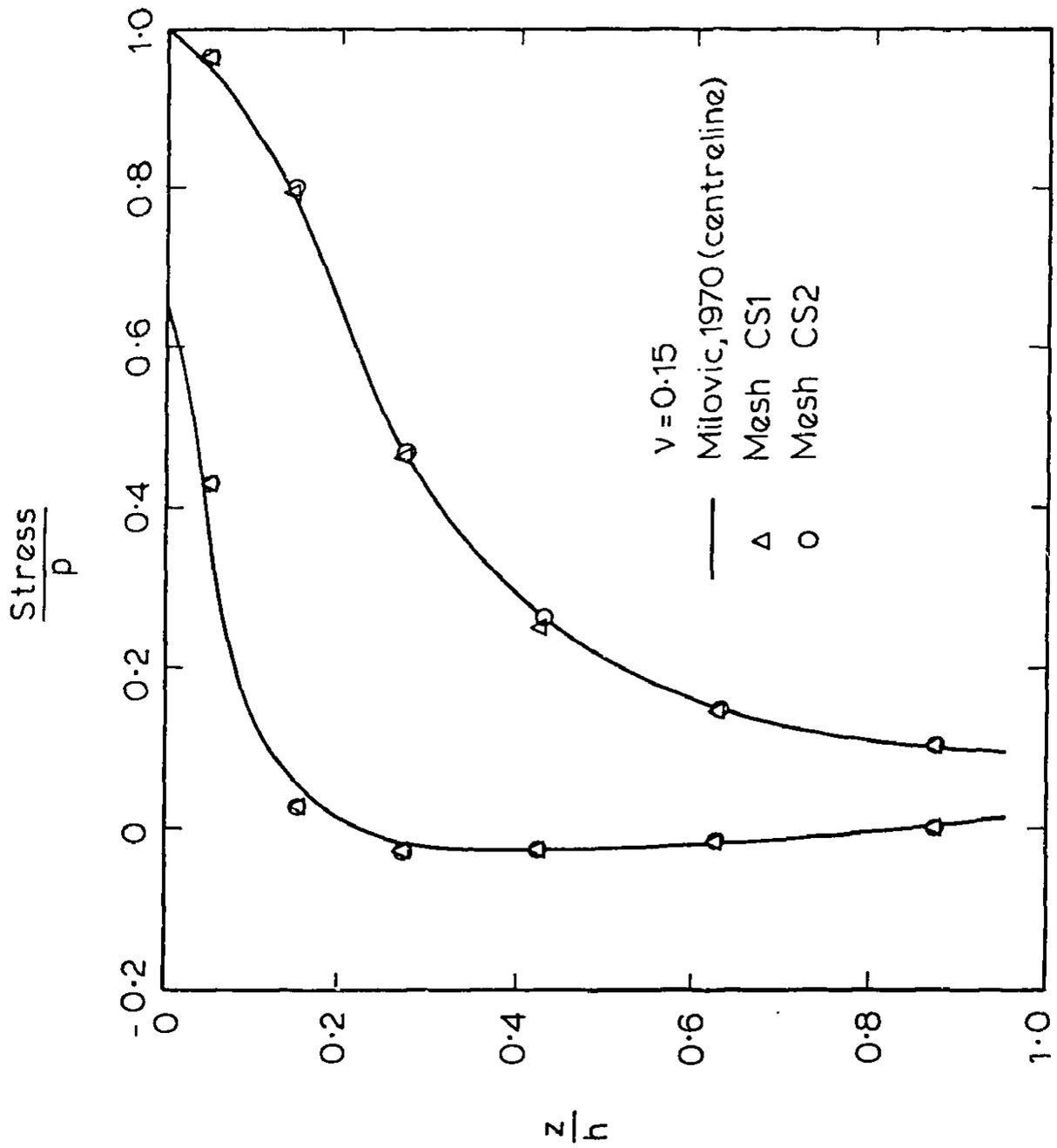

FIG. 3.23 ELASTIC STRESS DISTRIBUTIONS - MESHES CS1, CS2

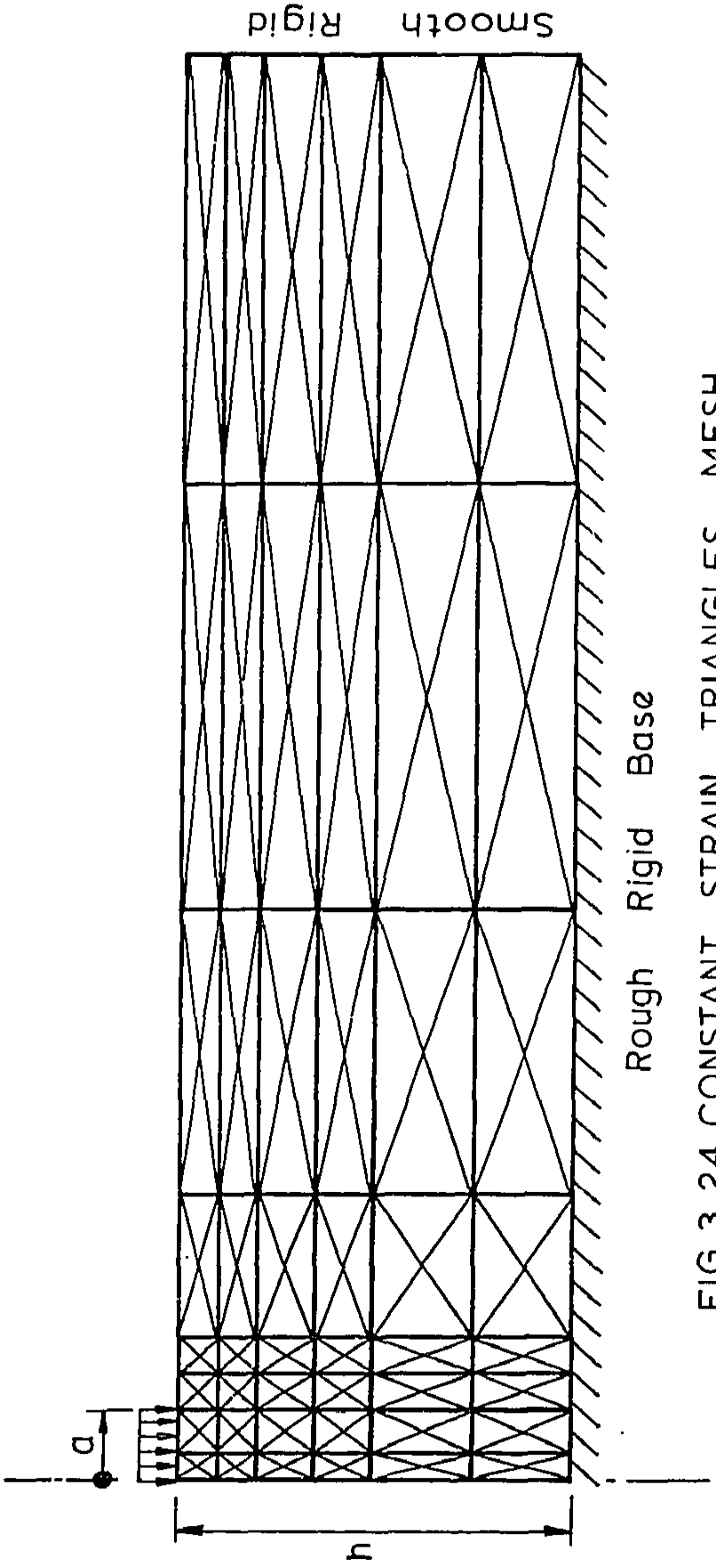

FIG.3.24 CONSTANT STRAIN TRIANGLES MESH

CS1 - 111 NODES

ciously. Finally, it is worth noting that considerable care needs to be exercised when evaluating the relative performance of element types in this manner, as the curves shown in Fig. 3.22 are not unique but depend on the astuteness of the user in subdividing the continuum.

3.5.3 Elasto-Plastic Analyses - The Two Elements Compared

Meshes IS2 and CS1 were used for elasto-plastic analyses of both a flexible and a smooth rigid footing to evaluate the relative performances of the two element types for non-linear analyses. The material was taken to be purely cohesive with cohesion c_u and a Poisson's ratio $\nu = 0.48$ which approximates incompressible behaviour. The Mohr-Coulomb criterion is used and the initial stress method of solution employed. The parameters chosen correspond to undrained loading of a fully saturated homogeneous soil layer. The same load increments and convergence criterion were used so that valid comparisons of computer times could be made.

3.5.3 (i) Flexible Footing Analyses

The results of the flexible footing analyses are shown in Fig. 3.25. The elastic central deflections given by the two meshes are in close agreement with Giroud's solutions for an incompressible material ($\nu = 0.5$). The finite element solutions are .1% (mesh IS2) and 4.5% (mesh CS1) smaller respectively. The two meshes give very similar load-deflection curves. The central processor time for the analysis using isoparametric elements was 1.67 times longer than for the analysis using the constant strain triangles mesh. However, for the isoparametric elements, considerable computation is involved in

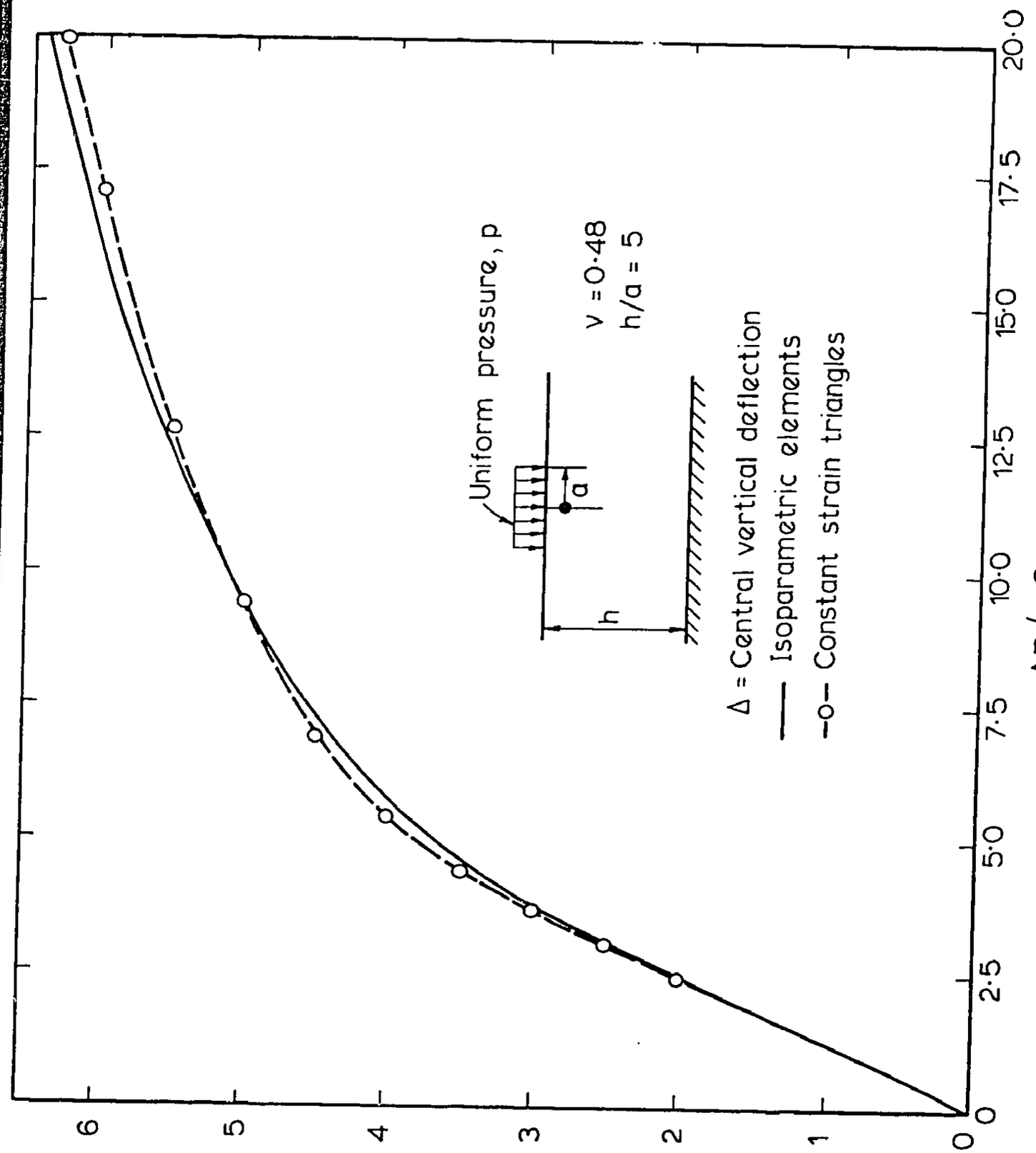

FIG. 3.25 ELASTO-PLASTIC ANALYSES - FLEXIBLE FOOTING

assembling the strain matrix [B]. A significant saving would be made in non-linear analyses by storing these strain matrices and thus avoiding reassembly when yielding occurs.

The growth of the yielded zones is shown in Figs. 3.26 and 3.27 for both meshes. For the isoparametric elements, when the stresses at a Gauss point satisfy the yield criterion, an equivalent zone of influence within the element has been shaded. The growth of the plastic zones obtained from the two element types is very similar.

3.5.3 (ii) Rigid Footing Analyses

The results of the analyses of a smooth rigid circular footing are shown in Fig. 3.28. Although the elastic response of the two meshes is different the elasto-plastic behaviour is very similar.

The elastic settlement obtained from meshes CS1 and IS2 are significantly different to the available published solutions (Poulos, 1968b). Carrier and Christian (1973) have reported errors of 10-13% in finite element solutions for the settlement of a rigid circular plate resting on a homogeneous elastic half space.

Mesh CS1 which has only 3 nodes beneath the footing gives a value for settlement which is 18.8% less than the Poulos solution. The solution computed from mesh IS2 is 9.4% too small. This improvement is partly due to the two extra nodes beneath the footing as improved accuracy is obtained by increasing the number of nodes beneath the footing. A mesh of 340 constant strain triangles which has 6 nodes beneath the footing gave a value for settlement which is 15.5% too small.

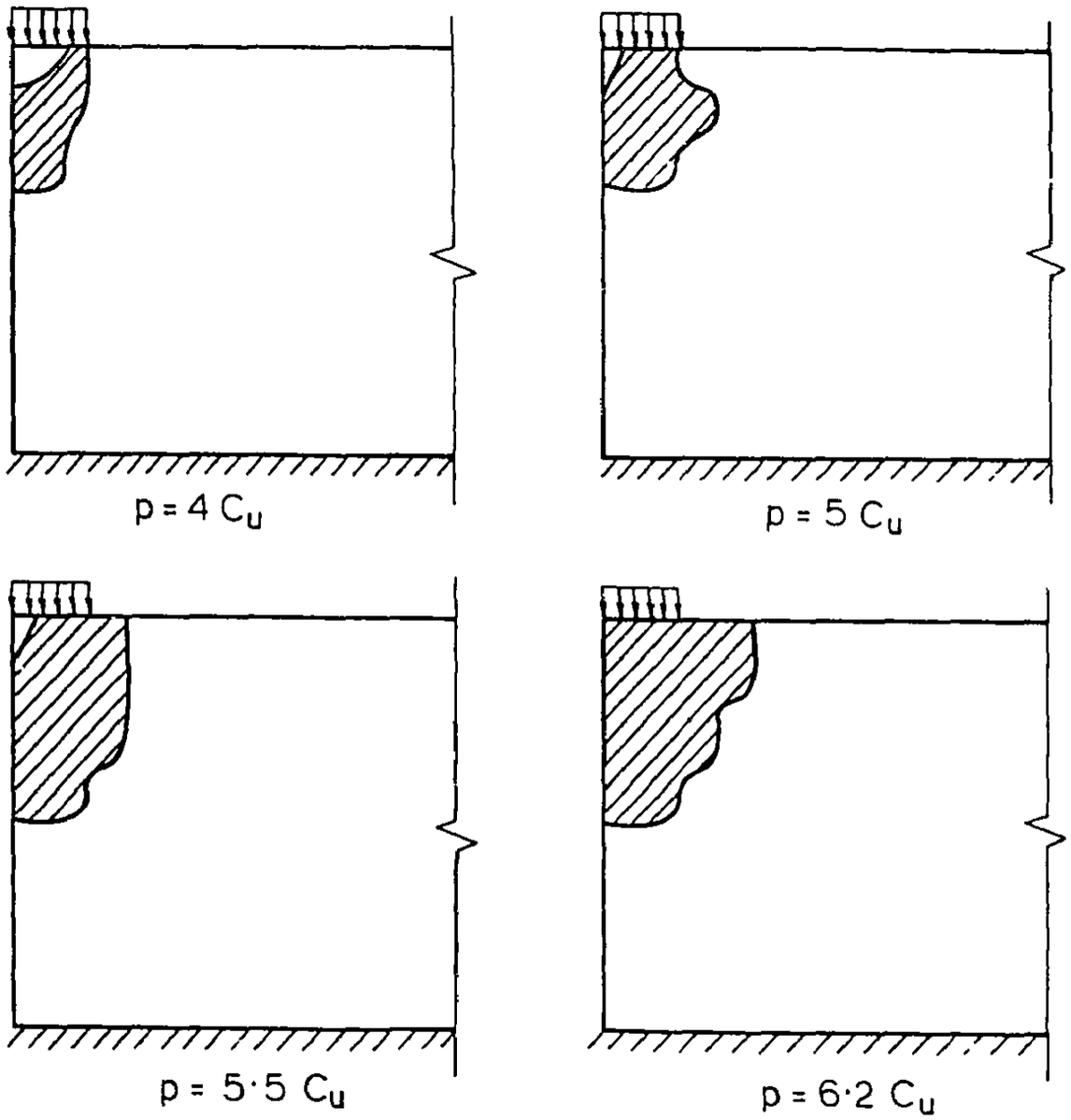

FIG. 3.26 GROWTH OF PLASTIC ZONES - ISOPARAMETRIC MESH IS2

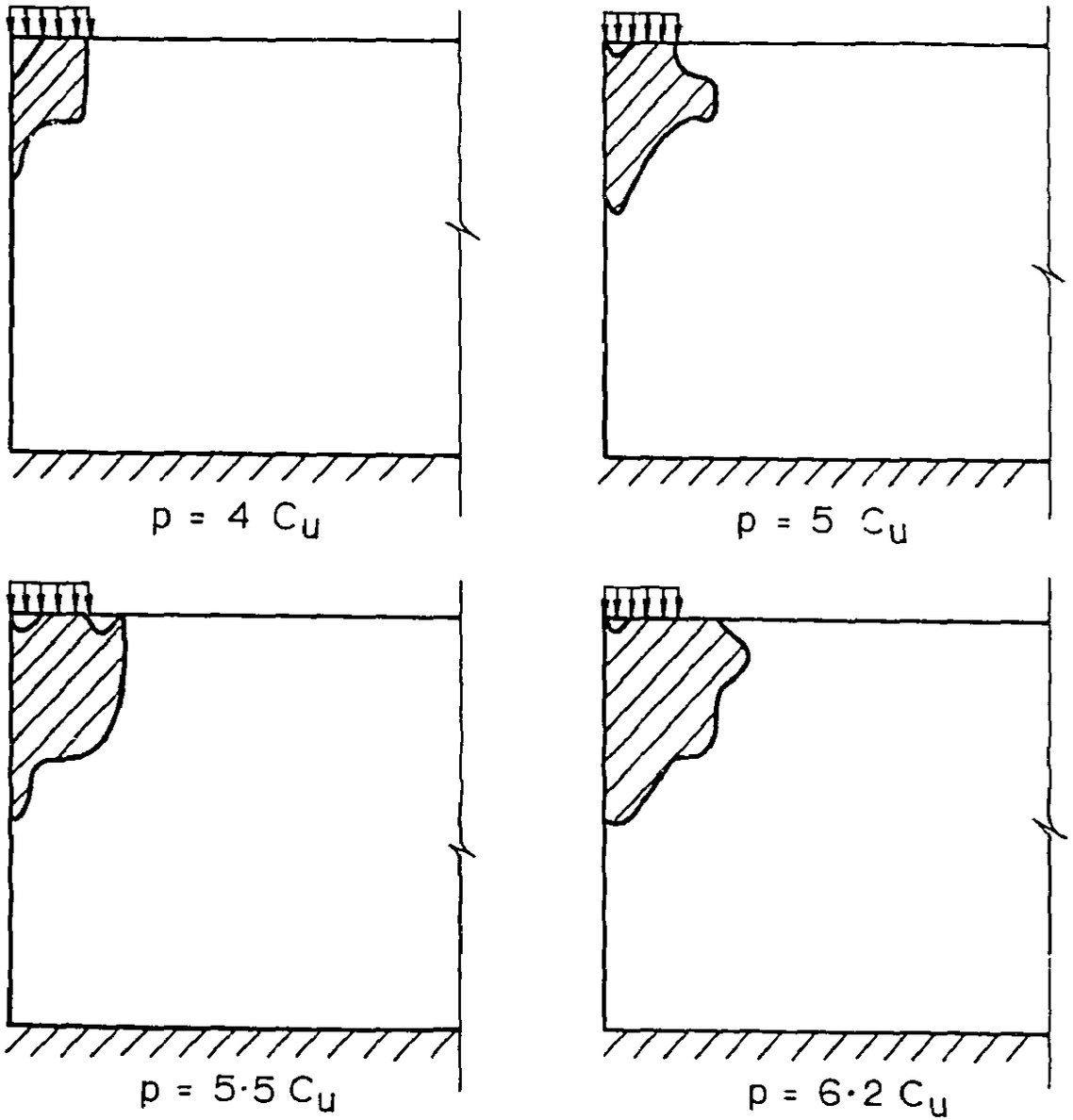

FIG. 3.27 GROWTH OF PLASTIC ZONES - CONSTANT STRAIN MESH CS1

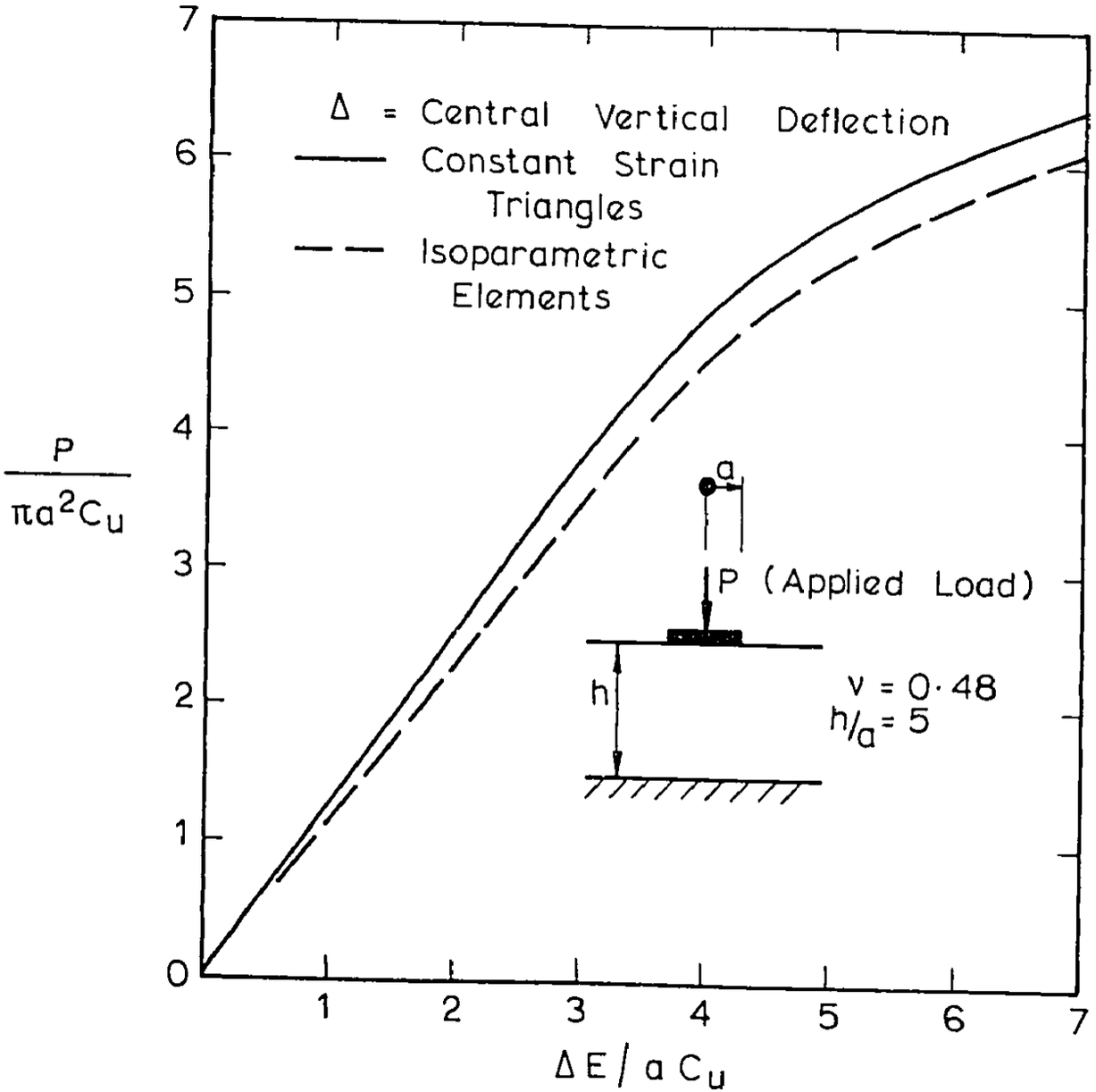

FIG. 3.28 ELASTO - PLASTIC ANALYSES - RIGID FOOTING

In Fig. 3.29 the results of several elastic analyses using this mesh are presented. These results show the effect of the value of Poisson's ratio on the magnitude of the error. The solution for $\nu = 0$ is 15% too small. If the number of nodes beneath the footing were increased further, the number of divisions down the layer also needs to be increased to avoid long thin elements. Therefore the number of elements becomes very large. This can be avoided by reducing the value of h/a. A mesh of 628 constant strain triangles which has 11 nodes beneath the footing was used to analyse a homogeneous layer with Poisson's ratio $\nu = 0$ where $h/a = 2$. The settlement was compared with the solutions of Poulos (1968b) and Brown (1969) and found to be 11.6% and 9.8% too small respectively. The solutions for $h/a = 5$ (6 nodes beneath footing) and $h/a = 2$ (11 nodes beneath footing) with $\nu = 0$ indicate that for constant strain triangles, slight improvement in accuracy can be gained from increasing the number of nodes beneath the footing but very large numbers of elements are required.

The results of this investigation show that finite element solutions for the settlement of a rigid circular raft are too small by 10-20% because of the inability of the elements to represent the discontinuity in stress at the edge of the footing. The results also suggest that the errors are reduced considerably by employing isoparametric elements for rigid footing analyses.

3.5.4 Conclusions

The main conclusions drawn from the results presented in this section are

(a) For a comparable degree of accuracy, isoparametric elements

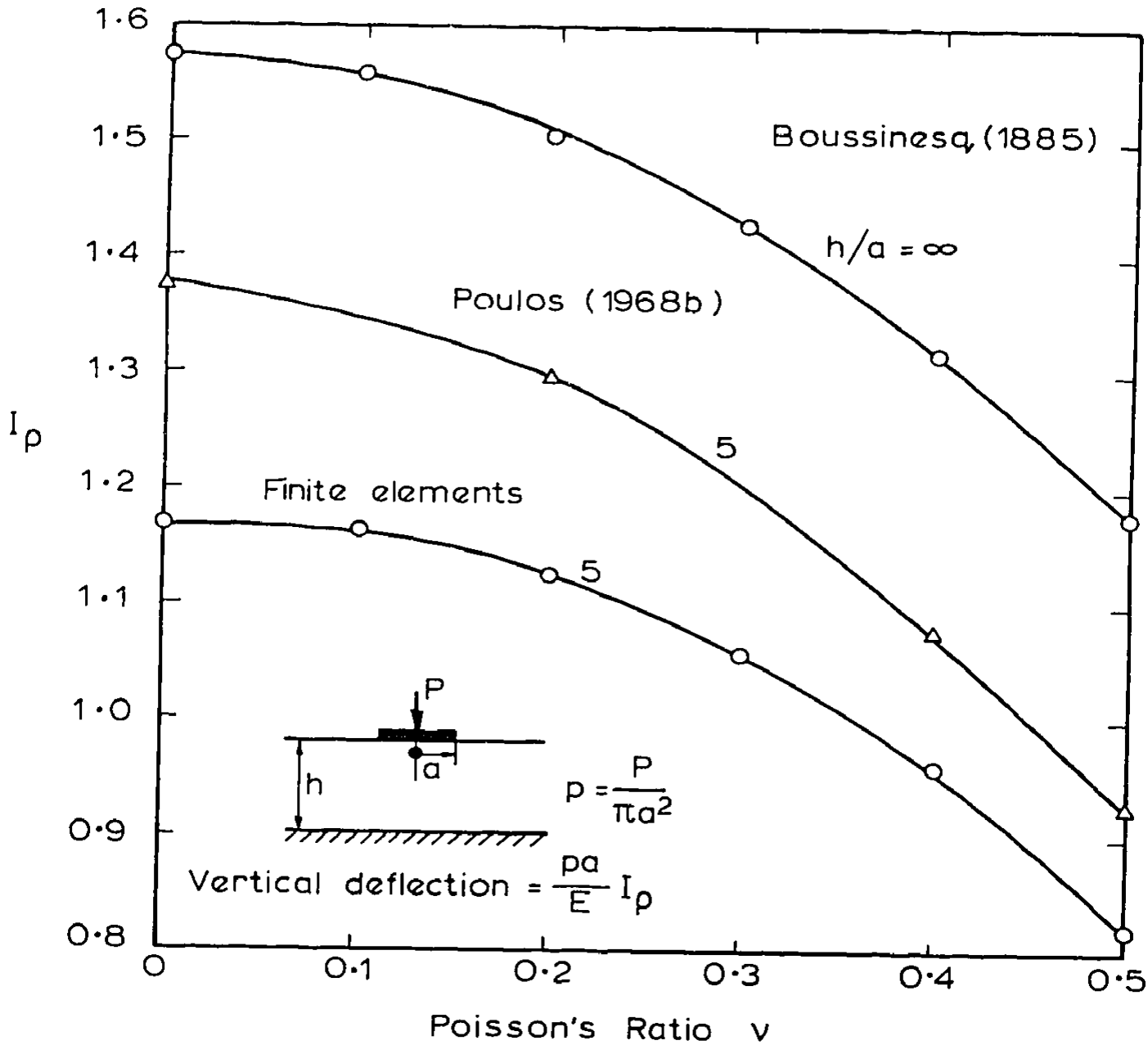

FIG.3.29 FINITE ELEMENT SOLUTIONS FOR SETTLEMENT OF RIGID FOOTING

require much less data storage than constant strain triangles for elastic flexible footing analyses.

(b) Finite element solutions for rigid circular footing settlements are too small when compared with available published solutions. However, the use of isoparametric elements result in significant improvement in accuracy.

(c) Elasto-plastic analyses of rigid and flexible footings give nearly identical results for the same order of computational effort.

APPENDIX 3A

ELASTICITY MATRIX

For an axisymmetric stress analysis, if the relationship between the stresses and strains is expressed in the usual notation ie.

$$\{\sigma\} = [D]\{\epsilon\} \tag{3A.1}$$

where $$\{\sigma\}^T = \{\sigma_z \ \sigma_r \ \sigma_\theta \ \tau_{rz}\} \tag{3A.2}$$

$$\{\epsilon\}^T = \{\epsilon_z \ \epsilon_r \ \epsilon_\theta \ \gamma_{rz}\} \tag{3A.3}$$

and $[D]$ = elasticity matrix

$$= \frac{E(1-\nu)}{(1+\nu)(1-2\nu)} \begin{bmatrix} 1 & \frac{\nu}{1-\nu} & \frac{\nu}{1-\nu} & 0 \\ & 1 & \frac{\nu}{1-\nu} & 0 \\ & & 1 & 0 \\ \text{symmetric} & & & \frac{1-2\nu}{2(1-\nu)} \end{bmatrix} \tag{3A.4}$$

then the elasticity matrix can be rewritten in terms of the Shear (G) and Bulk (K_B) moduli thus,

$$[D] = \begin{bmatrix} K_B + \frac{4}{3}G & K_B - \frac{2}{3}G & K_B - \frac{2}{3}G & 0 \\ & K_B + \frac{4}{3}G & K_B - \frac{2}{3}G & 0 \\ & & K_B + \frac{4}{3}G & 0 \\ \text{symmetric} & & & G \end{bmatrix} \tag{3A.5}$$

APPENDIX 3B

EXPRESSIONS FOR NODAL FORCES

A. Constant Strain Triangles - Linear Edge Displacements

Consider a uniform pressure p applied along the edge of element m [Fig. 3B1(a)]. If node i deflects w_i and node j w_j; then the displacement w for the edge can be written as

$$w = N_i(r).w_i + N_j(r).w_j \tag{3B.1}$$

$$\text{where } N_i(r) = \frac{(r-r_j)}{(r_i-r_j)} \tag{3B.2}$$

$$N_j(r) = \frac{(r-r_i)}{(r_j-r_i)} \tag{3B.3}$$

The equivalent nodal forces at nodes i and j given by Q_I and Q_J are required.

Equating the work done by the traction and the nodal forces

$$\int_{r_i}^{r_j} 2\pi r\, p\, w\, dr = Q_I.w_i + Q_J.w_j \tag{3B.4}$$

$$\int_{r_i}^{r_j} 2\pi r\, p\, w\, dr = \int_{r_i}^{r_j} 2\pi r\, p\, [N_i(r)\, w_i + N_j(r)\, w_j]\, dr$$

$$= \int_{r_i}^{r_j} 2\pi p \left[\frac{(r^2-rr_j)}{(r_i-r_j)} . w_i + \frac{(r^2-rr_i)}{(r_j-r_i)} . w_j \right] dr$$

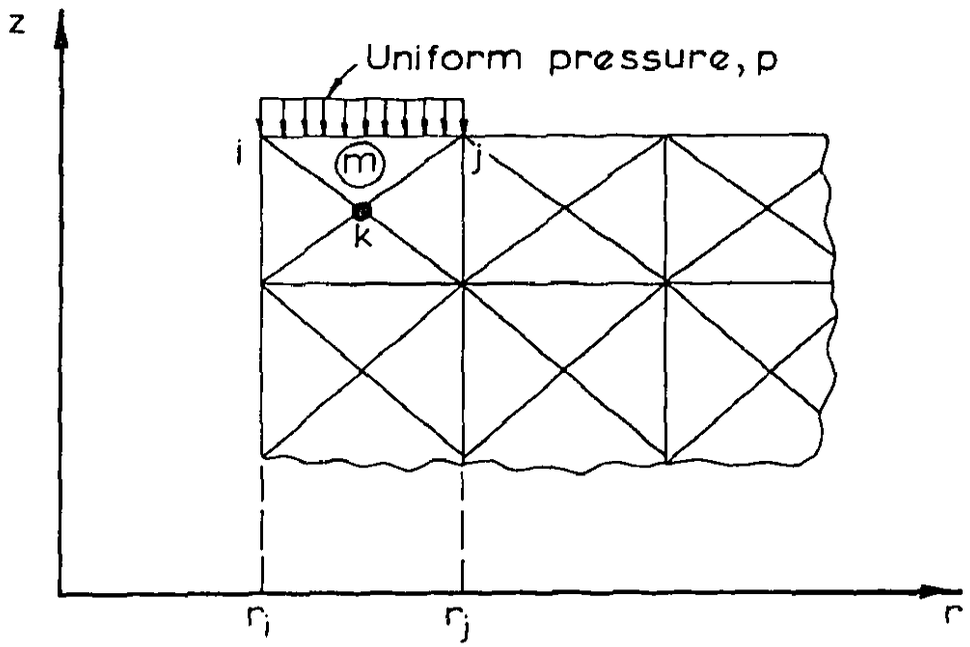

(a) Constant Strain Triangle

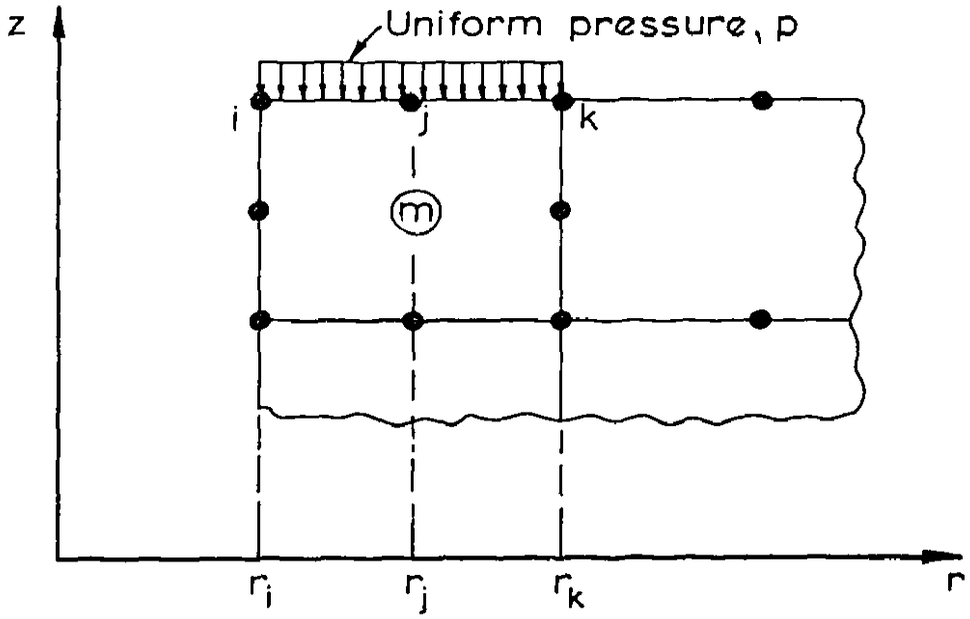

(b) Isoparametric Element

FIG. 3B.1 UNIFORM PRESSURE APPLIED TO THE TWO ELEMENT TYPES

$$= 2\pi p \left[\frac{r^3 w_i}{3(r_i - r_j)} - \frac{r^2 r_j w_i}{2(r_i - r_j)} + \frac{r^3 w_j}{3(r_j - r_i)} - \frac{r^2 r_i}{2(r_j - r_i)} \cdot w_j \right]_{r_i}^{r_j}$$

$$= 2\pi p \left[\frac{r_j^3 - r_i^3}{3(r_i - r_j)} - \frac{(r_j^2 - r_i^2)\, r_j}{2(r_i - r_j)} \right] w_i$$

$$+ 2\pi p \left[\frac{r_j^3 - r_i^3}{3(r_j - r_i)} - \frac{(r_j^2 - r_i^2) r_i}{2(r_j - r_i)} \right] w_j \qquad (3B.5)$$

Equivalent nodal forces:

$$Q_I = 2\pi p \left[\frac{r_j^3 - r_i^3}{3(r_i - r_j)} - \frac{(r_j^2 - r_i^2) \cdot r_j}{2(r_i - r_j)} \right] \qquad (3B.6)$$

$$Q_J = 2\pi p \left[\frac{r_j^3 - r_i^3}{3(r_j - r_i)} - \frac{(r_j^2 - r_i^2) \cdot r_i}{2(r_j - r_i)} \right] \qquad (3B.7)$$

B. Isoparametric Elements - Parabolic Edge Displacements

Consider a uniform pressure p applied along the edge of element m [Fig. 3B1(b)]. The deflections of nodes i, j, k are given by w_i, w_j and w_k. The displacement w for the edge can be written as

$$w = N_i(r) \cdot w_i + N_j(r) \cdot w_j + N_k(r) \cdot w_k \qquad (3B.8)$$

where $$N_i(r) = \frac{(r - r_j)(r - r_k)}{(r_i - r_j)(r_i - r_k)} \qquad (3B.9)$$

$$N_j(r) = \frac{(r - r_k)(r - r_i)}{(r_j - r_k)(r_j - r_i)} \qquad (3B.10)$$

$$N_k(r) = \frac{(r-r_i)(r-r_j)}{(r_k-r_i)(r_k-r_j)} \qquad (3B.11)$$

The equivalent nodal forces at nodes i, j and k given by Q_I, Q_J and Q_K are required.

Equating th work done by the traction and the nodal forces

$$\int_{r_i}^{r_k} 2\pi r\, p\, w\, dr = Q_I.w_i + Q_J.w_j + Q_K.w_k \qquad (3B.12)$$

$$\int_{r_i}^{r_k} 2\pi r\, p\, w\, dr = \int_{r_i}^{r_k} 2\pi r\, p\, [N_i(r).w_i + N_j(r).w_j + N_k(r).w_k]dr$$

$$= 2\pi p \int_{r_i}^{r_k} r\, N_i(r).w_i.dr + 2\pi p \int_{r_i}^{r_k} r\, N_j(r).w_j.dr$$

$$+ 2\pi p \int_{r_i}^{r_k} r.N_k(r).w_k.dr \qquad (3B.13)$$

$$\therefore \quad Q_I = 2\pi p \int_{r_i}^{r_k} r.N_i(r)\,dr \qquad (3B.14)$$

$$Q_J = 2\pi p \int_{r_i}^{r_k} r.N_j(r)\,dr \qquad (3B.15)$$

$$Q_K = 2\pi p \int_{r_i}^{r_k} r.N_k(r).dr \qquad (3B.16)$$

Evaluating these integrals gives:

$$Q_I = \frac{2\pi p}{(r_i - r_j)(r_i - r_k)} \left[\frac{(r_k^4 - r_i^4)}{4} - \frac{(r_j + r_k)(r_k^3 - r_i^3)}{3} + \frac{r_j r_k}{2} (r_k^2 - r_i^2) \right] \quad (3B.17)$$

$$Q_J = \frac{2\pi p}{(r_j - r_k)(r_j - r_i)} \left[\frac{(r_k^4 - r_i^4)}{4} - \frac{(r_i + r_k)(r_k^3 - r_i^3)}{3} + \frac{r_k r_i}{2} (r_k^2 - r_i^2) \right] \quad (3B.18)$$

$$Q_K = \frac{2\pi p}{(r_k - r_i)(r_k - r_j)} \left[\frac{(r_k^4 - r_i^4)}{4} - \frac{(r_i + r_j)(r_k^3 - r_i^3)}{3} + \frac{r_i r_j}{2} (r_k^2 - r_i^2) \right] \quad (3B.19)$$